8-2002

Development and Application of the Zero Length Column (ZLC) Technique for Measuring Adsorption Equilibria

Federico Brandani

DEVELOPMENT AND APPLICATION OF THE ZERO LENGTH COLUMN (ZLC) TECHNIQUE FOR MEASURING ADSORPTION EQUILIBRIA

By

Federico Brandani

Laurea Degree Universita' degli Studi di L'Aquila, 2000

A THESIS

Submitted in Partial Fulfillment of the

Requirements for the Degree of

Doctor of Philosophy

(in Chemical Engineering)

The Graduate School

The University of Maine

August, 2002

Advisory Committee:

Dr. Douglas M. Ruthven, Professor of Chemical Engineering, Advisor

Dr. Brian G. Frederick, Professor of Chemistry

Dr. William J. DeSisto, Professor of Chemical Engineering

Dr. John C. Hassler, Professor of Chemical Engineering

Dr. David J. Neivandt, Professor of Chemical Engineering

DEVELOPMENT AND APPLICATION OF THE ZERO LENGTH COLUMN (ZLC) TECHNIQUE FOR MEASURING ADSORPTION EQUILIBRIA

By Federico Brandani

Thesis Advisor: Dr. Douglas M. Ruthven

An Abstract of the Thesis Presented
in Partial Fulfillment of the Requirements for the
Degree of Doctor of Philosophy
(in Chemical Engineering)
August, 2002

This thesis reports the results of an experimental study aimed at developing the "zero length column" (ZLC) method as a useful technique for measuring adsorption equilibria. In a ZLC experiment a small sample of adsorbent is pre-equilibrated with the sorbate, at a known partial pressure, in a He carrier. Information concerning the sorption kinetics and equilibria can be obtained from the desorption curve when the flow is switched to a pure He purge under carefully controlled conditions. This technique has been widely used to measure intraparticle diffusivities but, when operated at sufficiently low flow rate, it provides a simple and convenient way to obtain equilibrium data, including both Henry's Law constants and complete isotherms.

The practical viability and limitations of this approach have been explored by measuring the adsorption isotherms for CO_2 on several different zeolites on the same

adsorbents and under the same conditions at which the isotherms had been measured, at the Air Products Laboratory, by a conventional volumetric/piezometric method. It was shown that, with careful attention to the details of the experiment, the ZLC measurement replicates the volumetric/piezometric isotherms within a few percent. The ZLC method has advantages of speed and simplicity and thus provides a useful tool for adsorbent screening studies.

The ZLC method was used to measure the isotherms for CO_2 (and some other sorbates) on a range of different cationic forms of zeolite X. The data, when analyzed using localized adsorption models, suggest adsorption site densities that are reasonably consistent with structural information concerning the distribution of the cations in these materials.

The ZLC approach has been extended to the measurement of separation factors in binary adsorption systems and the separation factors measured in this way are shown to be consistent with the values derived from standard binary isotherm measurements.

In a further development it is shown that the ZLC method can be easily coupled with a temperature programmed desorption (TPD) measurement. This allows determination of any residual "irreversibly" adsorbed sorbate and provides a simple way to study the effect of a strongly held adsorbate on the isotherm for a weaker species. The effect of water on the isotherm for CO_2 on several type X zeolites has been investigated in this way.

The advantages and limitations of the ZLC method are reviewed and experimental precautions needed to obtain reliable results are discussed in detail.

ACKNOWLEDGEMENTS

The present study was made possible, first of all, thanks to the support of my thesis advisor, Prof. Douglas Ruthven. His valuable advice and active collaboration allowed me to the project in a timely manner. Working with him has been not only an honor but also a pleasure. Thanks are also due to my advisory committee especially to Dr. David Neivandt for his constructive comments on the thesis draft.

Special thanks are due to Dr. Charles Coe of the AirProducts and Chemicals Inc. for both financial and technical support and for his many comments and suggestions during the course of the project.

I have also to thank my brother, Dr. Stefano Brandani of University College, London for introducing me to ZLC technique, for all his advice and for his help in the implementation of the mathematical models for binary equilibria.

I am sincerely grateful to all the staff of the Chemical Engineering department for providing help when needed. In particular, I would like to thank Amos Cline for his creative suggestions and for his speedy assistance in resolving technical problems related to the experimental systems.

Sincere thanks are also due to my parents and my wife Cristiana for supporting and encouraging me all these months.

Lastly, but not least, my deep gratitude goes to Patricia and Douglas Ruthven for hosting me in their house and considering me a member of the family. Thanks to them I was able to focus exclusively on the project. They will always have a special place in my heart.

Table of Contents

List of Tables

List of Figures

List of Symbols

b	Langmuir equilibrium constant
C	total concentration in fluid phase
c	sorbate concentration in fluid phase
c_0	sorbate initial steady state concentration in fluid phase
D	diffusion coefficient
F	volumetric flow rate
$-\Delta H$	heat of adsorption
K	dimensionless Henry's law adsorption equilibrium constant
K_0	pre-exponential factor [Eq.4.1]
k	calibration content [Eq.6.1]
L	parameter defined in Eq.2.7
n	adsorbed concentration [Eq.1.6]
P	equilibrium pressure [Eq.1.6]
p	sorbate partial pressure
q	sorbate concentration in adsorbed phase
q_0	initial adadsorbed phase concentration
$\bar{q}$	value of q averaged over crystal and pellet
q_s	saturation limit
q^*	equilibrium value of q
q'	total quantity of water [Eq.6.1]
R	gas constant; particle radius

r	radial coordinate for microparticle or crystal
T	absolute temperature
t	time
$\bar{t}$	mean retention time
ΔU_0	internal energy change on sorption
V	detector signal intensity [Eq.6.1]
V_{col}	volume of a chromatographic column
V_g	fluid phase volume
V_s	adsorbent volume
y	sorbate mole fraction in fluid phase
y_0	initial value of y
x	water loading [Eq.6.2]

Greek Letters

α	separation factor defined in Eq.2.23; temperature dependent parameter [Eq.6.2]
β_n	nth root of Eq.2.6
ε	voidage of adsorbent bed
γ	parameter defined in Eq.2.7

CHAPTER 1

Introduction

The practical importance of adsorption as an energy efficient separation process has grown greatly over the past thirty years. The large majority of adsorption processes depend on differences in adsorption equilibrium to achieve the desired separation. The measurement, correlation and prediction of adsorption equilibrium isotherms are therefore very important from both practical and theoretical points of view. The established experimental techniques for isotherm measurement are somewhat tedious and time consuming especially when applied to binary or multicomponent systems. This thesis describes the development and application of a new technique for measuring adsorption isotherms based on following the desorption curve for a small sample of adsorbent, pre-equilibrated with sorbate under known conditions. This approach proves easier and faster than conventional methods and thus provides a useful technique for adsorbent screening studies where rapid approximate data are required for a large number of samples.

This chapter contains a brief review of the traditional methods used for studying adsorption equilibria, a review of the relevant zeolite structures, the choice made for the molecule to use as a probe molecule and finally an outline of the structure of the thesis.

1.1 Adsorption Equilibrium

1.1.1 Henry's Law

Adsorption equilibrium is generally characterized by the adsorption isotherm – a plot of the adsorbed phase concentration against the gas phase concentration or partial pressure (of a specific sorbate) at equilibrium. From basic statistical thermodynamic principles it may be shown that for physical adsorption at sufficiently low concentrations the isotherm should approach a simple linear form. The region of approximate linearity is known as the Henry's law region and the slope (or the constant of proportionality between adsorbed phase and gas phase concentrations) is known as the Henry's constant.

Formally it is defined:

$$K(dimensionless) = \left.\frac{dq}{dc}\right|_{q\to 0} \tag{1.1}$$

$$K_p\left(\frac{moles}{cm^3 atm}\right) = \left.\frac{dq}{dp}\right|_{q\to 0} \tag{1.2}$$

The two constants are obviously related by:

$$K = (RT)K_p \tag{1.3}$$

Defined in this way the Henry constant is in fact an equilibrium constant and, as such, it shows the usual vant Hoff temperature dependence:

$$K = K_{\infty}\, exp(-\Delta U_0/RT); \qquad K_p = K_{p\infty}\, exp(-\Delta H_0/RT) \tag{1.4}$$

where ΔU_0 and ΔH_0 represent respectively the changes in internal energy and enthalpy on adsorption at very low loading.

The Henry constant measures the intrinsic affinity of the adsorbent for a specific sorbate. Consequently the Henry constants (or the limiting energy of adsorption) are commonly used to provide quantitative comparisons of adsorption affinity.

1.1.2 The Langmuir Isotherm

At loadings beyond the Henry's Law region the isotherm typically becomes curved. For a microporous adsorbent the isotherm is generally of type I form i.e. the curvature is monotonic and the isotherm approaches a saturation limit at high partial pressures (see Fig.1.1)

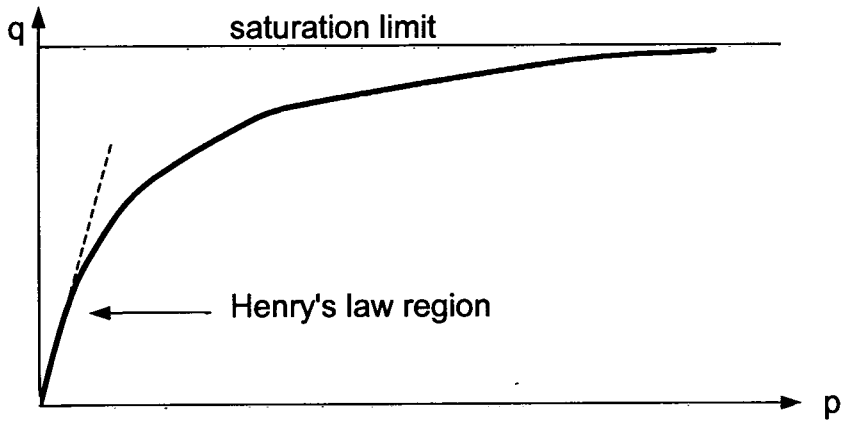

Figure 1.1: Sketch Showing the Typical Form of a Type I Isotherm

The simplest model capable of representing such behavior is the ideal Langmuir model:

$$\frac{q}{q_s} = \frac{bp}{1+bp} \tag{1.5}$$

where q_s represents the saturation limit and b is another adsorption equilibrium constant, related to the Henry constant by $K_p = bq_s$. Eq.1.5 is easily derived from the following assumptions:

1. Adsorption occurs at a fixed number of distinct sites
2. All sites are energetically equivalent
3. Each site can accommodate one sorbate molecule
4. No interaction between sorbate molecules on adjacent sites

This is clearly a reasonable model for localized adsorption. However, even when the adsorbed molecules are mobile the isotherm can often be approximated by Eq.1.5 so the Langmuir model is widely used as a correlating equation even when the above assumptions are not really fulfilled.

1.1.3 Localized and De-Localized Models

The Langmuir isotherm is the simplest example of a localized adsorption model. The sorbate molecules are regarded as either attached to localized adsorption sites (as in chemisorption) or confined within the low energy regions near such centers (localized physisorption). For adsorption of polar or quadrupolar molecules

(e.g. H_2O or CO_2) on a zeolite the accessible cations can be identified as the most favorable adsorption sites. The Henry constant is determined by the sorbate-cation interaction energy and any of shielding of the cations by adsorption of a strongly polar sorbate can be expected to have a major effect on the Henry constant for other guest molecules.

On less energetically heterogeneous surfaces the adsorbed molecules are more mobile, jumping rapidly from site to site or, at high temperatures, moving freely over the surface (2-dimensional gas model). Subject to certain assumptions it may be shown that the Langmuir expression for the isotherm is a reasonable approximation even for delocalized adsorption. The Henry constant is then determined by the average interaction energy rather than by the site energy.

1.2 Traditional Techniques for Studying Adsorption Equilibria

1.2.1 Gravimetric Method

In the gravimetric technique, the adsorption isotherm is determined by measuring the change in weight of an adsorbent sample when it is exposed to a known partial pressure of sorbate and allowed sufficient time to reach equilibrium. A schematic of a gravimetric apparatus is shown in Figure 1.2. The electronic balance accurately monitors the weight of the sample. The isotherm is determined by successively adding sorbate at increasing pressures. The equilibrium pressure is determined with a pressure transducer. Depending on the equilibrium pressures and the difference in pressure between the sample and the balance compartment, the

measurements have to be corrected to include buoyancy effects given by the difference between the volume displaced by the sample and the counterweight, condensation of the sorbate on the balance mechanism and thermal transpiration effects. For binary or multicomponent equilibria an on-line mass-spectrometer has to be included for analysis of the gas phase. The composition of the adsorbed phase may then be deduced from the mass balance but careful attention to details of the experiment is necessary to avoid cumulative errors (Rees and Shen[1]).

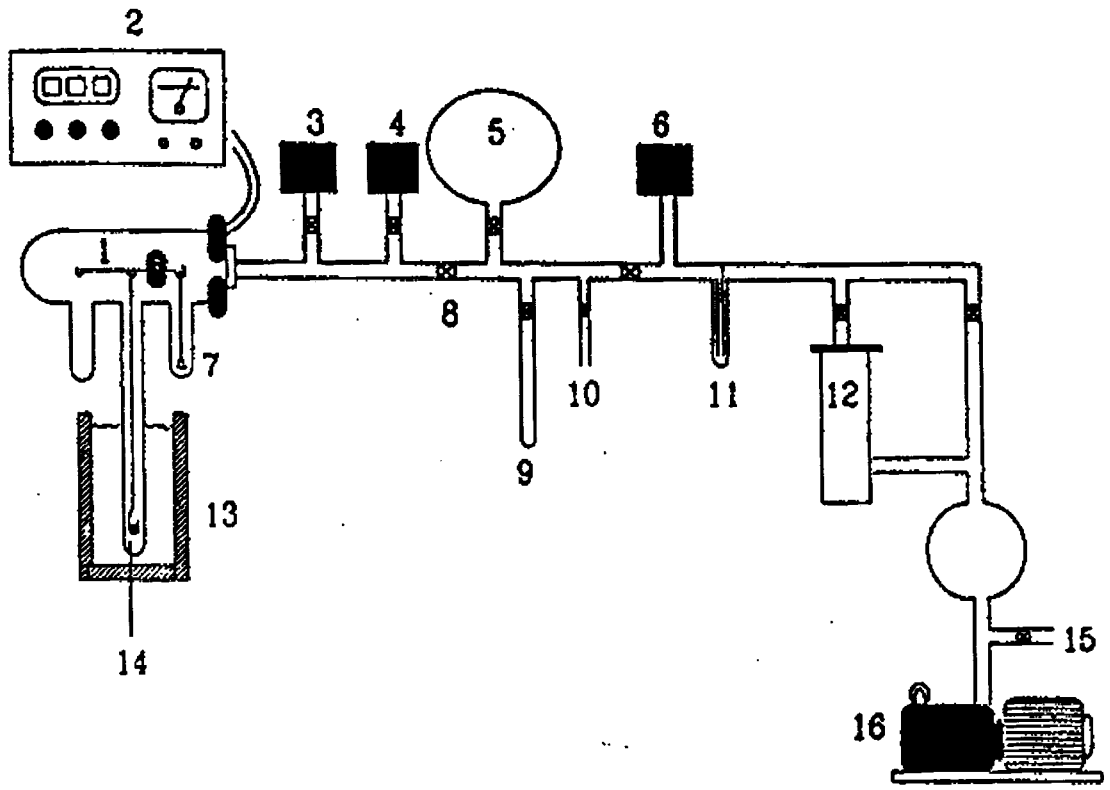

Figure 1.2: Example of a Gravimetric System (see Rees and Shen[1])

1. Electrobalance
2. Cahn 2000 Electrobalance
3. Baratron pressure transducer
4. Baratron pressure transducer
5. Gas reservoir
6. Pirani gauge
7. Counterweight
8. High vacuum taps
9. Liquid sorbate
10. Gas inlet
11. Cold finger
12. Oil diffusion pump
13. Water bath or tube furnace
14. Zeolite sample
15. Air inlet
16. Rotary pump

1.2.2 Volumetric/Piezometric Method

The basic elements of a volumetric/piezometric system are shown in Figure 1.3. In addition to the vacuum line, pressure transducer and adsorbent sample holder, the system is connected to a gas line with one or more calibrated gas volume fitted with a pressure transducer. All volumes are carefully calibrated using He, which is essentially non-adsorbing at room temperature. After pre-conditioning the adsorbent (under vacuum at elevated temperature), the system is evacuated and then charged to a known pressure from the calibrated gas dosing volume. Knowing the pressures in both the doser and the system and the relevant volumes, the quantity of gas adsorbed can be deduced by straightforward mass balance. Knowing the weight of adsorbent in the sample holder this yields directly one point on the experimental isotherm. This procedure is then repeated successively at different pressures to generate the complete isotherm. It is desirable that the entire system be contained in a constant temperature enclosure since temperature gradients in the system reduce the accuracy with which the mass balance can be calculated. At low pressures, the pressure measurement also becomes unreliable when there is a thermal gradient.

The main disadvantage of the volumetric/piezometric approach compared to the gravimetric method is that the amount of sorbate adsorbed is not measured directly and this may lead to cumulative errors in successive dosing. The balance calibration with standard masses is generally more accurate than the volume calibration. The volumetric/piezometric method requires corrections for non-ideal behavior of the sorbate, while the gravimetric technique does not depend on the ideal

gas law although it does require buoyancy corrections and at elevated temperatures it is subject to thermal transpiration errors (Rees and Shen[1], Ruthven and Post[2]).

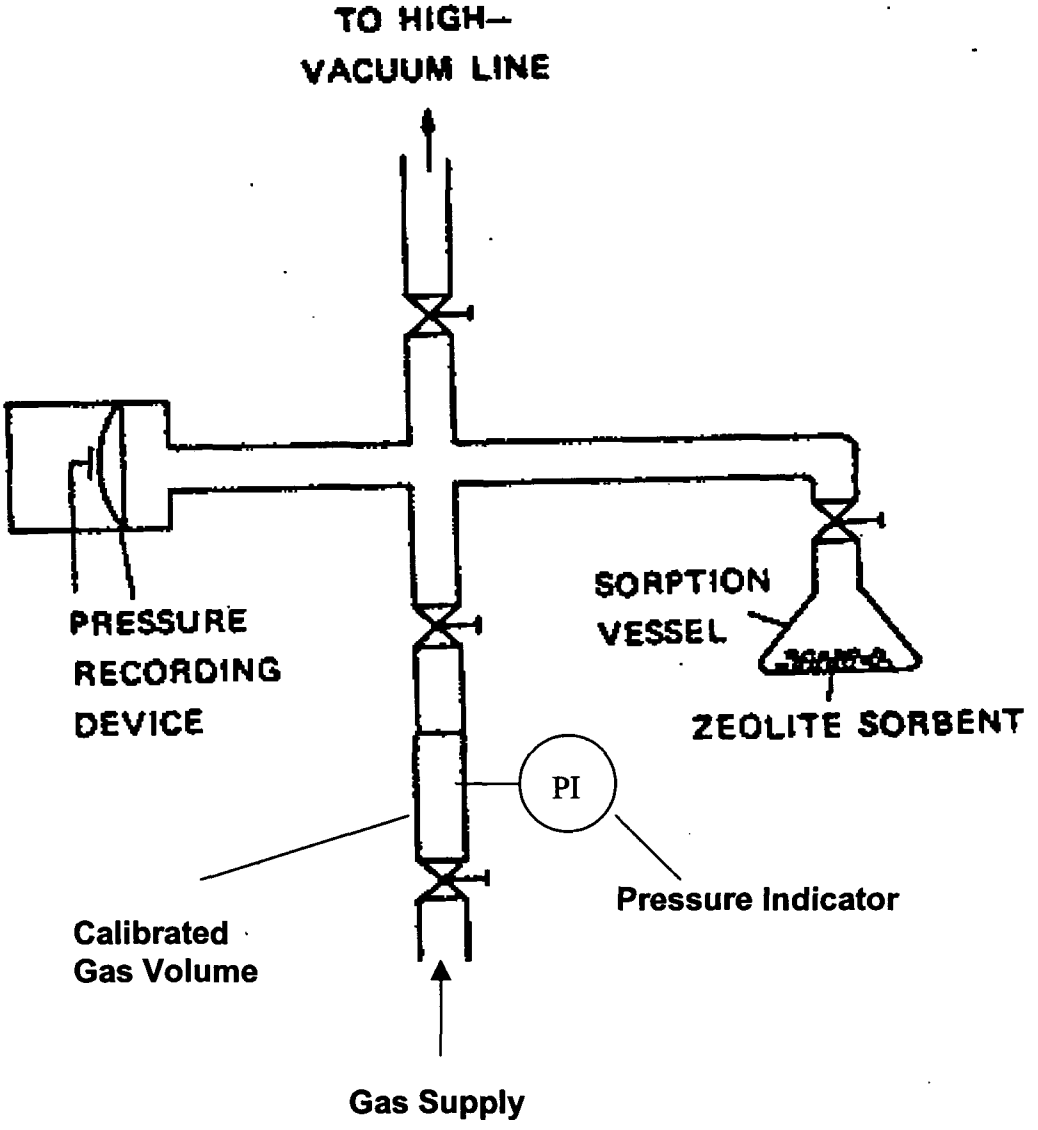

Figure 1.3: Experimental Set-Up for Volumetric/Piezometric Measurement of Sorption Equilibria (see Ruthven and Post[2])

1.2.3 Isosteric Method

Experimentally this technique is similar to the volumetric method. The main difference is that there is a large amount of adsorbent in the sample chamber while the volume of the gas phase is kept as low as possible. A schematic of the system is given in Figure 1.4. The principle of the technique is to maintain the adsorbed phase loading constant and determine the equilibrium pressure as a function of temperature (the isostere) by successively increasing the temperature of the system.

From the Clausius-Clapeyron equation for an ideal gas:

$$R\left[\frac{\partial \ln P}{\partial(1/T)}\right]_q = \Delta H \tag{1.6}$$

where P is the equilibrium pressure at the absolute temperature at the constant adsorbed concentration q. It can be seen that, at constant loading, a plot lnP vs. 1/T should yield a straight line from the slope of which the heat of adsorption $(-\Delta H)$ can be determined. By repeating the procedure for different sorbate loadings a series of isosteres can be obtained. The isotherms can be determined from this plot by drawing constant temperature lines and determining the adsorbed phase loading and equilibrium pressure at the points where the isothermal lines intercept the different isosteres. In the case of binary or multicomponent measurements, in addition to the total amount adsorbed, the adsorbed phase composition also has to be maintained constant. This is a serious

practically difficult so the method is not really useful for measuring binary or multicomponent isotherms.

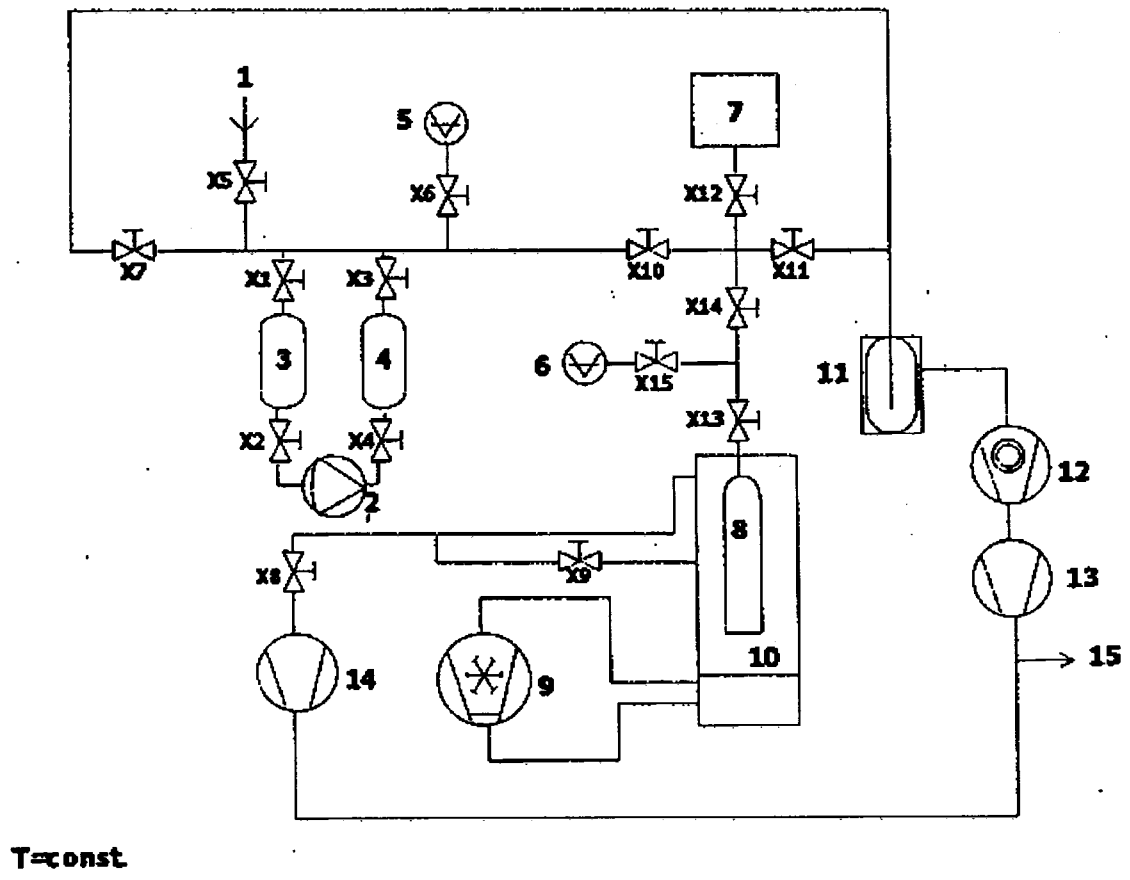

Figure 1.4: Isosteric Apparatus (see Rees and Shen[1]).

1. Gas supply
2. Circulating pump
3. Calibrated doser volumes
4. Calibrated doser volumes
5. Pressure sensor
6. Pressure sensor
7. Mass spectrometer
8. Sample holder
9. Cryostat
10. Cryostat

11-15 Vacuum system

1.2.4 Chromatographic Method

In addition to the well established gravimetric and volumetric/piezometric methods, during the last twenty years there have been several attempts to develop chromatographic methods for measuring isotherms (Ruthven[3]). The chromatographic measurement of the Henry constant is now a well established technique. The retention volume for a packed column, which is easily determined from the first moment of the chromatographic response $(\bar{t})$ at a known flow rate is directly related to the dimensionless Henry constant:

$$\frac{Retention\ Vol}{Column\ Vol} = \frac{F\bar{t}}{V_{col}} = \varepsilon + (1-\varepsilon)K \tag{1.3}$$

so the chromatographic determination of the Henry constant requires only measurements of the mean residence time under carefully controlled conditions.

The method can be extended to measuring the complete isotherm by using mixed feed streams containing known proportions of the sorbate plus an inert carrier and making small perturbations in the concentration about the base composition. In this situation the retention volume measurement yields the slope of the isotherm at the loading corresponding to the base feed composition. The complete isotherm may then be found by integration from zero up to the required concentration level. Further details are given by van der Vlist and van der Meijden[4] and Ruthven and Kumar[5].

A similar approach has also been developed to measure binary isotherms by using a mixed stream containing two adsorbable components. However, this method

is not particularly accurate and it requires the use of a model isotherm with only a few constants that are of the correct form to represent the binary isotherm. The viability of this approach has been demonstrated and while it is probably quicker than conventional methods for binary isotherm measurements it still requires many measurements to establish the isotherm. The current situation is that while chromatographic techniques are very useful for Henry constant measurements their use in the determination of isotherms at higher loading and for measurements of separation factors in binary adsorption systems remains quite limited.

1.3 Zeolite Structures

The present study has been focused on the study of the adsorption equilibria on various zeolite adsorbents. Zeolites are crystalline aluminosilicalites which can be found in nature or may be produced synthetically. The basic structural units in zeolites are the SiO_4 or AlO_4 tetrahedra which are joined together in regular structures through shared oxygen atoms. The crystal lattice is sufficiently open to admit molecules and is completely regular. This structural regularity distinguishes the zeolites from other microporous materials such as activated carbon, activated alumina and silica gel. The zeolitic structure can be thought of as an assemblage of polyhedral units which are made of several SiO_4 or AlO_4 tetrahedra. These polyhedra can be represented with an aluminum or silicon atom centered at each apex and with the oxygens centered near the midpoint of each edge. A representation of the units is shown in Figure 1.5. Each aluminum atom introduces a negative charge on the

framework which has to be balanced by an exchangeable cation. These cations are located at energetically preferred sites within the framework. The nature and the location of the exchangeable cations are important in determining the adsorptive properties. The zeolitic structures are also characterized by the Si/Al ratio which cannot be less than 1.0 but may be very large, as in silicalite, which is essentially a pure silica structure. The value of the Si/Al ratio determines the cation density and therefore the affinity of the adsorbent for polar molecules such as water. The transition between hydrophilic and hydrophobic materials occurs for values of the Si/Al ratio between 8 and 10 (Ruthven[3]).

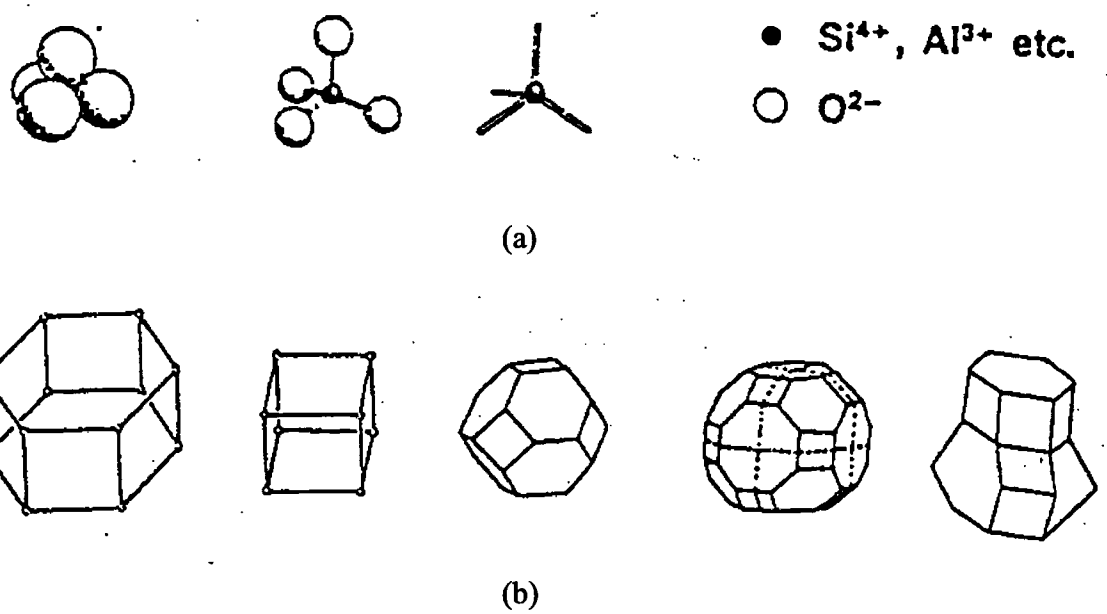

Figure 1.5: (a) Primary Units and (b) Building Polyhedra Occurring in Zeolite Structures

There are about 120 known zeolite frameworks but in this study only types A, X and silicalite were used.

1.3.1 Zeolite A

The structure of zeolite A is shown in Figure 1.6. Eight octahedral units, called sodalite cages, are located at the corners of a 12.3 Å cube and connected through four-membered oxygen rings. This arrangement forms a cage of 11.4 Å free diameter accessible through eight-membered oxygen windows. Each cage has 24 SiO_2 or AlO_2 tetrahedra so that for the ideal structure (Si/Al= 1.0) there are 12 monovalent exchangeable cations. There are three distinct types of cation sites- see Figure 1.6. The strongest sites (site I) are located near the centers of the six-membered oxygen rings- 8 per cage. These have the lowest energy and tend to be preferentially occupied. The next most favorable sites (type II) lie within the eight-membered oxygen window, displaced from the center. Since each window is shared between two cages there are three type II sites per cage. The type III sites have the highest energy and are located within the cage near one of the four-membered oxygen rings.

The 4A zeolite contains 12 Na^+ cations per cage so all the type I and type II sites are occupied with the twelfth cation in site III. Each of the eight-membered windows is therefore obstructed by a Na^+ cation reducing the effective aperture to about 4 Å (4A sieve). If the Na^+ is replaced by K^+ the window is further obstructed by the larger K^+ cation reducing the aperture to about 3 Å (3A sieve). If more than 67%

of the Na^{+} is replaced by Ca^{++} the total number of cations per cell drops to below 8. All cations can then be accommodated in site I so the windows are unobstructed (5A sieve).

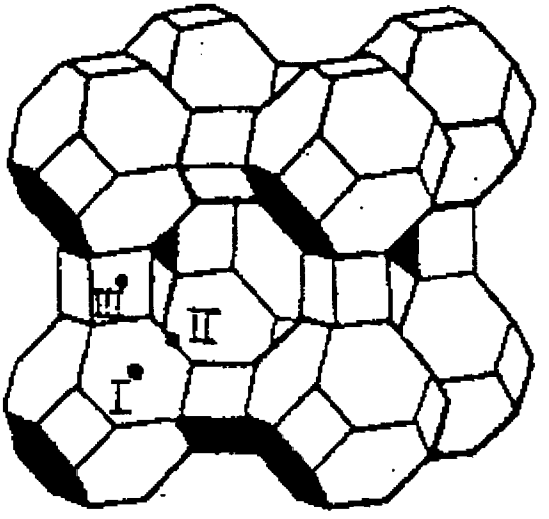

Figure 1.6: Schematic Representation of the Zeolite A Structure Showing the Cation Sites Type and Location

1.3.2 Zeolite X

The structure of zeolite X is shown in Figure 1.7. Like the A structure it is composed of eight sodalite cages each containing 24 SiO_2 or AlO_2 tetrahedra. The sodalite cages are however joined through six-membered oxygen rings in a tetrahedral arrangement. The large cavity or supercage (~11.6 Å in diameter) is accessible through twelve-membered oxygen rings of about 7.5 Å diameter. The Si/Al ratio varies from 1.0 to 1.5 and the number of exchangeable univalent cations

per cage varies correspondingly from 12 to about 7. The location of the sites is also shown in Figure 1.7.

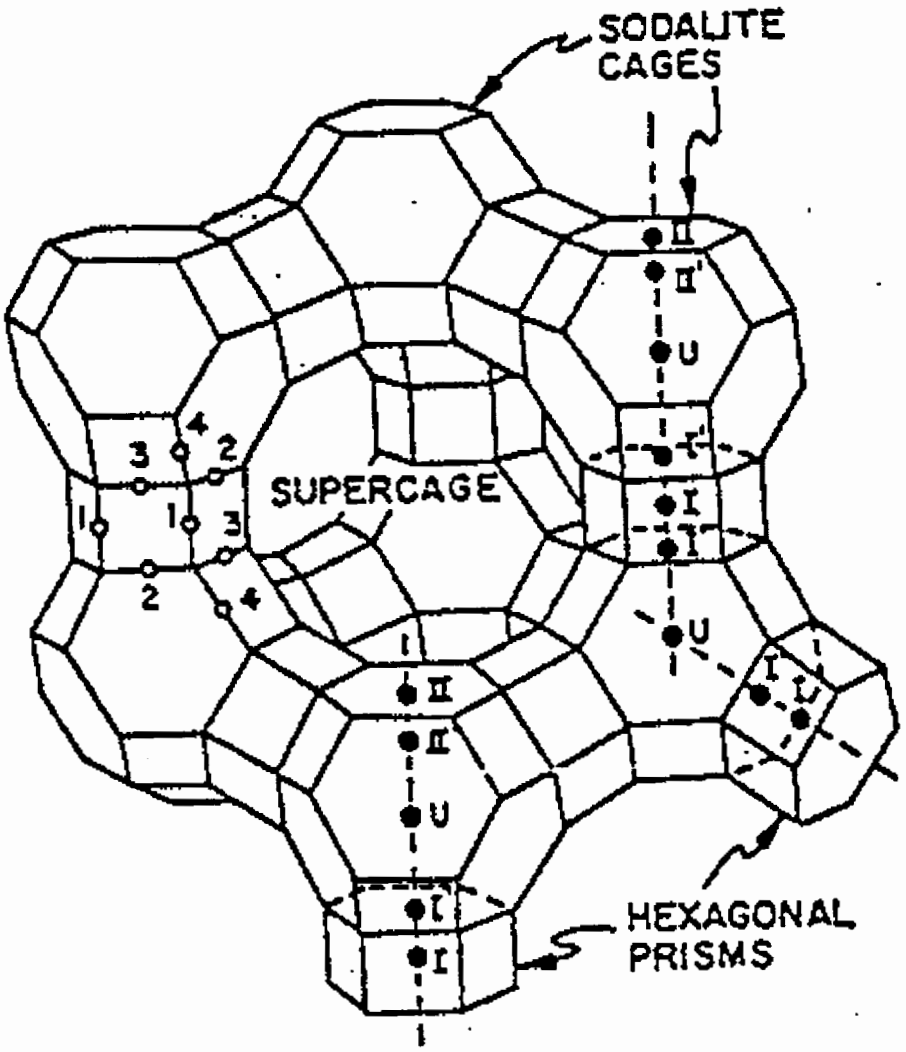

Figure 1.7: Schematic Representation of the Zeolite X (or Y) Structure Showing the Cation Sites Type and Location. The X and Y structures differ only in the Si/Al ratio. Roman numerals denote the different cation sites. Arabic numerals denote different oxygen ions.

The cation distribution in X zeolites is more complicated than for zeolite A and depends on both the nature and number of the cations. Sites I, I' and II are generally the most favorable energetically and so these sites tend to be preferentially occupied. The less favorable type III sites are only occupied when the Si/Al ratio is low and the cation density correspondingly high. A more detailed discussion on cation location in Zeolite X is given in Chapter 4.

1.3.3 Silicalite

Silicalite is a pure silica zeolite analog in which the channel structure (with free diameter approximately 6 Å) are defined by ten-membered oxygen rings. This material is hydrophobic and adsorbs CO_2 much less strongly than aluminum rich zeolites. In this study it was used only as a basis for comparison with the A and X zeolites (Chapter 4) and as a weak adsorbent for water in the calibration of the mass spectrometer (Chapter 6).

1.4 Choice of Sorbate

As a result of their ionic structure zeolite adsorbents are energetically heterogeneous. Polar or quadrupolar molecules (e.g. H_2O, CO_2) interact with the strong electric field in the region of the cations and therefore tend to be adsorbed preferentially at the cation sites. Non-polar sorbates interact much less strongly with the cations and are therefore less sensitive to changes in the nature and distribution of

the cations. CO_2 is useful as a probe molecule since it is adsorbed sufficiently strongly at the cationic sites to make the isotherms sensitive to differences in the nature and distribution of the cations but not so strongly that the isotherm becomes almost irreversible (as is the case for water). The isotherm measurements reported in this thesis were therefore carried out primarily with CO_2 since this allowed not only validation of the experimental technique but also provided useful insights into the way in which the adsorption isotherm is affected by changes in the number and nature of the cations. Measurements were also made with other non-polar species (CH_4, C_3H_8, C_2H_4 etc) to provide a basis of comparison.

1.5 Thesis Outline

The basic theory underlying the ZLC method is summarized in Chapter 2 while the practical realization of the method and the necessary precautions required to obtain reliable results are considered in Chapter 3.

The main experimental results are presented in Chapters 4-6. Chapter 4 deals with the experimental verification of the technique and its application to the measurement of single component equilibrium isotherms. Chapter 5 describes the extension of this method to the measurement of separation factors in binary systems and the coupling of ZLC with temperature programmed desorption (TPD). This approach was used to study the effect of water on the isotherms for CO_2 on several type X zeolites. General conclusions including a review of the advantages and limitations of the ZLC method for isotherm measurements are presented in Chapter 7.

CHAPTER 2

The ZLC Method: Background and Theory

The ZLC technique was originally developed as a simple and versatile way of measuring intracrystalline or intraparticle diffusion in zeolite based adsorbents (Ruthven et al.[6], Ruthven and Brandani[7]). The method depends on exposing a small sample of adsorbent to an adsorbate at known partial pressure in an inert carrier stream and following the desorption when the sample is purged by pure carrier. The column consists of only a few layers of adsorbent and it can be considered as a well mixed cell. Assuming spherical particles (radius R), the system can be described by the following mathematical model:

2.1 Mathematical Model

Fluid phase mass balance

$$V_s \frac{d\bar{q}}{dt} + V_g \frac{dc}{dt} + Fc = 0 \tag{2.1}$$

Solid phase mass balance

$$\frac{\partial q}{\partial t} = D\left(\frac{\partial^2 q}{\partial r^2} + \frac{2}{r}\frac{\partial q}{\partial r}\right) \tag{2.2}$$

Initial conditions

$$q(r,0) = q_0 = Kc_0; \quad c(0) = c_0 \tag{2.3}$$

Boundary conditions

$$\left(\frac{\partial q}{\partial r}\right)_{r=0} = 0; \quad q(R,t) = Kc(t) \tag{2.4}$$

It has been shown that the solution to this set of equations is given by:

$$\frac{c(t)}{c_0} = \sum_{n=1}^{\infty} \frac{2L}{\beta_n^2 + \left(1 - L + \gamma\beta_n^2\right) + L - 1 + \gamma\beta_n^2} exp\left(-\beta_n^2 \frac{D}{R^2} t\right) \tag{2.5}$$

where β_n are the positive roots of:

$$\beta_n \cot \beta_n + L - 1 - \gamma = 0 \tag{2.6}$$

with:

$$L = \frac{1}{3} \frac{F}{KV_s} \frac{R^2}{D}; \quad \gamma = \frac{1}{3} \frac{V_g}{KV_s} \tag{2.7}$$

At high purge flow rates (large values of L) the desorption rate is controlled by the diffusion of the sorbate out of the particle. At low purge flow rate, contact time is large compared with the diffusion time (R^2/D) and the desorption rate is determined

by convection under equilibrium conditions (Brandani and Ruthven[8]). The present study is directed towards equilibrium measurements and the experiments are therefore carried out at low flow rates under condition of equilibrium control.

2.2 Linear Equilibrium

Assuming linear equilibrium, the isotherm is given by:

$$\bar{q} = q^* = Kc \tag{2.8}$$

where $\bar{q}$ represents the average sorbate concentration through a particle and q^* represents the equilibrium value.

In a trace system the flow rate (F) is constant and with the initial condition:

$$t = 0, \quad q = q_0 = Kc_0 \tag{2.9}$$

The integration of Eq.2.1 yields the concentration response curve:

$$\frac{c}{c_0} = exp\left(\frac{-Ft}{KV_s + V_g}\right) \tag{2.10}$$

A plot of $\ln(c/c_0)$ vs. time (or the product Ft) should yield a straight line through the origin with slope $-F/(KV_s+V_g)$ (or $-1/[KV_s+V_g]$). For strongly adsorbed species (K large, $KV_s>>V_g$) and the slope yields directly the value of the dimensionless Henry constant (K). For weakly adsorbed species KV_s is of the same order of magnitude of V_g but the dead volume of the cell can be easily obtained by performing an experiment with no adsorbent in the cell. In this case, a plot of $\ln(c/c_0)$ vs. Ft yields directly the value of V_g.

2.3 Langmuir Equilibrium

Beyond the Henry's Law region the isotherm may be approximated by the Langmuir expression:

$$\frac{q^*}{q_s} = \frac{bc}{1+bc} \tag{2.11}$$

The equilibrium conditions are:

$$\frac{d\bar{q}}{dt} = \frac{dq^*}{dt} = \frac{dq^*}{dc} \cdot \frac{dc}{dt} \tag{2.12}$$

Differentiation of Eq.2.11 yields:

$$\frac{dq^*}{dc} = \frac{bq_s}{(1+bc)^2} = \frac{K}{(1+bc)^2} \tag{2.13}$$

Substituting into Eq.2.1 and integrating from the initial condition $c = c_0$ at $t = 0$

$$\ln\left(\frac{c}{c_0}\right) = \frac{-Ft}{KV_s + Vg} - \frac{KV_s}{KV_s + Vg}\left[\frac{1}{1+bc} - \frac{1}{1+bc_0} + \ln\left(\frac{1+bc_0}{1+bc}\right)\right] \tag{2.14}$$

In the long time region, $c \rightarrow 0$, the plot $\ln(c/c_0)$ vs. Ft approaches a linear asymptote of slope $-1/(KV_s+V_g)$, which represents the linear response, with negative intercept given by $\left[KV_s/(KV_s + V_g)\right] \cdot \left[1 - 1/(1+bc_0) + ln(1+bc_0)\right]$. The Henry constant can therefore be found from the slope of the long time asymptote. However, for highly non-linear systems ($bc_0 >> 1$) this may not be practical as the long time asymptote will be buried in the baseline.

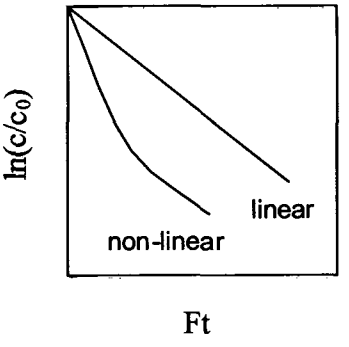

Figure 2.1 Sketch Showing Qualitative Linear and Non-Linear Behavior for a ZLC Response Curve

Eqs.2.10 and 2.14 show that under equilibrium control the response curve should be independent of flow rate, depending only on the product Ft which represents the total volume of purge gas. Conformity between the response curves measured at different flow rates thus provides a simple experimental test of the equilibrium assumption.

2.4 Calculation of the Complete Isotherm

Implicit in the derivation of Eqs.2.10 and 2.14 is the assumption that the flow rate remains constant. This is a valid approximation for a trace system (small mole fraction of sorbate in the carrier stream) but to extend the analysis to higher sorbate concentration it is necessary to allow for the variation of the effluent flow rate as desorption proceeds. Eq.2.1 may be re-written in the more general form:

$$FC\frac{y}{1-y} = -V_s\frac{dq^*}{dt} - V_gC\frac{dy}{dt} \tag{2.15}$$

where y represents the mole fraction of sorbate in the effluent gas stream. At $t = 0$, $y = y_0$ and $q^* = q_0^*$. Integration of Eq.2.15 yields:

$$q^* = q_0^* - \frac{V_gC}{V_s}\cdot(y - y_0) - \frac{FC}{V_s}\cdot\int_0^t \frac{y}{1-y}dt \tag{2.16}$$

For $t = \infty$, $y = 0$ and $q^* = 0$ and q_0^* can be then calculated from Eq.2.17:

$$q_0^* = -\frac{V_g C}{V_s} \cdot y_0 + \frac{FC}{V_s} \cdot \int_0^{\infty} \frac{y}{1-y} dt \tag{2.17}$$

which represents the adsorbed phase concentration at equilibrium with concentration c_0 in the gas phase. Substituting Eq.2.17 in 2.16 yields:

$$q^* = \frac{FC}{V_s} \cdot \int_0^{\infty} \frac{y}{1-y} dt - \frac{FC}{V_s} \cdot \int_0^{t} \frac{y}{1-y} dt - \frac{V_g C}{V_s} \cdot y \tag{2.18}$$

To evaluate the first integral complete desorption of the sample is required. This can present a practical problem for strongly adsorbed species since, when K is large, the slope of the long time asymptote (Eq.2.14) is very small. The desorption curve then has a long tail which may be difficult to distinguish from the baseline. The completeness of desorption can, however, be easily checked experimentally simply by increasing the temperature to carry out a thermal desorption at the end of the run. If no significant TPD peak is observed the isothermal desorption process must have been essentially complete.

2.5 Extension of the ZLC Method to Binary Systems

In a binary ZLC experiment the adsorbent sample is pre-equilibrated with a gas stream containing the two adsorbable species (components A and B) in an inert (He) carrier and then desorbed by switching, at time zero, to a pure He purge, monitoring the mole fractions of both components in the effluent stream. As with the single component measurements the purge flow rate must be sufficiently low that the effluent stream is essentially at equilibrium with the adsorbed phase. Varying the purge rate provides a simple experimental test for this condition since, under conditions of equilibrium control, the desorption curve, when plotted against the volume of the effluent gas, should be independent of flow rate. For component A, the differential mass balance for the ZLC cell then becomes:

$$V_s \frac{dq_A^*}{dt} + V_g C \frac{dy_A}{dt} + \frac{FCy_A}{1 - y_A - y_B} = 0 \tag{2.19}$$

At $t = 0$, $y_A = y_{A0}$ and $q_A^* = q_{A0}^*$. Integration of Eq.2.19 yields:

$$q_A^* = q_{A0}^* - \frac{V_g C}{V_s} \cdot (y_A - y_{A0}) - \frac{FC}{V_s} \cdot \int_0^t \frac{y_A}{1 - y_A - y_B} dt \tag{2.20}$$

the adsorbed phase concentration q^*_{A0} at equilibrium with concentration $c_{A0}\,(y_{A0}\cdot C)$ in the gas phase can be evaluated from Eq.2.20 by substituting for $t=\infty$, $y_A=0$ and $q^*_A=0$:

$$q^*_{A0}=\frac{FC}{V_s}\cdot\int_0^\infty\frac{y_A}{1-y_A-y_B}dt-\frac{V_gC}{V_s}\cdot y_{A0} \tag{2.21}$$

Substituting in Eq.2.20 yields:

$$q^*_A=\frac{FC}{V_s}\cdot\int_t^\infty\frac{y_A}{1-y_A-y_B}dt-\frac{V_gC}{V_s}\cdot y_A \tag{2.22}$$

similar expressions may be derived for component B. The experimental desorption curves thus yield $q^*_A(t)$ and $q^*_B(t)$ as functions of the partial pressures $p_A(t)$ and $p_B(t)$, from which the separation factor α may be calculated as a function of time:

$$\alpha\equiv\left(q^*_A/p_A\right)/\left(q^*_B/p_B\right) \tag{2.23}$$

In the low loading limit the separation factor should approach the ratio of the Henry constants for the two components (K_A/K_B).

The complete binary isotherm can be thought of as a surface showing the variation of α as a function of p_A and p_B together with a second surface showing the variation of total loading in the same coordinates (p_A and p_B). The ZLC desorption curve yields a section through these surfaces, starting at the initial equilibration point (q_{Ao}, q_{Bo}, p_{Ao}, p_{Bo}) and ending at the zero loading point (the origin). However, the path followed is generally not a simple rectilinear section since the composition of the adsorbed phase changes continuously as the loading decreases. The less strongly adsorbed species desorbs preferentially in the initial region leaving an adsorbed phase that, in the long-time region, consists almost entirely of the more strongly held species. When the affinities of the two sorbates are very different the desorption actually occurs in two distinct stages, with the weaker component being removed initially with very little change in the loading of the strong component which then desorbs, as if from a single component system, during the later stages of the process. To represent the information concerning the variation of separation factor derived from a single experiment it is therefore necessary to consider both the variation in separation factor with loading and the associated variation in the composition of the adsorbed phase along the desorption path.

CHAPTER 3

The ZLC Method: Practical Implementation

In this chapter the general experimental issues related to a simple ZLC experiment such as the experimental set-up (sec.3.1), preparation of feed mixture and equilibration time (sec.3.2), acquisition and data processing (sec.3.3), dead volume and choice of detector (sec.3.4), drying of gas streams and regeneration temperature (sec.3.5), are discussed.

The particular experimental procedures required in the study of binary systems and the study of effects of traces of water on CO_2 isotherms are discussed in chapters 5 and 6.

3.1 Experimental Set-Up

The experimental set-up was subject to several modifications during the project resulting from changes in the experimental requirements (for example extending the studies to binary systems) or by feedback derived from analysis of the preliminary experimental results. This highlighted the need to incorporate molecular sieve dryers in the gas streams. Fig.3.1 shows a simplified schematic diagram of the most recent "version" of the system.

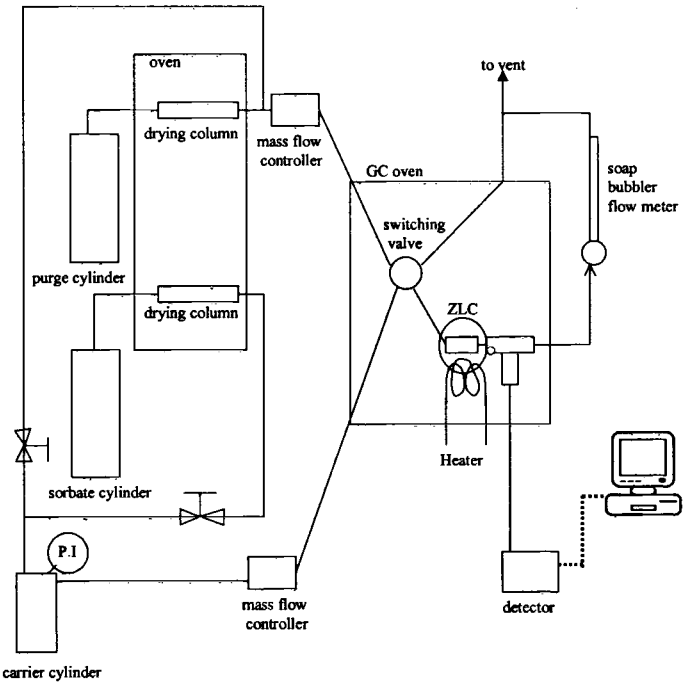

Figure 3.1: Zero Length Column (ZLC) Experimental Set-Up

The ZLC cell consists of a small sample of zeolite adsorbent (1-6 mg) sandwiched between two sintered discs and contained within a 1/8" Swagelok® fitting. The switch valve is a standard high temperature *Valco* valve, operable up to 250-300°C. A small electric heater with its own temperature control surrounds the ZLC cell thus allowing the adsorbent to be regenerated *in situ* at temperatures up to 400°C without exposing the valve to these temperatures. The detector is an on-line quadrupole mass spectrometer (Ametek Dycor™ Quadrupole Gas Analalyzer Model No. MA200HDEF with a Balzers turbomolecular pump). The gas leaving the cell is sampled continuously through a silica capillary connected to the chamber of the mass spectrometer. The ZLC cell and the switch valve are placed in a gas chromatograph oven (Varian Vista series 6000). This allowed the use of a thermal conductivity

detector (TCD) when the turbomolecular pump had to be replaced. The mass spectrometer is essential for self-diffusion or multi-component system studies but for single component systems the TCD is quite satisfactory. The effluent concentration response curves are recorded in digital form for data processing. The flow rates of both feed and purge streams are controlled by mass flow controllers (Matheson model 8270 equipped with mass flow transducers model 8272-0411).

3.2 Experimental Procedures

The ZLC column consists of a 1/8" Swagelock® union. A 1/8" nickel sinter disk is placed on one end of the union and made seal by tightening with a piece of tubing and a nut. Then the sample, previously weighed with an electronic scale (Sartorious model AC210P), is placed on the sinter disk, on the external side of the union, and a second disk is added to complete the cell. The result is a few layers of adsorbent material sandwiched in between the two sinter disks. If the amount of adsorbent required is greater than about 3 mg, the zeolite is introduced directly within the union. In this case the second sinter disk is used to close the remaining open end of the union.

The feed was pre-mixed by using the carrier tank. To measure the amount of gas introduced into the tank a pressure indicator was used. The procedure followed was to first introduce partially the inert, then add the desired amount of sorbate, finally filling the tank with He to the desired pressure. When the sorbate had to be changed the carrier tank was filled several times with He and flushed by using a

vacuum pump (SpeediVac E.B.3 Vacuum Pump & Compressor No.1045) connected to the tank. The sample of adsorbent material is then equilibrated with the carrier stream. The time of equilibration depends on the value of the Henry constant for the system studied. For weakly adsorbed species a few minutes is sufficient but for strongly adsorbed species at low concentrations longer times are required to provide a sufficient supply of sorbate to fully equilibrate the sample. For consistency, replicate runs at different equilibration time should be performed. Following the equilibration step the run is started by switching, at time zero, to a pure He purge. The concentration of the adsorbable species in the effluent stream is then followed continuously for a sufficiently long period to ensure complete desorption of the sample.

3.3 Data Collection and Analysis

The Dycor gas analyzer is equipped with an RS-232 interface, to convert analog signal into digital, connected with a PC on which is installed software (MOTF) for data acquisition. The analog signal from the TCD was connected to a PC equipped with a card for converting the analog signal into digital form. When using the TCD as the detector Vissim was used as the software for data acquisition.

For ZLC experiments, the concentration of the sorbates in the gas stream is relatively low (3-6% vol is the initial concentration). The response of the detectors then, with reasonable accuracy, can be considered linear and directly proportional to the concentration of the sorbate in the effluent stream. This was confirmed in

preliminary studies. The analysis of ZLC data requires the response curves normalized relative to the initial concentration. Calibration of the detector is therefore not required.

The experimental response was normalized by using the following equation:

$$\frac{c(t)}{c_0} = \frac{\sigma(t) - \sigma_{inf}}{\sigma_0 - \sigma_{inf}} \tag{3.1}$$

As shown in figure 3.2, σ_0 is the value of the signal at time zero and σ_{inf} is the value of the signal when the desorption is completed.

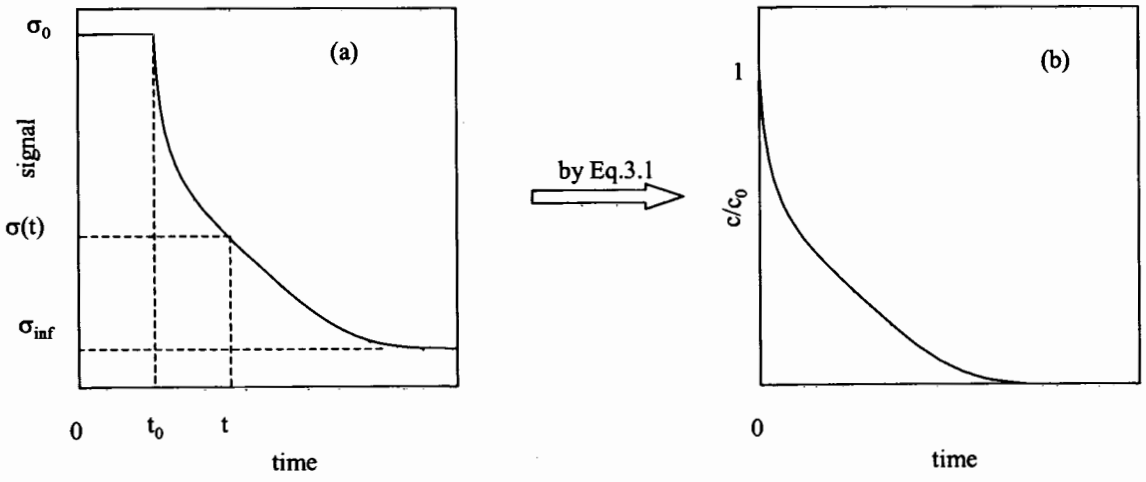

Figure 3.2: Qualitative (a) "Raw" ZLC Response and (b) Corresponding Normalized Response Curve

In order to clearly evaluate σ_0 the data acquisition is started t_0 seconds before switching to a pure He purge. Consequently, the time scale from the data acquisition has to be shifted back by t_0 seconds.

3.4 Dead Volume Determination

In Chapter 2 when analyzing Eq.2.10, it was pointed out that for weakly adsorbed species the determination of the dead volume V_g is important. Here the problem is discussed more quantitatively. The dead volume in the ZLC system represents the sum of the volume of the cell and the volume of the piping between the switching valve and the detector. V_g is determined by performing a ZLC experiment with no adsorbent in the cell. In Figure 3.3 representative experimental blank response curves are shown. The response curves, plotted against the product Ft are clearly independent of flow rate or the nature of the sorbate and show the expected experimental decay, in conformity with Eq.2.10. Four CH_4 runs at different initial sorbate concentrations were performed. The responses show no significant differences thus validating the assumption of linearity of the response of the mass spectrometer with concentration. The dead volume derived from the slope is about 0.15-0.16 ml. Since in a ZLC experiment the volume of the adsorbent in the cell is of the order $1-5\times10^{-3}$ ml, for values of the Henry constant less than 100 the product KV_s is of the same order of magnitude of V_g.

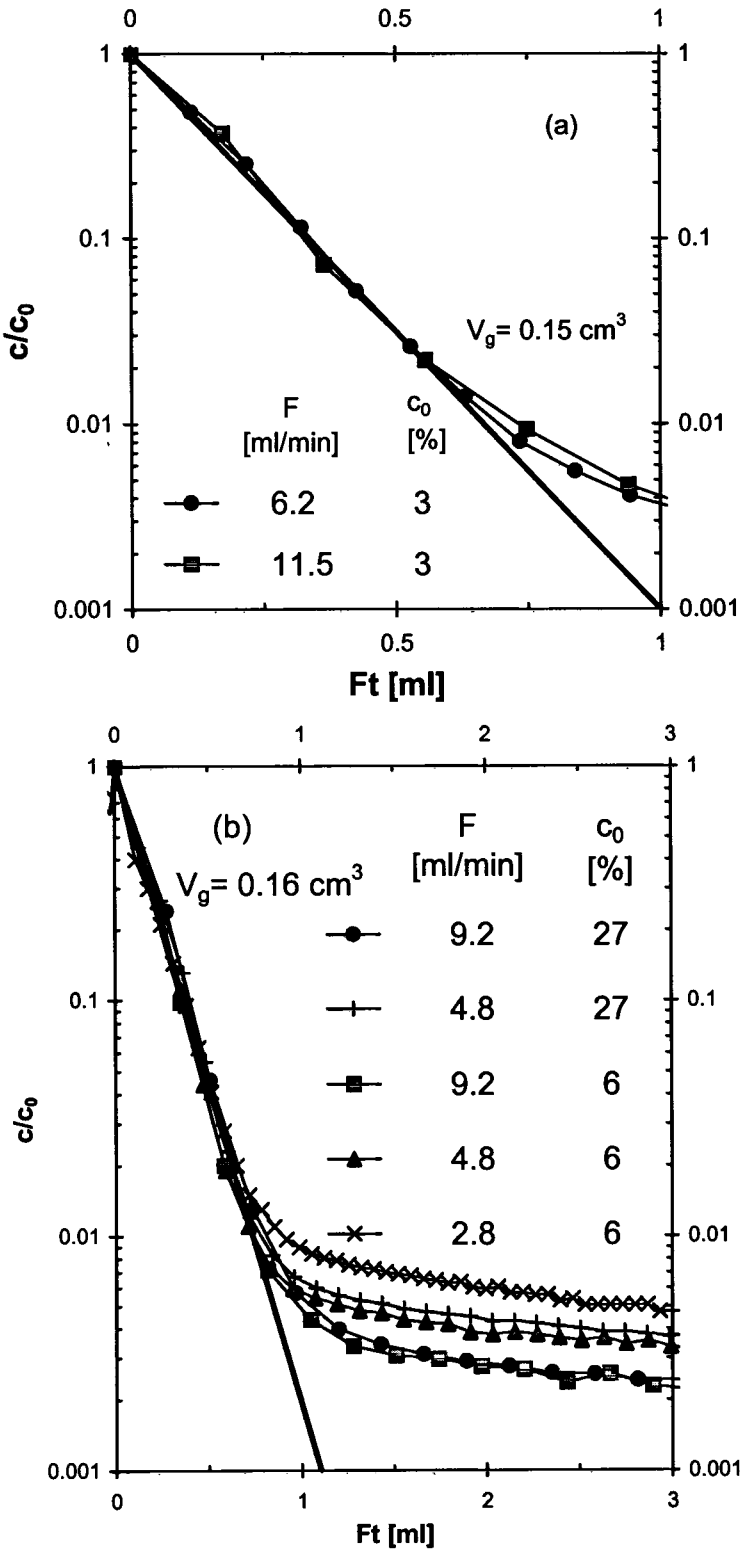

Figure 3.3: ZLC Blank Response for (a) CO_2 and (b) CH_4 Plotted Against Ft.

For gas analysis, an on-line mass spectrometer was chosen. This offers a better sensitivity compared with a TCD and it is also required for binary systems. Nonetheless, some of the preliminary studies had to be carried out using a TCD as a detector because the turbomolecular pump broke down and had to be replaced, which took some time. To ensure consistent results, the system CO_2-silicalite was studied by using both detectors. Figure 3.4a shows response curves plotted against Ft and Figure 3.4b shows a vant Hoff plot showing temperature dependence of the dimensionless Henry constant for this system. It can be seen that there is no significant difference in the response measured using the two different detectors.

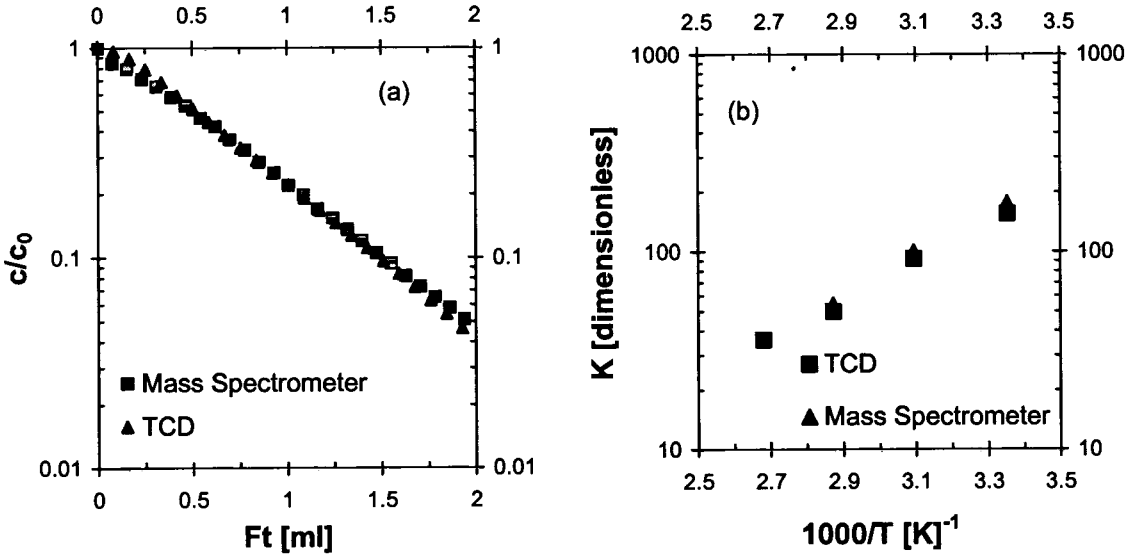

Figure 3.4: (a) Response Curves and (b) Vant Hoff Plot for CO_2-Silicalite Using Different Detectors

3.5 Elimination of Traces of Water Vapor

Preliminary experiments on hydrophilic adsorbents quickly revealed that it is important to pay careful attention to dehydration of both feed and purge streams as well as to the regeneration of the adsorbent. Various arrangements for drying the gases were tried but the system that worked best utilized individual drying columns, 8" long and 3/8" O.D., packed with 5A zeolite in each of the gas lines. These columns were contained in a separate oven which allowed regeneration at up to 400°C. During operation the drying columns were immersed in ice to enhance their affinity for water vapor. A limited series of experiments using dry ice showed no significant difference. It was concluded that, with well regenerated drying columns, operation at 0°C is sufficient to ensure satisfactory dehydration of the gas stream.

Another important issue was the regeneration temperature of the sample in the ZLC cell. Molecular sieve adsorbents retain water very strongly so a high regeneration temperature (~400°C) is necessary to eliminate any residual water. The original configuration allowed regeneration only at temperatures up to 250°C since the switch valve was rated for 250°C-300°C (regeneration at 275°C had no significant effects). For this reason, the ZLC cell was placed in a brass tube surrounded by a heater (Omegalux M2181/0395 Band Heater). With this arrangement the sample could be regenerated in situ at a temperature of 400°C.

Finally, all the connections in the system were periodically inspected for leakage. The most effective procedure was to pressurize the system and to check the fittings with a solution of water and soap.

CHAPTER 4

The ZLC Method: Single Component Systems

The project was focused on studying the characteristics of adsorption on zeolite based adsorbent material of industrial interest in separation processes. Details of the zeolite based adsorbent materials are given in Table 4.1. These zeolites, being of cationic form, have strong intracrystalline electric fields, the strength of which depends on the Si/Al ratio and on the nature of the exchangeable cations. It was decided to use CO_2 as a probe molecule since CO_2 has a strong quadrupole moment making its adsorption sensitive to the strength (or more correctly the gradient) of the electric field. Because of their sensitivity to the electric field gradient the CO_2 isotherm provide information concerning the number and strength of the cation adsorption sites. Other gas molecules that were studied include N_2, CO and various hydrocarbon gases.

Table 4.1: Zeolite Adsorbents used in this Study

Zeolite	Si/Al	cationic form	cations/supercage	(molecules/cage)/(mmole/g)
Silicalite	>1000	-	-	-
LiLSX*	1.0	Li^+	12	1.8
NaLSX*	1.0	Na^+	12	2.0
NaX*	1.25	Na^+	10.6	1.95
CaX	1.25	Ca^{++}	5.3	1.65
CaA	1.0	Ca^{++}	6	1.68

* Containing about clay 18% binder.
Other samples are binderless. All samples are fully cation exchanged.

4.1 Linear Sytems/Henry Constants

Representative response curves showing plots of ln (c/c_o) vs t and Ft are shown in Figures 4.1 and 4.2. In conformity with Eq.2.10, the response curves plotted vs. Ft are essentially linear and independent of flow rate, thus confirming both the validity of the equilibrium approximation and the linearity of the isotherms. The small curvature in the initial region probably arises from uncertainty in the zero time resulting from the small delay in the gas sampling system.

Measurements were made for several different systems over a range of temperature. Examples of the vant Hoff plots showing the temperature dependence of the dimensionless Henry constant are shown in Figures 4.3-4.5. The resulting parameters, calculated from the vant Hoff expression:

$$K = K_0 \exp(-\Delta U_0 / RT) \tag{4.1}$$

are summarized in Table 4.2.

The ZLC Henry constants for CO_2 – silicalite (Figure 4.3) are generally consistent with although slightly higher than the gravimetric data reported by Graham et al.[9]. The ZLC data for N_2-5A (Figure 4.4) are also broadly consistent with, although slightly higher than, previously reported data for this system and agree well with the values derived from the equilibrium isotherms measured on samples of the same zeolite in the Air Products Laboratory.

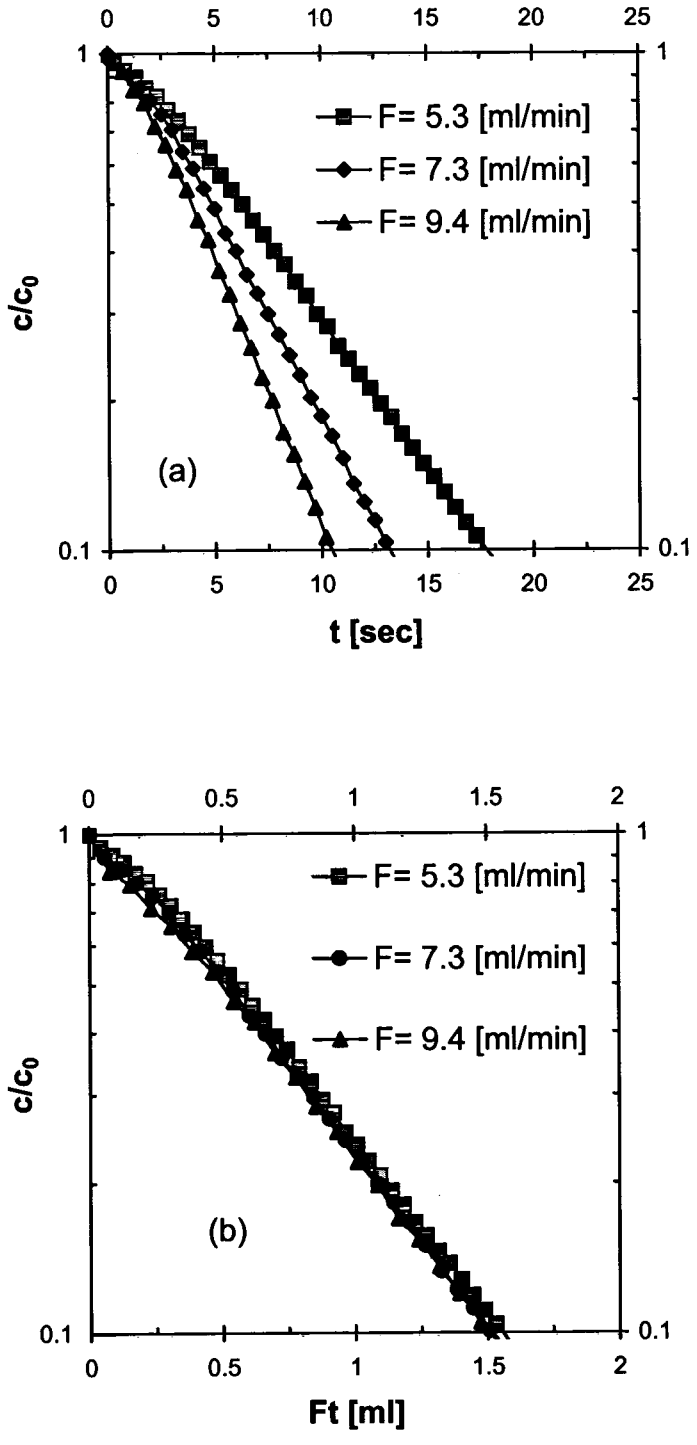

Figure 4.1: ZLC Response Curves for CO_2-Silicalite at 25°C Plotted Against (a) t and (b) Ft.

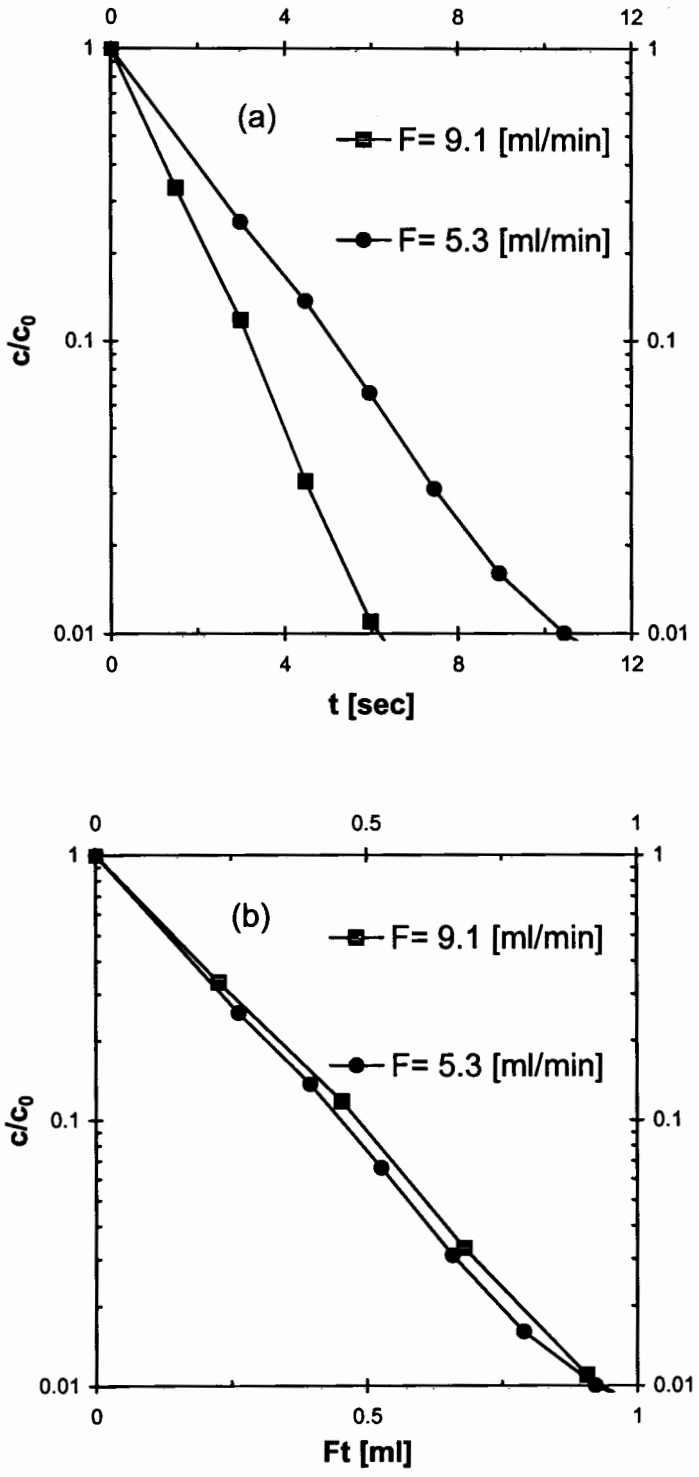

Figure 4.2: ZLC Response Curves for CH_4-NaLSX at 0°C Plotted Against (a) t and (b) Ft

Table 4.2: Summary of Vant Hoff Constants Giving Temperature Dependence of Henry Constants According to Eq.4.1

Sorbate	Sorbate	Temp. Range (K)	$K_o x 10^3$ (dimensionless)	$-\Delta U_o$ (kJ/mole)
CO_2	Silicalite	298-373	59.2	19.8
	Graham et al[10]	273-343	33.0	20.4
	CaA	323-448	10.4	38.4
	CaA-Air Products	348-448	7.0	40.4
	5A-Haq[11]	420-465	6.5	32.8
	CaX	323-423	0.6	50.5
	NaX	312-398	1.2	40.6
	NaLSX	293-423	2.4	39.9
	LiLSX	308-448	0.5	48.6
N_2	5A[11]	293-360	4.6	20
	5A[12]	200-300	4.4	18.8
	CaA-Air Products	263-303	2.2	23.8
CO	CaX	308-398	0.1	40.9
CH_4	NaX	195-273	0.1	26.0

The strong effect of traces of water is evident from the CO_2-CaA data shown in Figure 4.5. Early ZLC measurements yielded Henry constants slightly larger than the values derived from the chromatographic measurements of Haq and Ruthven[10]. However careful measurements carried out in the Air Products laboratory (by the volumetric/piezometric method) yielded substantially higher K values which were replicated by the ZLC data only after the incorporation of drying columns (at 0°C) in the purge and feed streams and provision for *in situ* regeneration of the adsorbent at elevated temperature (see section 3.5). The good agreement finally achieved provides convincing evidence of the validity of the ZLC approach.

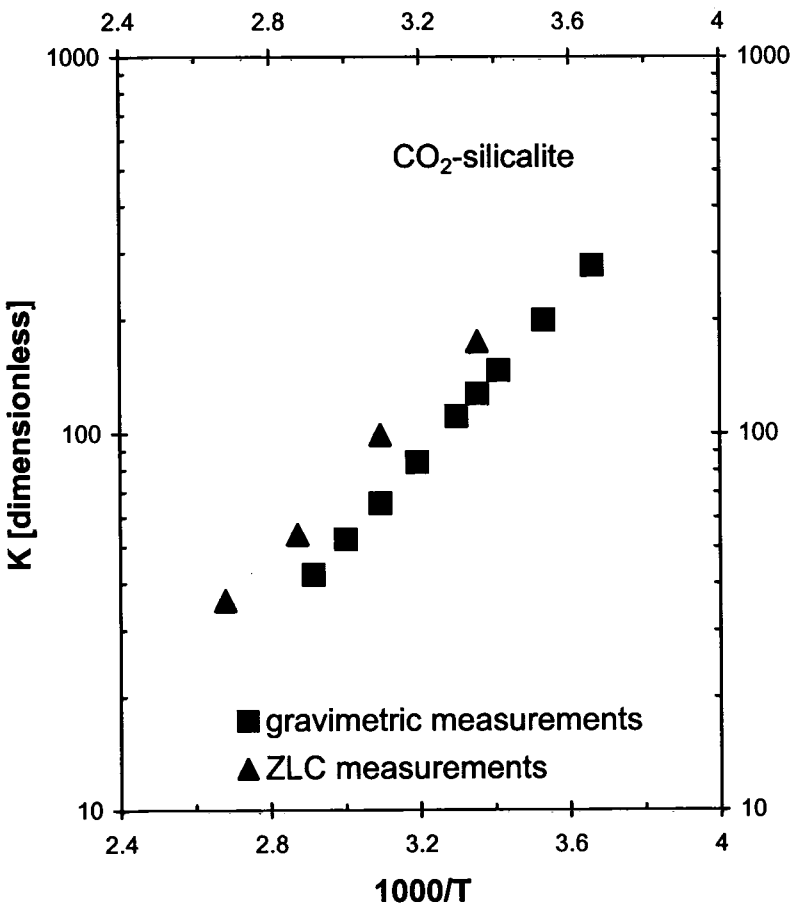

Figure 4.3: Vant Hoff Plot Showing Temperature Dependence of Henry Constants for CO_2-Silicalite

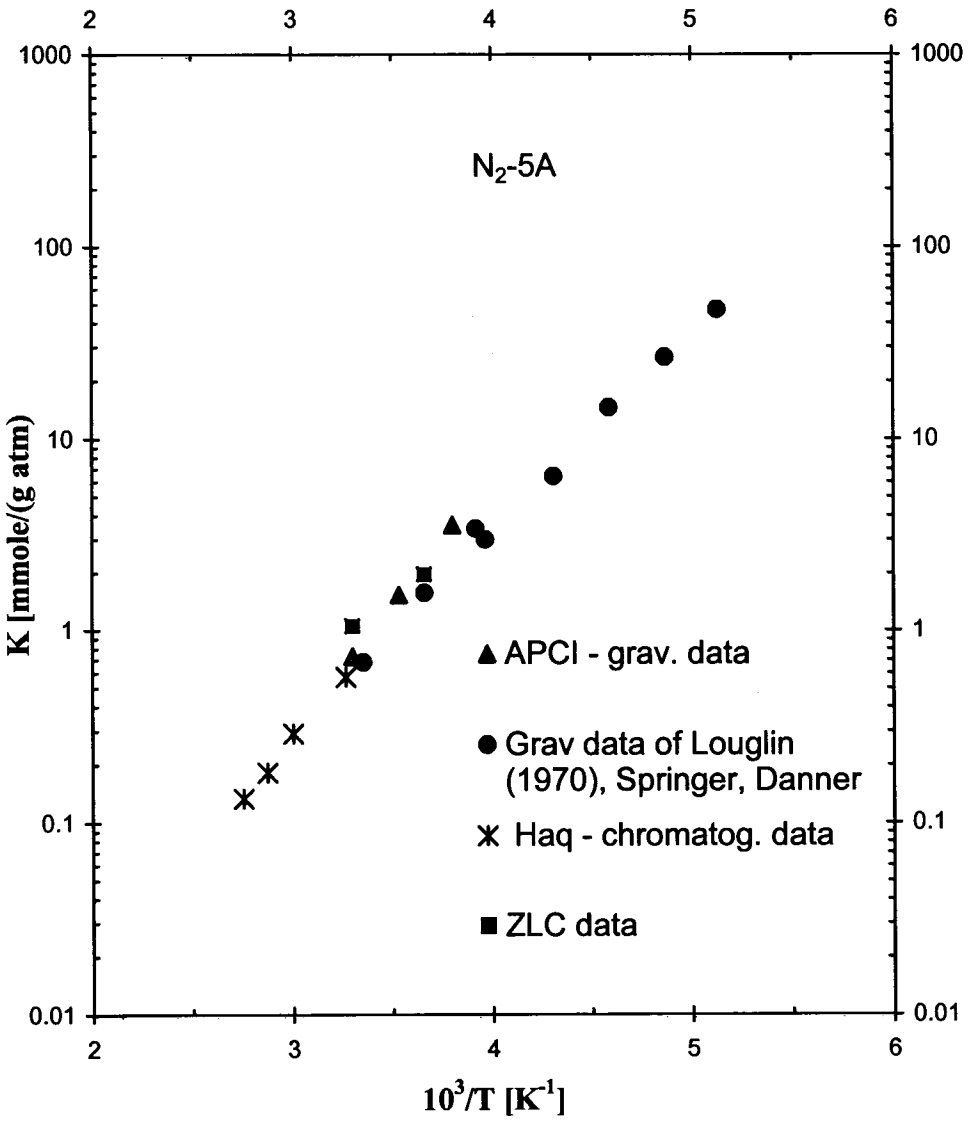

Figure 4.4: Vant Hoff Plot Showing Temperature Dependence of Henry Constants for N_2-5A

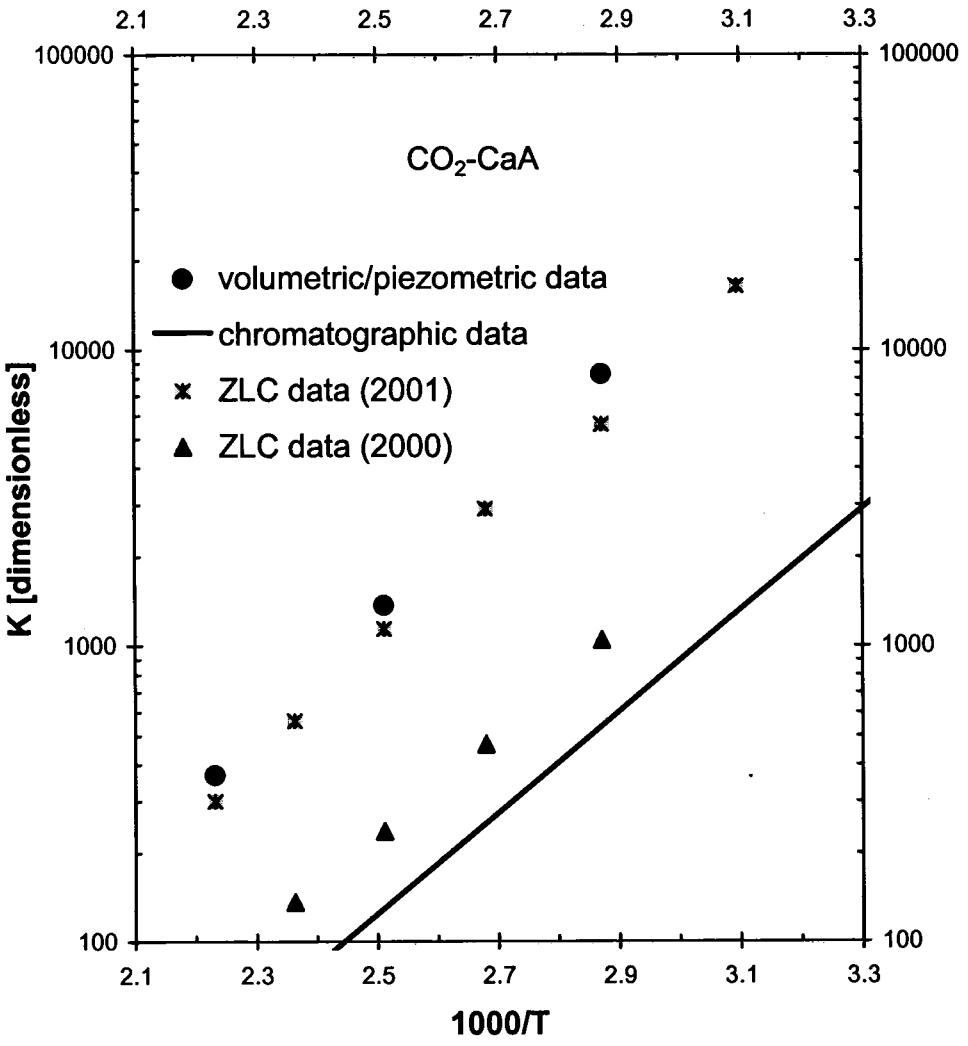

Figure 4.5: Vant Hoff Plot Showing Temperature Dependence of Henry Constants for CO_2-CaA. 2001 Data Obtained with On-Line Drying Columns.

The vant Hoff plots for CH_4, CO and CO_2 on various different forms of zeolite X are shown in Figures 4.6-4.8; the derived parameters are included in Table 4.2. The ΔU_o values for CO_2 in A and X zeolites show clearly how the difference in the strength of the most favorable adsorption sites depends on the nature of the cation. The sequence, for the X zeolites, correlates well with structural data relating to cation

positions, as shown in Table 4.3. However, the large difference in ΔU_o between CaX and CaA seems surprising since the cation sites (type II) in both the materials are similar. It can be seen that the adsorption energies in these (cationic) zeolites are all substantially greater than for silicalite (non-polar) thus providing convincing evidence of the importance of electrostatic forces in these systems.

Table 4.3: Variation of Limiting Adsorption Energies for CO_2 at Low Loading Levels in Different Cationic Forms of Zeolite X

Material	$-\Delta U_o$ (kJ/mole)	Dominant Site
CaX	50.5	Ca^{++} in site II
LiLSX	48.6	Li^{+} in site III
NaX	40.6	Na^{+} in site IIi
NaLSX	39.9	Na^{+} in site III
Silicalite[18]	20.0	Framework

From Figure 4.6 it is clear that the Henry constants and adsorption energies for methane on NaX and NaLSX are almost identical. Since methane is non polar and has a rather small polarizability the adsorption is dominated by the van der Waals interaction with the framework; the cations have very little effect. Since NaX and NaLSX have the same framework and differ only in the occupancy level of the cation sites the similarity in their adsorption behavior is understandable.

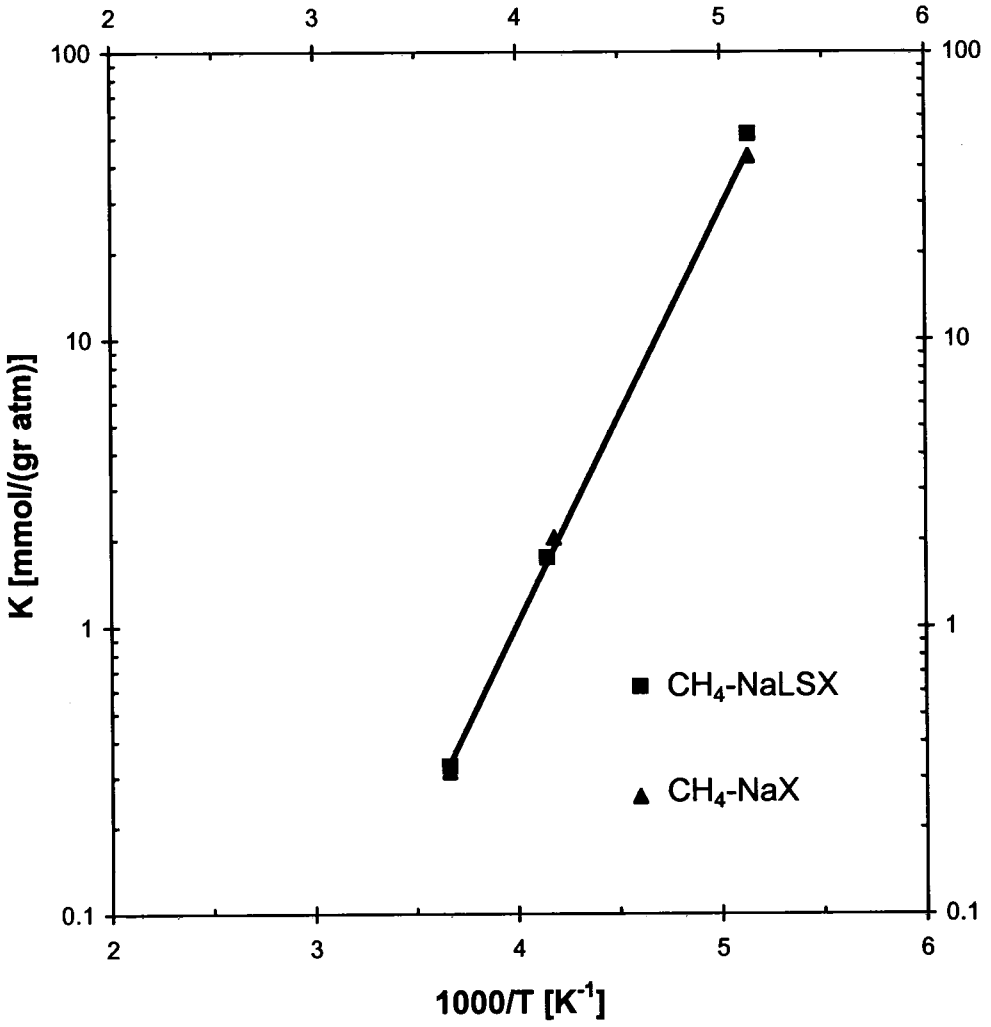

Figure 4.6: Vant Hoff Plot Showing Temperature Dependence of Henry Constants for CH_4-NaX and CH_4-NaLSX

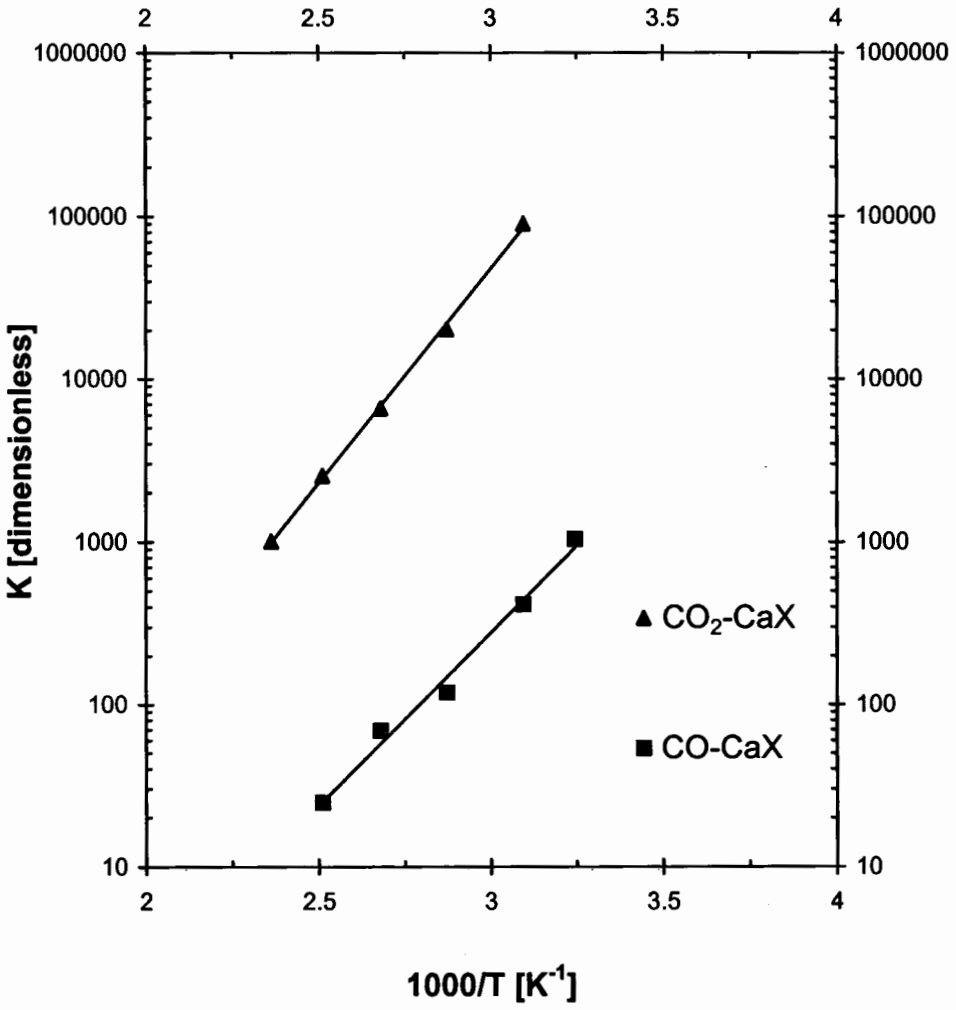

Figure 4.7: Vant Hoff Plot Showing Temperature Dependence of Henry Constants for CO_2-CaX and for CO-CaX.

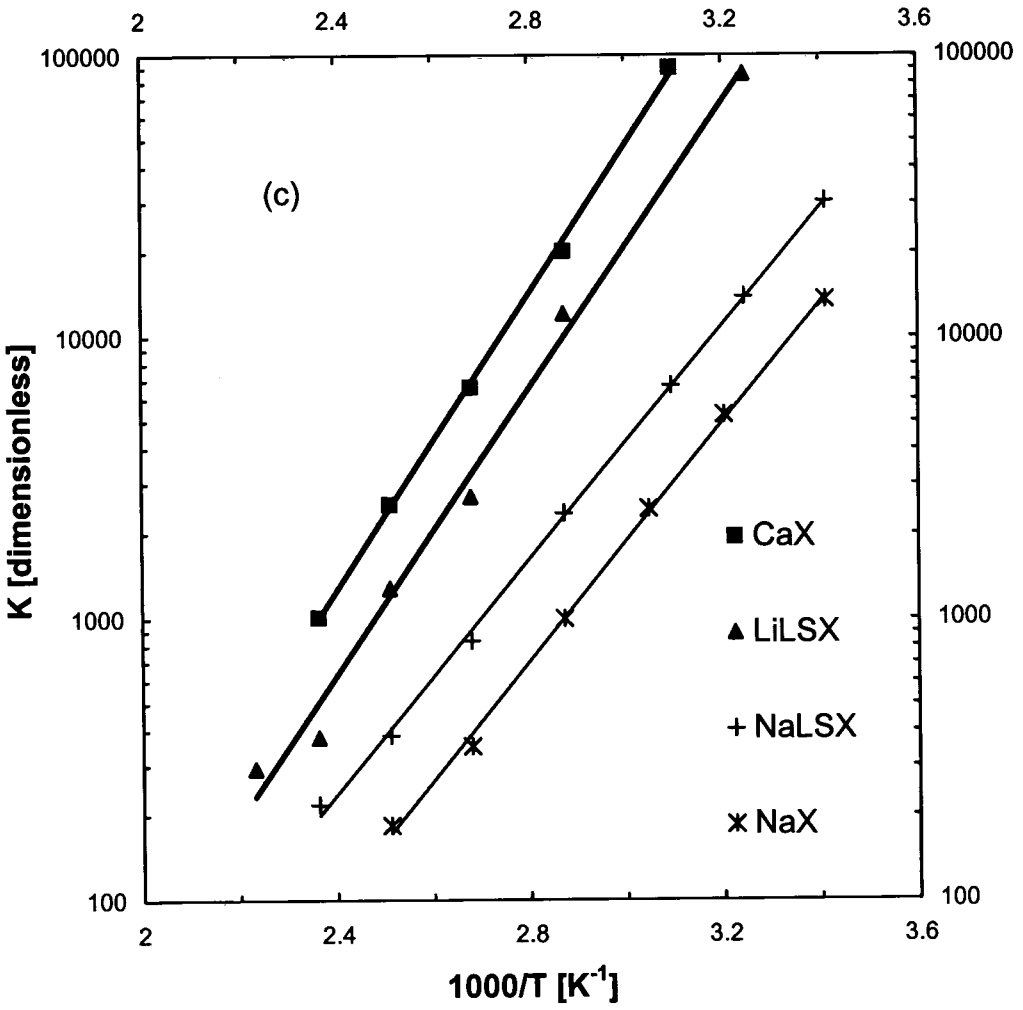

Figure 4.8: Vant Hoff Plot Showing Temperature Dependence of Henry Constants for CO_2 on X Type Zeolites.

4.2 Non-Linear Systems

As an example of the behavior of a non-linear system Figure 4.9 shows the response curves for CO_2-CaX at 75°C at three different partial pressures of CO_2. The response curves, plotted in terms of Ft, are independent of flow rate showing that, in all cases, the equilibrium assumption is a valid approximation. All the response curves can be adequately represented by Eq.2.14 with a single pair of Langmuir constants (q_s=0.91 mmole/g, b= 17 atm^{-1}). These runs were carried out early in the study with an incompletely dehydrated adsorbent. As a result the Langmuir parameters are somewhat different from the values obtained later for the CO_2-CaX system under dry conditions (q_s= 1.4 mmole/g, b≅ 320 atm^{-1}).

4.3 Complete Isotherm Determination

Figures 4.10 (a-c) show examples of the complete isotherms for CO_2 on CaA and on NaLSX calculated by integration of the ZLC response curves. For these systems the isotherms were also measured by the piezometric/volumetric method, using the same adsorbent samples, at the Air Products Laboratory. In all cases the ZLC isotherms lie close to the piezometric/volumetric data, thus confirming the validity of the ZLC approach. For CO_2-NaLSX the recently reported experimental data of Siperstein and Myers[11] and Shen et al.[12] are also shown. The Shen and Siperstein isotherms are close to both the ZLC and the Air Products data suggesting

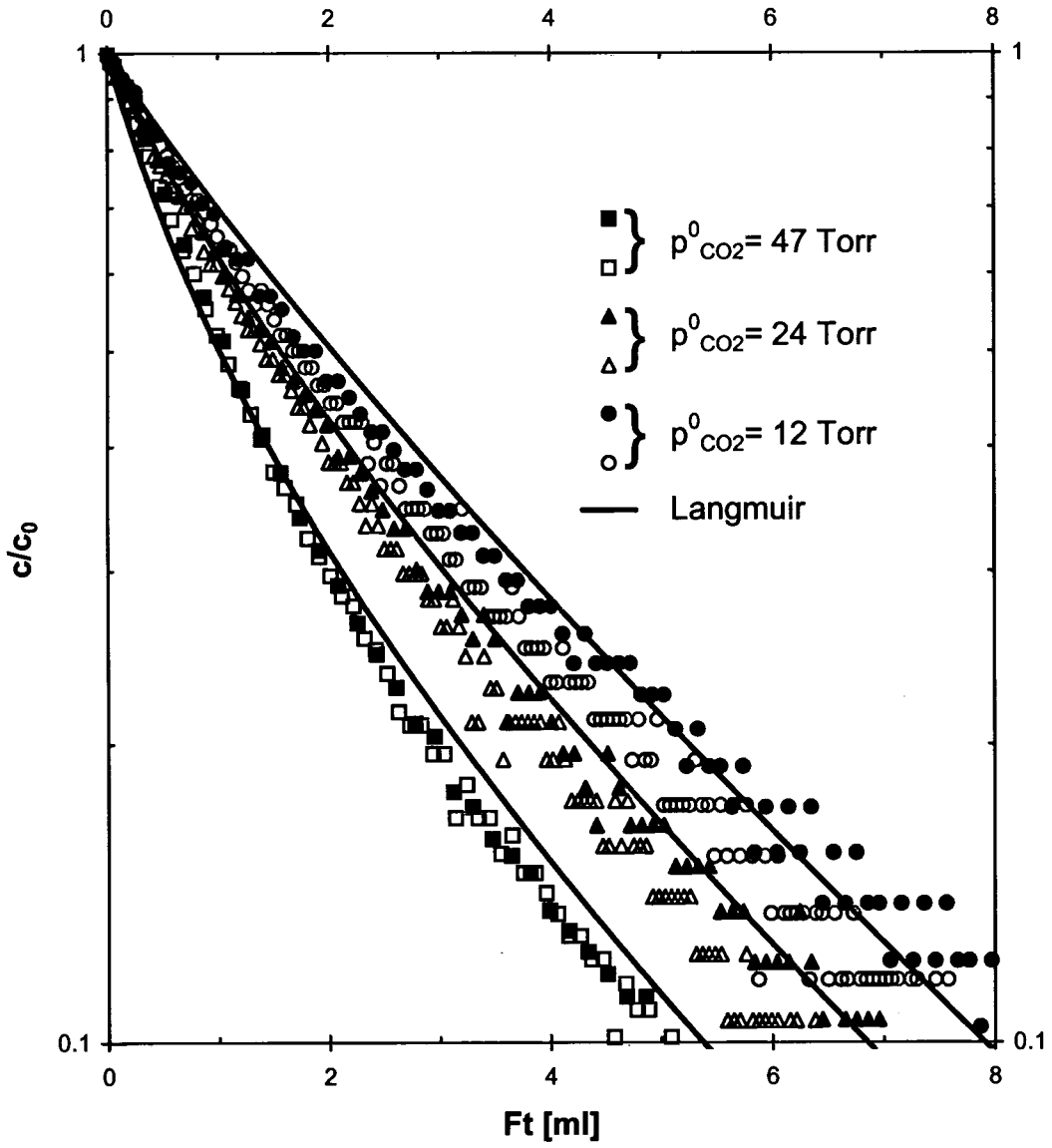

Figure 4.9: ZLC Response Curves for CO_2-CaX at 75°C Plotted Against Ft, Showing Comparison with Values Predicted by Langmuir Model. Filled and Open Symbols Represent Runs Carried Out at Different Purge Flow Rates.

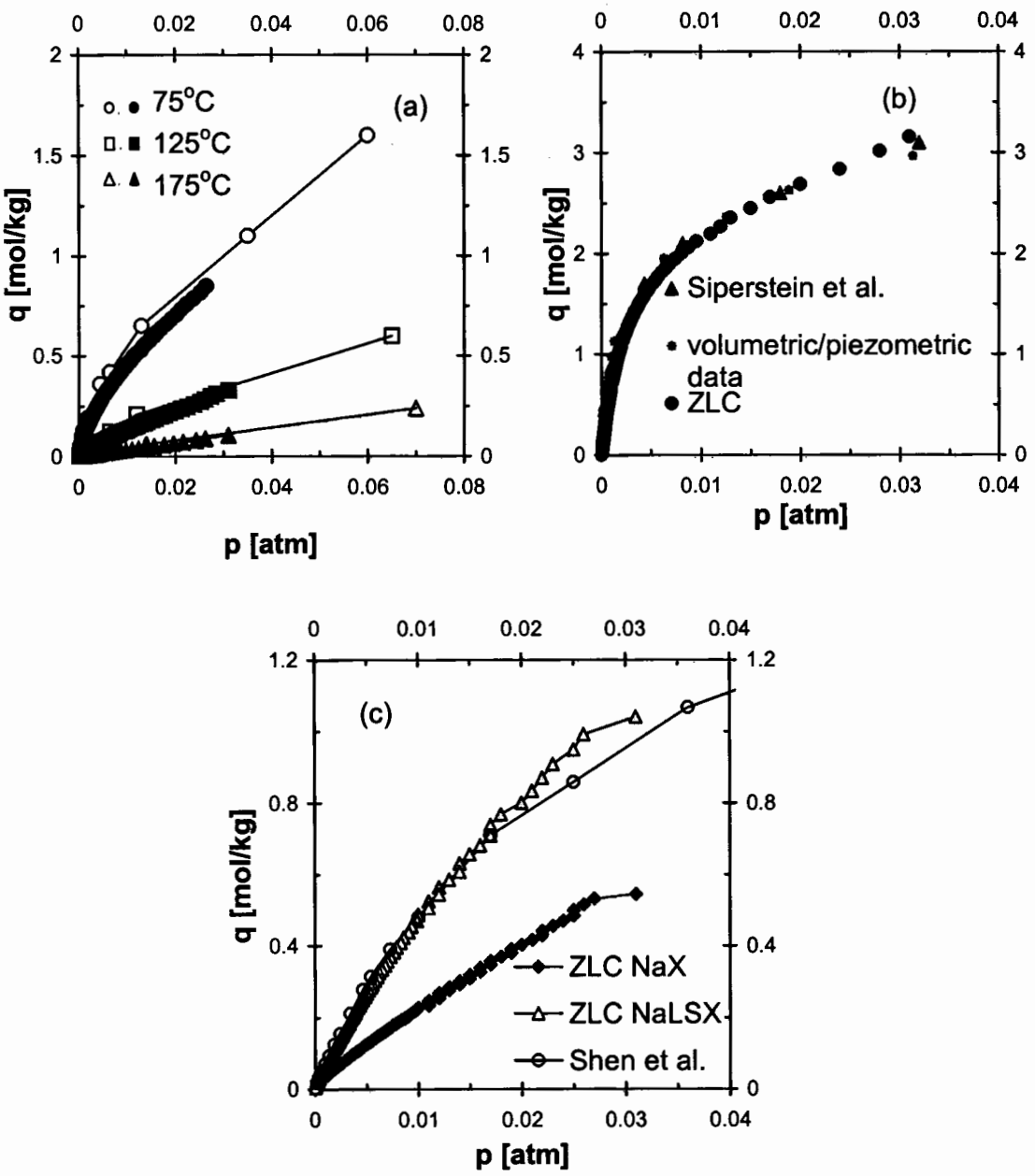

Figure 4.10: Comparison of (a) ZLC Isotherms (Full Symbols) for CO_2-CaA with Volumetric/Piezometric Data (Open Symbols), (b) ZLC Isotherm for CO_2-NaLSX at 20°C with Volumetric/Piezometric Data and Volumetric Data, (c) ZLC Isotherms for CO_2-NaX at 75°C with Volumetric Data.

that their NaX adsorbent must have been very similar to our NaLSX material. The isotherm for our regular NaX sample (at 75°C) is substantially lower.

As an example of isotherm measurement over a very wide loading range Figure 4.11 shows the data set obtained for CH_4-NaX at sub-ambient temperatures. The 195 K isotherm extends from the Henry's law region almost to the saturation limit. Also shown are the high pressure isotherms obtained at 298 K by Zhang et al.[13] and Rolniak and Kobayashi[14] which appear to be broadly consistent with the present data and show a similar saturation limit.

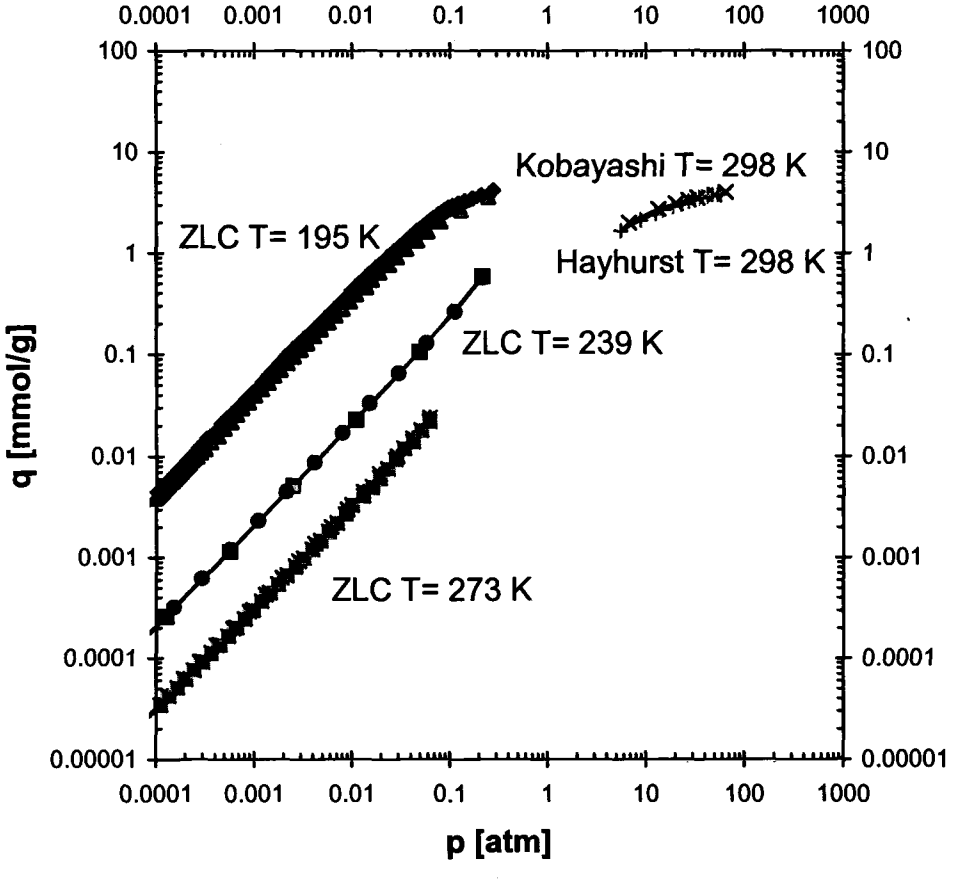

Figure 4.11: Equilibrium Isotherms for CH_4-NaX Showing Comparison with the High Pressure Data of Hayhurst[13] and Kobayashi[14].

4.4 Analysis and Interpretation of CO_2 Isotherms

Figures 4.12 and 4.13 show sets of isotherms for CO_2 on LiLSX, NaLSX, NaX, CaX and CaA measured at several temperatures by the ZLC method. The shapes of the isotherms for these adsorbents are obviously different. It seems reasonable to assume that, at least in the low to intermediate loading region, the quadrupolar CO_2 molecules are adsorbed mainly at the cation sites within the supercage. The slopes of the isotherms thus reflect differences in both the number and positions of the supercage cations. In zeolite X the cations within the supercage occupy two different types of site (II and III in the standard notation)[15] so the simplest isotherm model that may be expected to capture the essential features of the physical system is the double Langmuir expression:

$$q^* = \frac{b_1 q_{s1} p}{1 + b_1 p} + \frac{b_2 q_{s2} p}{1 + b_2 p} \tag{4.1}$$

where b_1, q_{s1} and b_2, q_{s2} are the characteristic parameters for sites of types 1 and 2. The first term is assumed to represent adsorption on the "strong" cation sites within the supercage while the second term represents adsorption on weak cation sites plus any additional contribution from delocalized adsorption or adsorption on the framework.

If there is a large difference in affinity between sites 1 and 2 one can expect that the most favorable (type 1) sites will be predominantly occupied in the low concentration region with significant occupation of the type 2 sites only at higher

loading. To interpret the experimental data, the low concentration region of the isotherm (from zero to just beyond the linear region) was fitted to the single Langmuir model (Eq.2.11) subject to the restrictions that, for a given sorbent, q_{s1}, which represents the density of "strong" cation sites, must be the same at all temperatures and the product bq_s must coincide with the Henry constant (with appropriate correction for units). For those systems which showed substantial deviation from the simple Langmuir model these values (b_1, q_{s1}) were then substituted in Eq.4.1 and the parameters b_2, q_{s2}, corresponding to the "weak" sites, were estimated by fitting the complete isotherms. Minor readjustments were then carried out to optimize the fit of the entire data set. The resulting parameters are summarized in Table 4.4 and the comparisons between the experimental data and the model isotherm are shown in Figures 4.12 and 4.13. It may be seen that the data

Table 4.4: Langmuir Constants and Saturation Capacities for CO_2 Adsorption on Zeolite X

T(K)	NaLSX	LiLSX		NaX	CaX	
	b_1 (atm^{-1})	b_1 (atm^{-1})	b_2	b_1 (atm^{-1})	b_1 (atm^{-1})	b_2
293	--	--	--	193.3	--	--
308	138	1462.5	63.5	--	--	--
312	--	--	--	80.0	--	--
323	68	312.5	5.4	--	1606.0	11.4
328	--	--	--	39.3	--	--
348	21.5	100.0	0.3	18.5	321.4	3.0
373	7.9	35.6	--	6.7	105.9	1.1
398	3.2	15.0	--	2.9	35.7	0.3
423	1.6	5.0	--	--	14.1	0.1
448	--	3.8	--	--	--	--
$-\Delta H_1$(kJ/mole)	41.6	48.1			53.3	
b_o (atm^{-1})	1.27×10^{-5}	7.0×10^{-6}			4.0×10^{-6}	
q_{s1} (m mole/g)	2.75	1.6		1.5	1.4	
q_{s2} (m mole/g)		2.0		2.4	2.2	

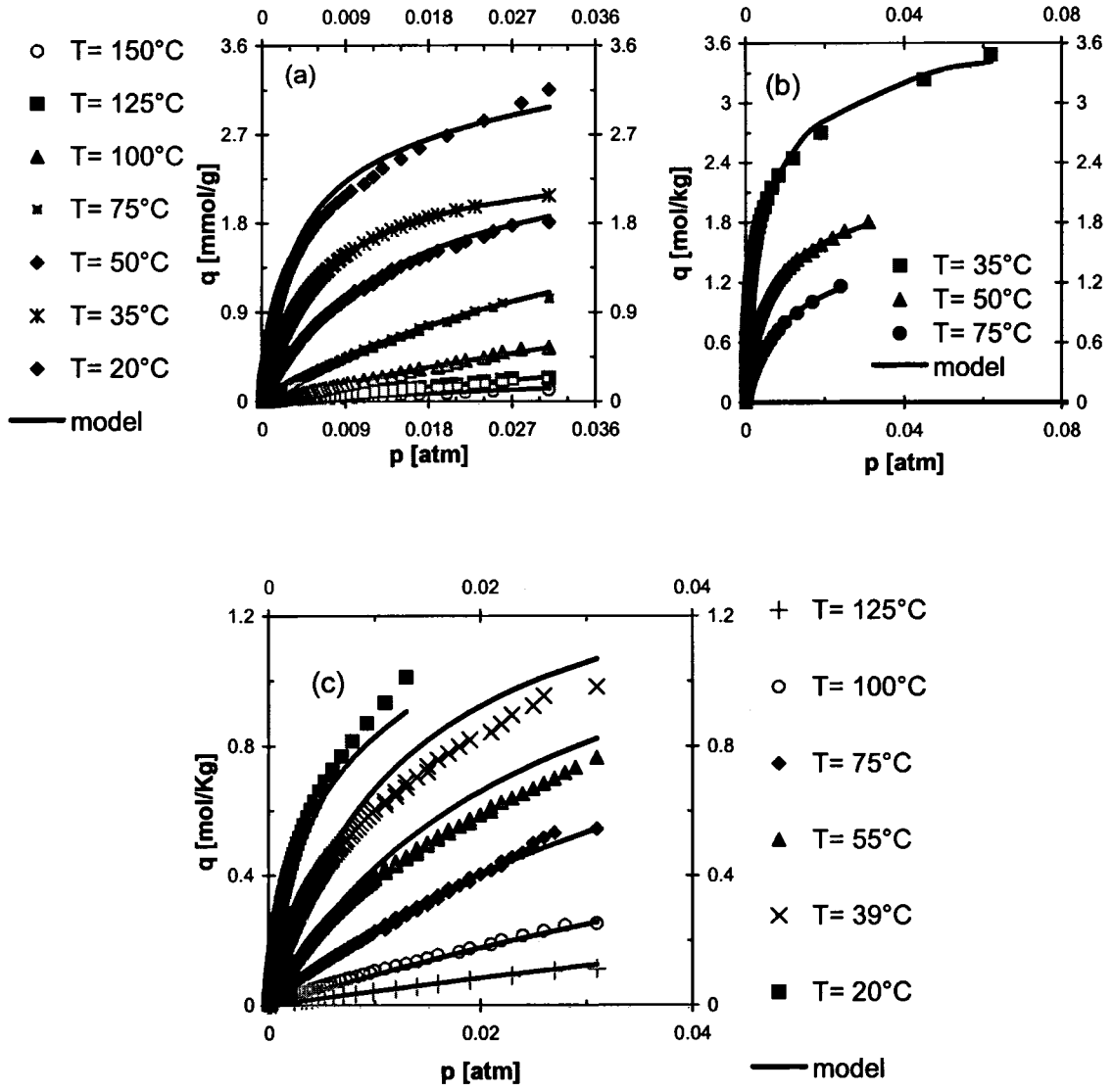

Figure 4.12: Equilibrium Isotherms for CO_2 on Na^+ and Li^+ Zeolites Showing Comparison of Experimental Data and Model Isotherms Calculated with Parameters Given in Table 4.4 (a) NaLSX – Ideal Langmuir Model (20°C Fitted with Dual Site Langmuir with b_2= 8.0 atm^{-1} and q_{s2}= 2.0 mmole/gm), (b) LiLSX- Dual Site Model, (c) NaX Ideal Langmuir Model.

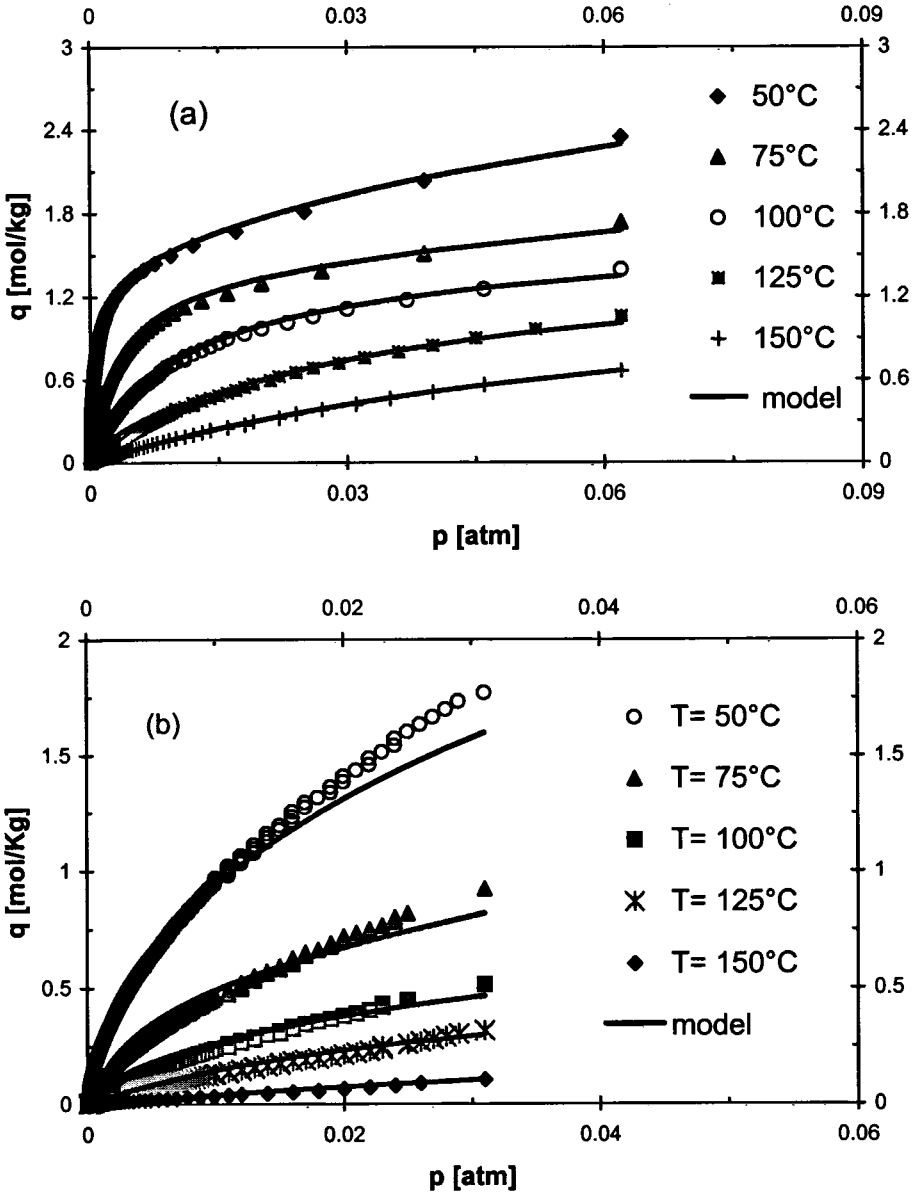

Figure 4.13: Equilibrium Isotherms for CO_2 on Ca^{++} Zeolites Showing Comparison of Experimental Data and Dual Site Model Isotherms Calculated with Parameters Given in Table 4.4 (a) CaX, (b) CaA.

for NaX and NaLSX (except at 20°C) can be reasonably well approximated by the ideal Langmuir model (Eq.2.11) with q_s independent of temperature. In contrast the ideal Langmuir model cannot adequately fit the data for LiLSX, CaX and CaA. The

isotherms for these sorbates are, however, reasonably well represented by the dual site model (Eq.4.1).

According to the dual site model the Henry constant is given by $K = b_1 q_{s1} + b_2 q_{s2}$ (with due correction for units). The Henry constants calculated in this way are close to but not identical to the values given in Table 4.2 (and Figures 4.5-4.8) which were derived directly from the ZLC response curves.

4.5 Density and Strength of Cation Sites

The locations of the cations in zeolite X have been studied extensively by X ray diffraction, neutron diffraction and other techniques[15-22]. The available information is summarized in Table 4.5. In principle it is possible to compare the q_s values derived from the CO_2 isotherms with the values that may be anticipated from structural considerations (the number of cations in the most favorable sites). However, it is well known that the distribution of cations between the available sites depends not only on the nature of the cation and the Si/Al ratio (which determines the total number of cations) but also on details of the sample dehydration and regeneration procedures[23], so such comparisons are not unambiguous.

Further structural information can be obtained from detailed calorimetric studies[12, 23-25], by molecular modeling[26, 27] and MASNMR[28, 29]. Like the diffraction data the results of the calorimetric studies are somewhat ambiguous. For LiX Shen and Bulow[23] found that, in the low loading region (up to 2.5 molecules/cage), the heat of adsorption is constant. This is consistent with structural information which

suggests that, for this sample (Si/Al= 1.28) with the idealized cation distribution, there should be 2.5 Li^+ cations per cage in the exposed Type III sites. However, Barrer and Gibbons[25], for an apparently similar LiX sample, found a continuous decline of heat of adsorption with CO_2 loading (at least above 1.7 molecules per cage) suggesting a more random distribution of cations among the available sites. Similarly for NaX and NaLSX most of the studies report a continuous decline in heat of sorption with loading[12, 23-25] although a few studies suggest that the heat of sorption approaches a constant value at low loadings[23].

Table 4.5: Structural Data, Cation Positions and Adsorption Capacities

Zeolite	LiLSX	LiX	NaLSX	NaX	NaX	NaX	NaX	CaX	CaX
Si/Al	1.0	1.28	1.0	1.1	1.1	1.2	1.25	1.0	1.25
Cations/ Cage	12	10.5	12	11.5	11.5	11	10.6	6	5.3
Site									
I	0	0	0	0	0.36		0	1.66	1.66
I′	4	4	4	4	3.64	4	4	0.63	0.63
II′	0	0	0	0	0	0	0	0.75	0.75
II	4	4	4	4	3.85	4	4	3.1	2.3
III+III′	4	2.5	4	3.5	3.65	3	2.6	0	0
Ref.	Plevert [20,21]	Shen[23]	--	Xhu[18]	Olson[17]	Vitale[19]	--	Breck[15]	*
q_{s1}	2.9		5.5				2.9		2.3
q_{s2}	3.6						4.3		3.6
$q_{s1}+q_{s2}$	6.5						7.2		5.9

q_s is expressed in molecules/cage. Conversion factors $(molecules/cage)/(mmole/g)$ are given in Table 4.1

Site I – hexagonal prism
Site I′, II′ – inside sodalite cage, near 6 – rings
} Inaccessible to gas

Site II – within supercage at the 6 – rings
Site III, III′ – within supercage at the 4 – rings
} Accessible to gas

See Breck[15] or Mortier[16] for a more detailed description of the cation sites.

*Calculated assuming occupation of sites I, I′ and II′ are the same as for the lower Si/Al sample.

Information concerning the accessibility of the cations to the guest molecules has been obtained from MASNMR with both ^{6}Li and ^{7}Li[27, 28] and from infrared spectroscopic studies[29, 30]. It seems clear from these results that Li^{+} in site II is essentially buried (at the center of the oxygen six ring) and is inaccessible to either N_2 or O_2 (and presumably also to CO_2). Li^{+} occupies site III only at high degrees of Li^{+} exchange and when the Si/Al ratio is sufficiently low but these are clearly the "strong" adsorption sites in LiLSX or LiX. By contrast Na^{+} and Ca^{++} in site II appear to be accessible to the gas molecules. In fact, for Na^{+}, there appears to be little difference in interaction energies for a guest molecule with cations in sites II and III.

CO_2-NaLSX *(Fig.4.12a)*

The structural data suggest that this material should contain four Na^{+} cations in type III sites and four in type II. Since cations in both these sites are accessible to the gas molecules with little energetic difference this would suggest up to eight "strong" sites per cell. Except at 20°C the experimental data are well represented by the ideal Langmuir model and suggest five equivalent (strong) sites—a much higher value than for LiLSX. The sorption data are thus seen to be qualitatively (although not quantitatively) consistent with the structural information. It seems possible that a fraction of the cations attributed to sites II and III in the idealized structure are in fact located in the interior sites (I, I', II').

***CO_2-LiLSX** (Fig.4.12b)*

For the ideal cation distribution shown in Table 4.5 one would expect four strong sites per cage corresponding to Li^+ in the type III sites. In fact it was found about 2.9 "strong" and 3.6 "weak" sites per cage. This might be interpreted as suggesting that, in practice, the type III (and III') sites are somewhat less fully populated than in the idealized structure.

***CO_2 – NaX** (Fig.4.12c)*

For a given CO_2 pressure and temperature the loading on NaX is substantially smaller than for NaLSX reflecting the lower cation density (see Figure 4.5c). Analysis of the experimental isotherms suggests about 3 strong sites and 4 weaker sites per cage ($q_{s1} = 2.9, q_{s2} = 4.3$). These values are close to the expected numbers of cation sites III (strong) and II (weak) respectively. Furthermore the equilibrium constants for the strong sites (b_1) for NaX and NaLSX are very similar suggesting that the difference in affinity is related to the difference in site densities, rather than to differences in the intrinsic affinity of an individual site. These conclusions are broadly consistent with the structural data except that in NaLSX the strength of the type II and type III cation sites appear to be similar while in NaX[16] there is a measurable difference (see Table 4.5).

CO_2 – CaX *(Fig.4.13a)*

The experimental isotherms are well represented by the dual site Langmuir model with $q_{s1} \cong 2.3$ sites per cage and $q_{s2} \cong 3.6$ sites per cage. This is reasonably consistent with the structural information (2.3 cation per cage in site II) if it is assumed that the occupancy of the internal sites is the same as for the lower silica material. The data suggest some additional adsorption on sites II but the b_2 values are very much smaller (by 2 orders of magnitude) than the b_1 values. This may suggest that, for this system, the second set of sites represents the framework rather than less favorable cation sites.

4.6 Effect of Water Vapor

The major problem with the ZLC technique is the need to eliminate all traces of water vapor. With hydrophobic adsorbents such as silicalite or even with hydrophilic adsorbents such as CaA or NaX this difficulty can be overcome relatively easily by careful attention to the obvious details of the experimental system. However, with strongly hydrophilic adsorbents such as LiLSX, for which the effect of ppm (or even ppb levels) of water can be significant, the problem may be more severe. Figure 4.14 shows the effect on the CO_2 isotherm of purging for several hours with cylinder He (without a molecular sieve dryer in the line). There is a perceptible decline in capacity within a few hours and after two days the capacity and affinity fall to very low levels characteristic of a non-cationic system, suggesting that all cation

sites have been deactivated by water adsorption. Heating under He purge at 400°C for a relatively short period (30 min) restored the capacity and affinity to the original level for a water free sample. Indeed the isotherms, determined after successive regenerations at 400°C showed no evidence of any permanent decline in capacity (see Fig.4.15).

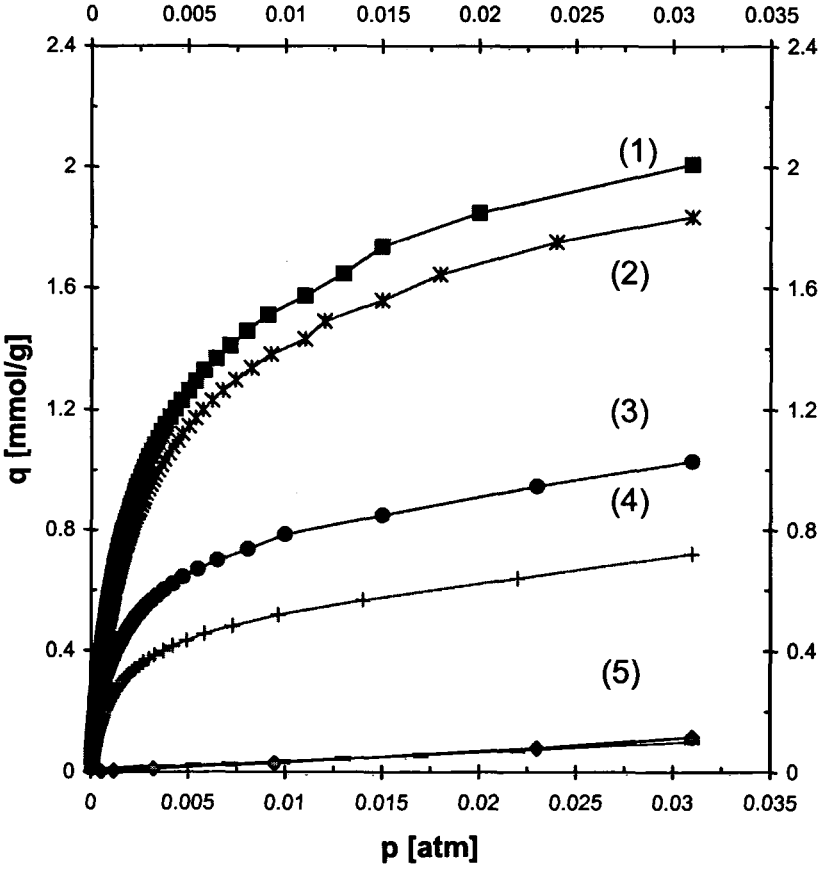

Figure 4.14: Isotherms for CO_2-LiLSX at 35°C Showing Deactivation on Time (1) Freshly Regenerated, (2) After 5 hrs, (3) After 24 hrs, (4) After 28 hrs, (5) > 48 hrs.

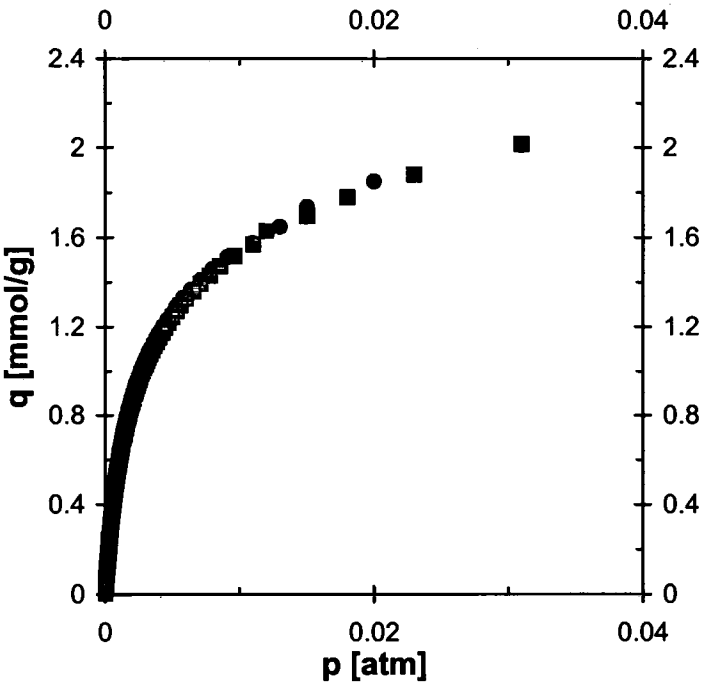

Figure 4.15: Replicate Isotherms for CO_2-LiLSX at 35°C Showing No Decline in Capacity After Successive Regeneration at 400°C

Results of a quantitative study of the effect of water traces on the CO_2 isotherm on various adsorbents will be presented in Chapter 6.

4.7 Conclusions

In this chapter the validity of the ZLC technique for measuring Henry constants and adsorption equilibrium has been shown. For strongly hydrophilic adsorbents it is essential to maintain the system dry as was discussed in Chapter 3. The Henry constants obtained with the ZLC technique for several hydrophilic systems are consistent with recent data obtained for these systems by conventional piezometric/volumetric methods but are higher than most of the earlier reported

values which suggests that the earlier studies may have been impacted by the presence of water.

The low and intermediate concentration regions of the isotherm for these systems can be interpreted assuming that adsorption occurs predominantly on the cations in the supercage. . The site densities derived by application of the simple Langmuir and dual site Langmuir models to the CO_2 isotherms are qualitatively consistent with the available information on cation site occupancy levels derived from structural data. For the NaX and CaX samples the correspondence between the density of strong adsorption sites and the expected cation occupancies of the sites $III + III'$ and site II is almost quantitative. For NaLSX and LiLSX the agreement is not as close although the cation occupancy levels and adsorption site densities are still similar.

CHAPTER 5

ZLC Measurement of Binary Equilibria

In the previous chapter it was shown that the ZLC technique provides a simple and rapid way to measure Henry constants and single component equilibrium isotherms. The same general method can be extended to the measurement of equilibria in binary (or higher order multicomponent) systems. This possibility has been explored in some detail and in this chapter the results of these studies are reported. The focus has been on systems containing both CO_2 (a quadrupolar sorbate) and a non-polar (hydrocarbon) species on cationic zeolite adsorbents. Since CO_2 is adsorbed strongly on the cation sites such systems show strong energetic heterogeneity, resulting in separation factors that vary strongly with loading.

5.1 Overview of Binary Experiments

The ZLC experimental procedure for binary systems is similar to that described for single component measurements. The adsorbent sample is pre-equilibrated with a gas stream containing the two adsorbable species (components A and B) in an inert (He) carrier and then desorbed by switching, at time zero, to a pure He purge, monitoring the mole fractions of both components in the effluent stream. As with the single component measurements the purge flow rate must be sufficiently low that the effluent stream is essentially at equilibrium with the adsorbed phase. Varying the purge rate provides a simple experimental test for this condition since,

under conditions of equilibrium control, the desorption curve, when plotted against the *volume* of the effluent gas (the product Ft), should be independent of flow rate. The expression of the adsorbed phase concentration is given by Eq.2.22 and the separation factor (α) by Eq.2.23.

An on-line mass spectrometer is a particularly convenient detector for binary measurements since it allows the desorption of more than one component to be followed simultaneously. In studying binary systems a practical problem may arise if the two sorbates have same m/e peaks from primary ion or fragments on the mass spectrometer. In this case, tables reporting the complete mass spectrum of various compounds can be consulted and peaks that do not superimpose can generally be found (Cornu and Massot[31]). Alternatively, the mass spectra may be determined by running the sorbates separately and recording all the peaks on the mass spectrometer. This procedure might be time consuming, since the system has to be flushed thoroughly with He between experiments to avoid traces of one sorbate interfering with the mass spectrum of the other. The use of a secondary mass peak to follow the desorption curve, however, generally results in a loss of sensitivity since the intensity of the secondary peaks is lower.

The complete binary isotherm can be thought of as a surface showing the variation of α as a function of p_A and p_B together with a second surface showing the variation of total loading in the same coordinates (p_A and p_B). The ZLC desorption curve yields a section through these surfaces, starting at the initial equilibration point (q_{Ao}, q_{Bo}, p_{Ao}, p_{Bo}) and ending at the zero loading point (the origin). However, the path followed is generally not a simple rectilinear section since the composition of the

adsorbed phase changes continuously as the loading decreases. The less strongly adsorbed species desorbs preferentially in the initial region leaving an adsorbed phase that, in the long-time region, consists almost entirely of the more strongly held species. When the affinities of the two sorbates are very different the desorption actually occurs in two distinct stages, with the weaker component being removed initially with very little change in the loading of the strong component which then desorbs, as if from a single component system, during the later stages of the process. To represent the information concerning the variation of separation factor derived from a single experiment it is therefore necessary to consider both the variation in separation factor with loading and the associated variation in the composition of the adsorbed phase along the desorption path.

The systems selected for study are listed in Table 5.1. The adsorbents are the same as those used for the single component experiments. These systems were selected from amongst those for which reliable binary adsorption equilibrium data, obtained by conventional methods, are available for comparison[11, 32, 33]. A second consideration relates to the requirement that the two sorbates should preferably be adsorbed with comparable affinities. If there is a large difference in affinity, the desorption occurs sequentially, with essentially complete desorption of the weaker component before any significant amount of the stronger component is removed. Analysis of the desorption curves then yields only the separation factor at the initial loading condition, together with the single component isotherm for the strong component. An example of such behavior is shown in Figure 5.1.

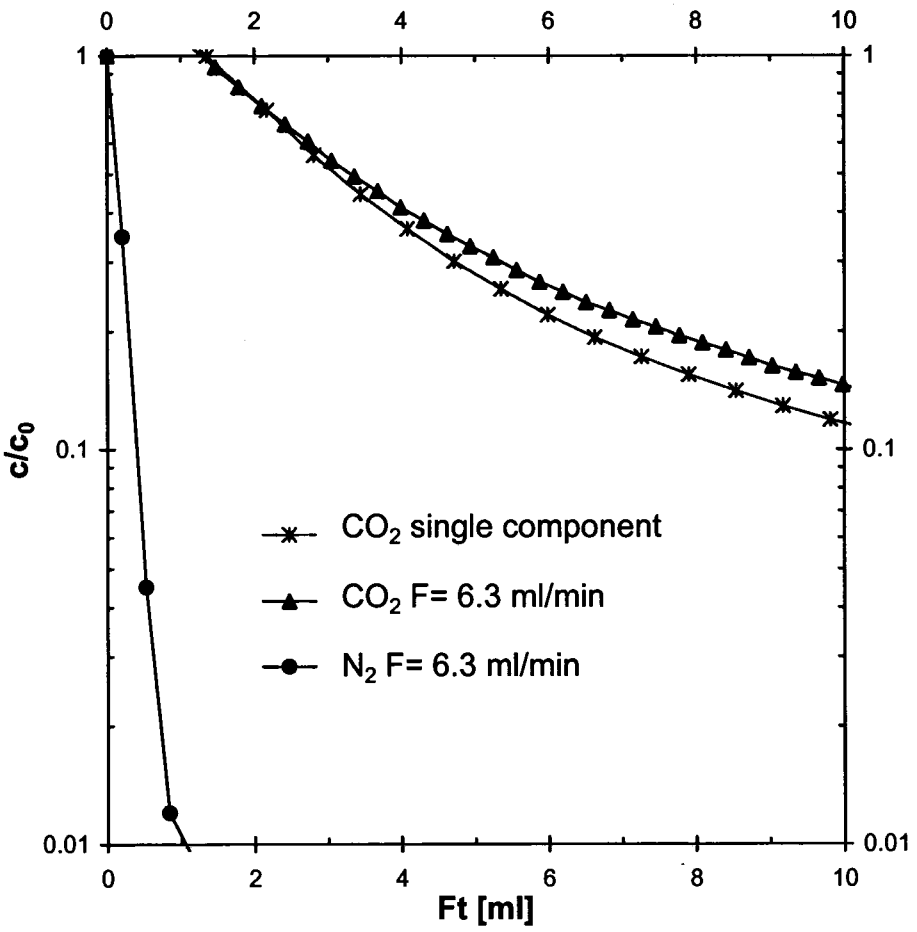

Figure. 5.1: Experimental Desorption Curves for N_2/CO_2 on CaX at 50°C. Note that desorption of the weakly adsorbed species (N_2) is essentially complete before any significant desorption of CO_2 has occurred. The CO_2 desorption curve is therefore almost the same as for the single component system.

Representative binary desorption curves are shown in Figure 5.2. The curves were integrated in accordance with Eq.2.22 to obtain q_A^* and q_B^* (together with the partial pressures p_A and p_B) as a function of time. Separation factors, defined according to Eq.2.23 were then calculated and the equilibrium data are presented as plots of separation factor against loading of the more strongly adsorbed species (q_A)

together with corresponding plots of q_B vs. q_A showing the path of the desorption. Calculation of the separation factors becomes unreliable when the adsorbed phase concentration of the weaker component approaches zero (see Eq.2.23) so the plots are truncated in this region.

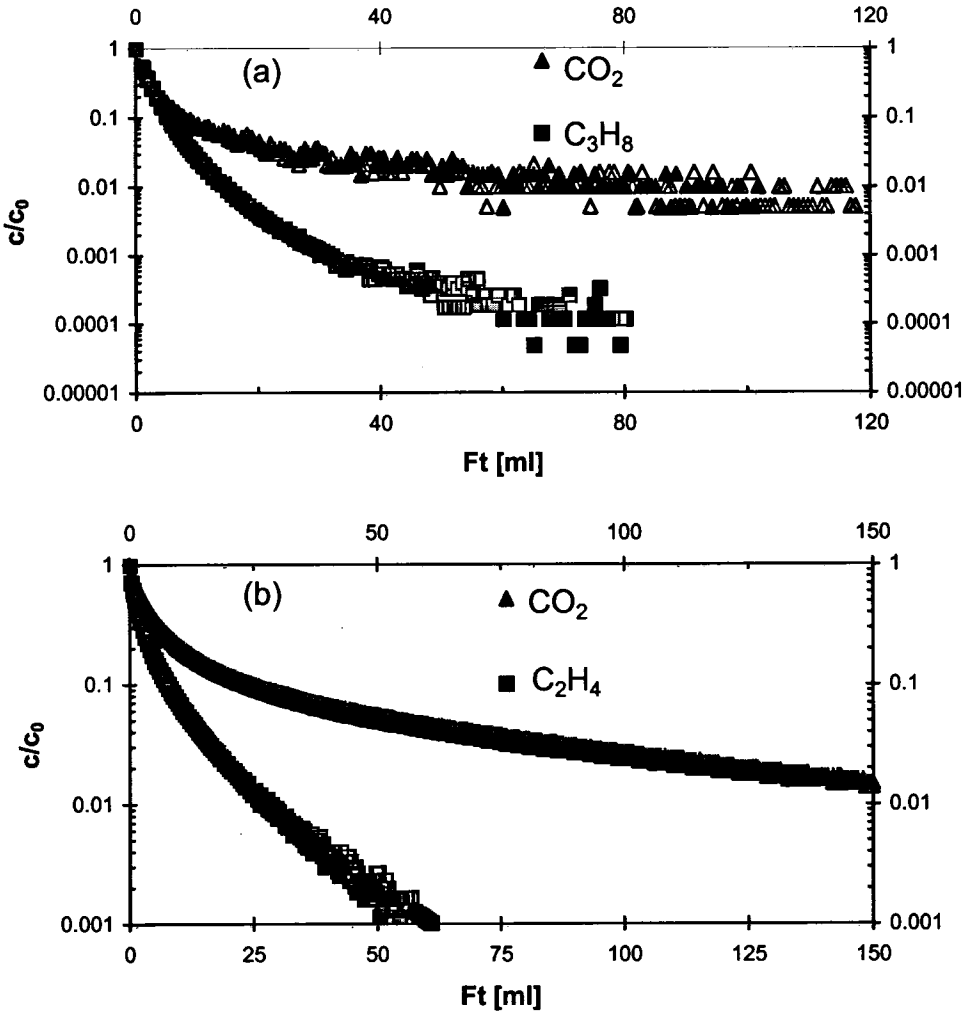

Figure 5.2: Experimental Desorption Curves for (a) C_3H_8/CO_2 onCaX at 50°C $p°CO_2$= 23.5 Torr, $p°C_3H_8$= 47 Torr, F= 7.7, 11.1 ml/min, for (b) C_2H_4/CO_2 on NaLSX at 20°C, $p°CO_2$= 23.5 Torr, $p°C_2H_4$= 23.5 Torr, F= 3.8, 10.0 ml/min.

For several systems a variant of this experiment was also carried out. The sample was pre-equilibrated with a mixture containing only the two adsorbable components at one atmosphere (no He), with one component in considerable excess. The sample was then desorbed by switching to a purge of the major component. Under these conditions the partial pressure of the major component remains almost constant. Integration of the desorption curve for the minor component then yields the isotherm for that component in the presence of a constant partial pressure of the major component (approximately one atmosphere).

5.2 Experimental Results

Representative single component isotherms showing the comparison between the experimental data and the comparison with the theoretical curves, calculated according to Eq.5.1, discussed in the next section, with the parameters given in Table 5.1, are shown in Figures 5.3-5.5. The binary equilibrium data are shown in Figures 5.6-5.13. For each system, the plots show the variation of separation factor with the CO_2 loading (q_A) and the corresponding variation in the adsorbed phase composition and loading during desorption as a plot of q_B vs. q_A. For CO_2, C_3H_8-CaX and CO_2, C_3H_8-CaA the partial isotherms giving the CO_2 loading in the presence of an atmosphere of propane (as a function of CO_2 partial pressure) are also shown in figures 5.12 and 5.13. The theoretical curves calculated from Eq.5.1 with the fitted parameters given in Table 5.1 are shown in all these figures.

Table 5.1: Summary of Experimental Systems and Equilibrium Parameters

Sorbent	NaLSX	NaLSX	NaX	CaX	CaA
Si/Al Ratio	1.0	1.0	1.25	1.25	1.0
Sorbate (A)	CO_2	CO_2	CO_2	CO_2	CO_2
Sorbate (B)	C_2H_4	C_3H_8	C_3H_8	C_3H_8	C_3H_8
p_A°	23.5	23.5 23.5	23.5	23.5 23.5	23.5
p_B°	23.5	23.5 47	23.5	47 94	23.5
T (Deg. C)	20	20	20	50	50
b_{1A}	463	471	318	1188	543
b_{2A}	28	20	0.1	9	15
b_{1B}	61	15.3	7.8	103.4	257
b_{2B}	17	41.3	17.6	6.9	13.1
q_{s1}	1.9	1.88	1.43	0.8	0.58
q_{s2}	2.77	3.66	3.0	2.0	3.51

p_A°, p_B° in Torr, b in atm^{-1}, q_s in m mole/gm

The trends shown by the experimental data are qualitatively consistent with theoretical expectation. In the low loading limit the separation factor approaches the ratio of the Henry constants. For an ideal Langmuir system the separation factor should be independent of loading whereas these systems all show a significant decline, strongest for CaX and weakest for CaA. The declining trend is understandable since CO_2 is adsorbed predominantly on the cationic sites for which it has a much higher affinity than either propane or ethylene. At higher loadings the cationic sites are largely occupied and the separation factor becomes increasingly dominated by the framework sites for which the affinities of CO_2 and the hydrocarbons are similar.

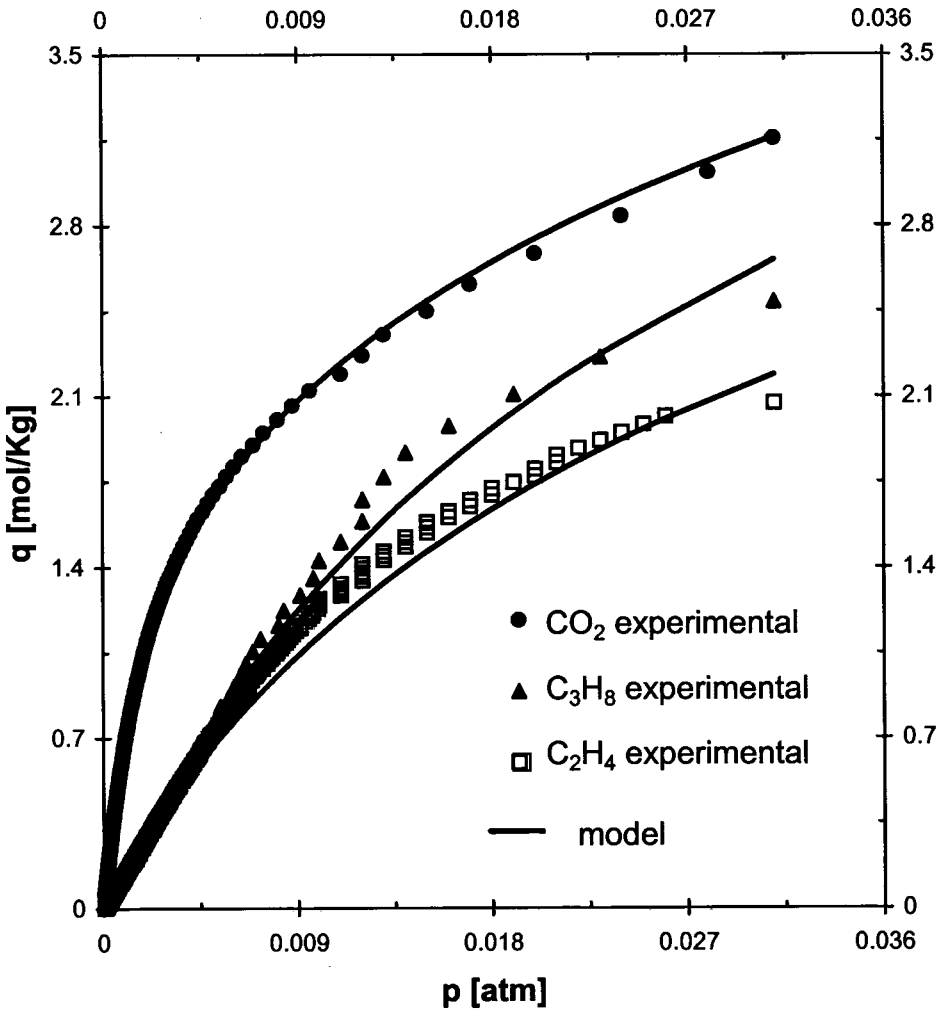

Figure 5.3: Single Component Isotherms for CO_2, C_3H_8 and C_2H_4 on NaLSX at 20°C. The theoretical curves are calculated from Eq.5.1 with the parameters given in Table 5.1.

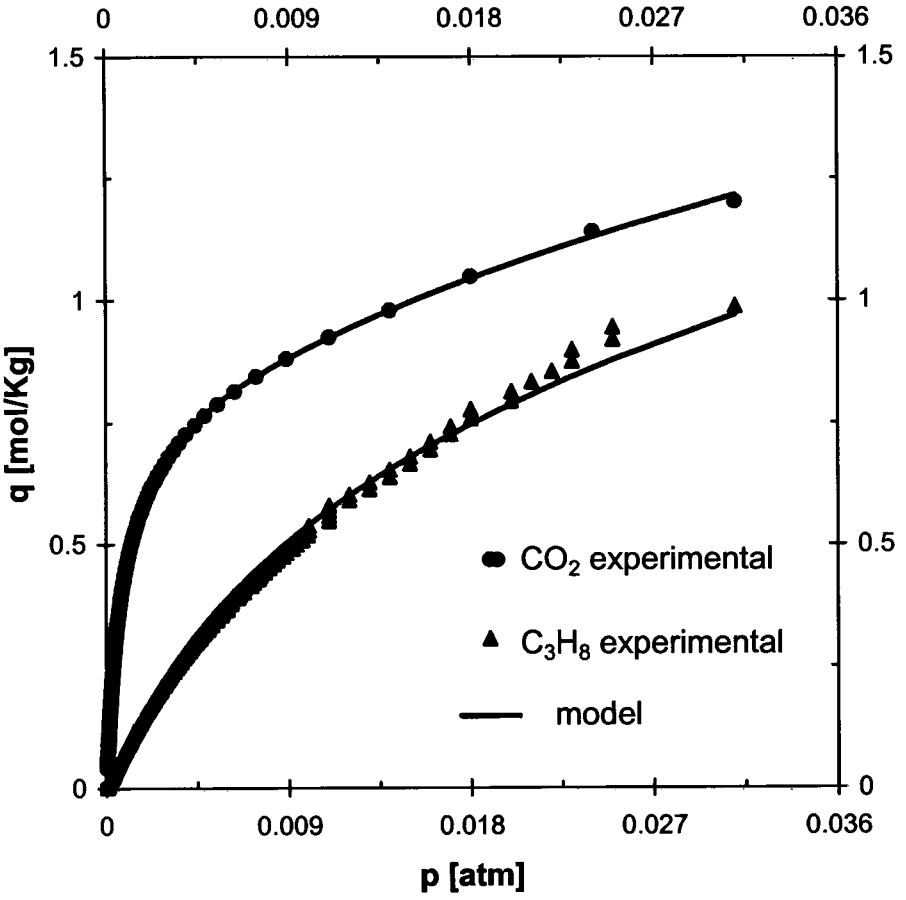

Figure 5.4: Single Component Isotherms for CO_2, C_3H_8 on CaX at 50°C. Theoretical curves are calculated from Eq.5.1 with parameters given in Table 5.1.

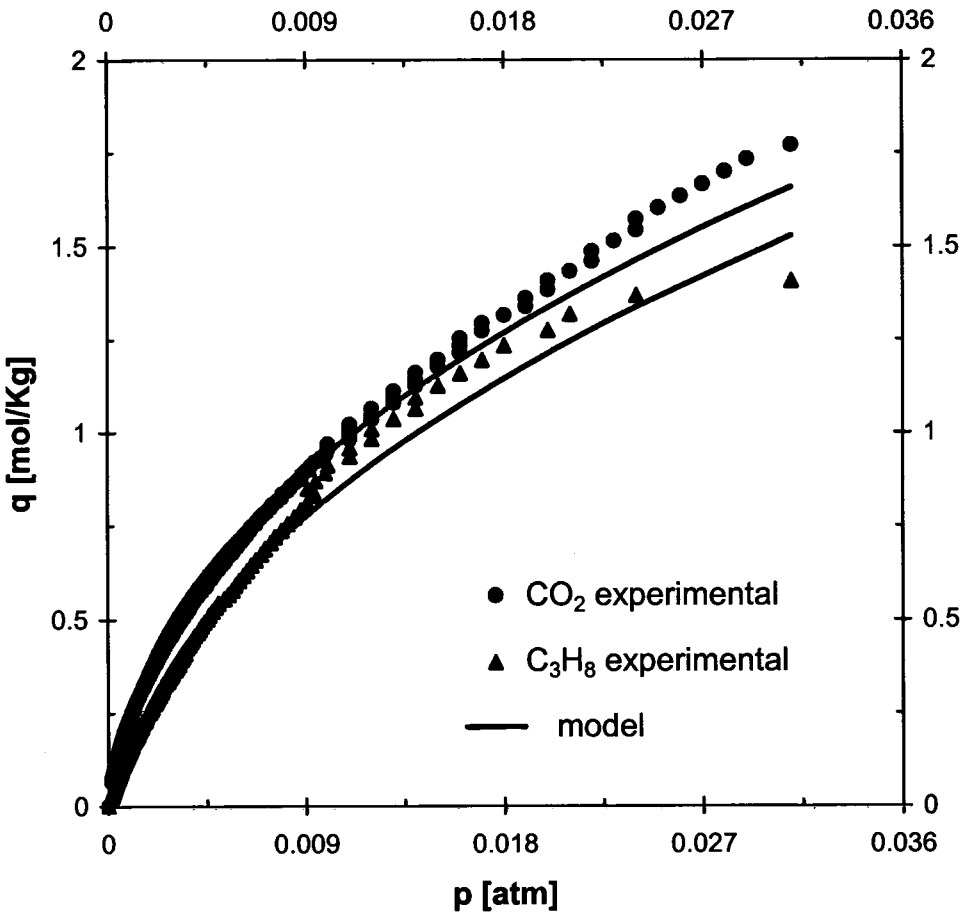

Figure 5.5: Single Component Isotherms for CO_2, C_3H_8 on CaA at 50°C. Theoretical curves are calculated from Eq.5.1 with parameters given in Table 5.1.

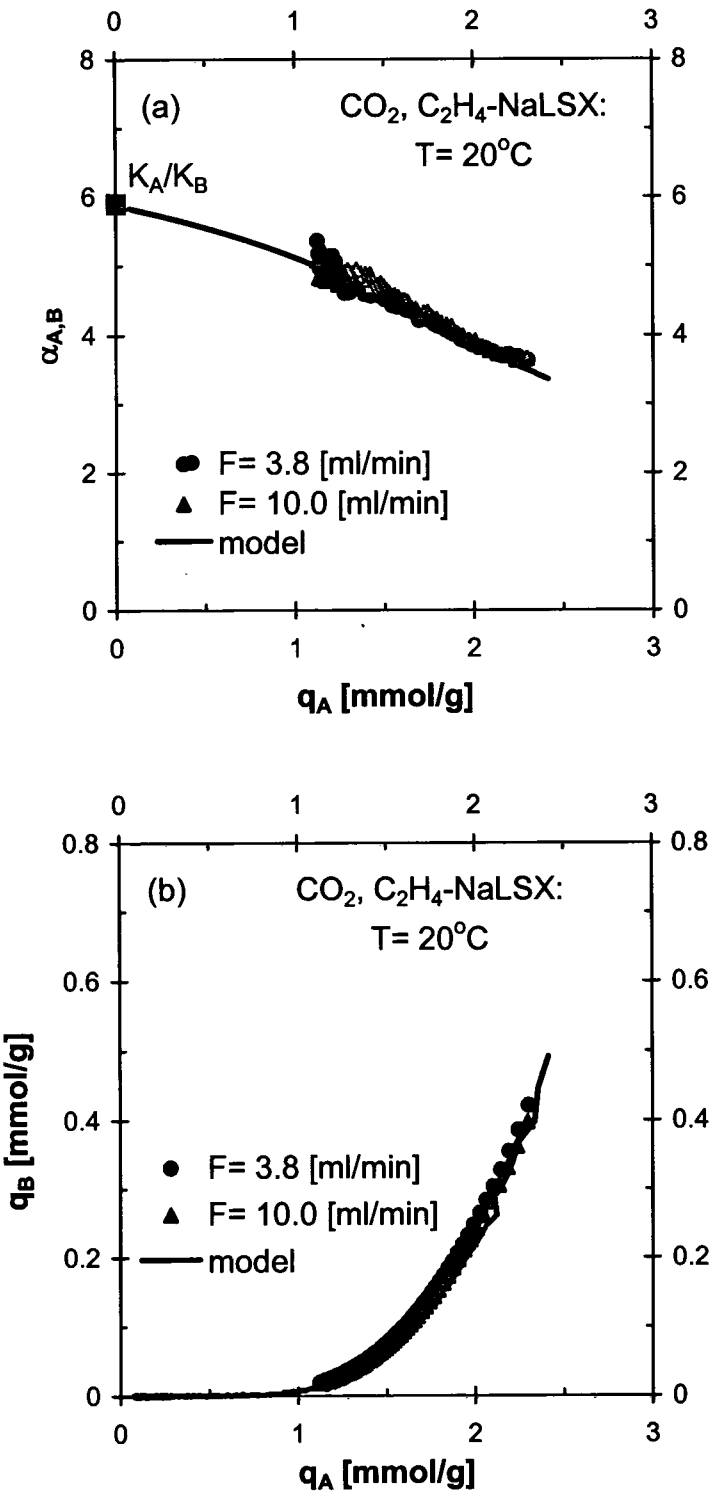

Figure 5.6: (a) Variation of Separation Factor with CO_2 Loading and (b) Path of Desorption for CO_2/C_2H_4 on NaLSX at 20°C, $p^o_A = p^o_B = 23.5$ Torr. Theoretical curves are calculated from Eqs 2.23 and 5.1 with parameters given in Table 5.1.

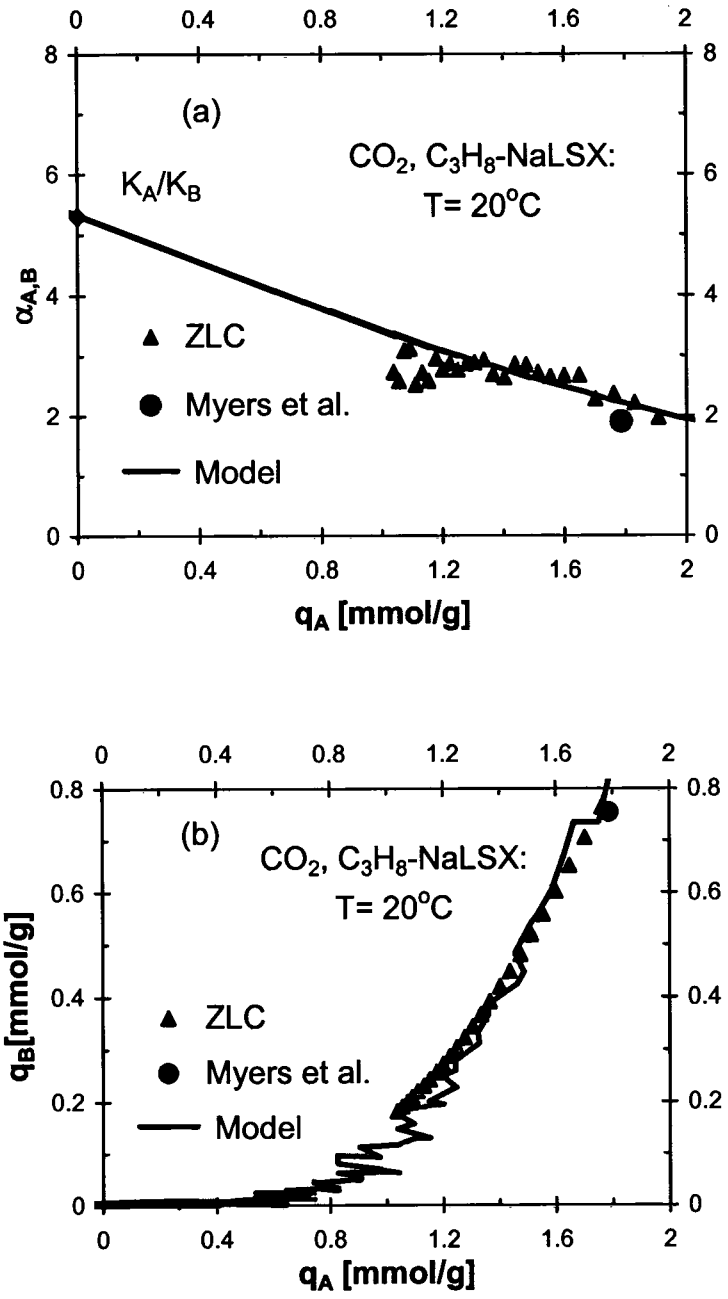

Figure 5.7: (a) Variation of Separation Factor with CO_2 Loading and (b) Path of Desorption for CO_2/C_3H_8 on NaLSX at 20°C, $p^\circ_A = p^\circ_B = 23.5$ Torr. An experimental point calculated from the data of Siperstein and Myers[11] is shown for comparison. Theoretical curves are calculated from Eqs 2.23 and 5.1 with parameters given in Table 5.1.

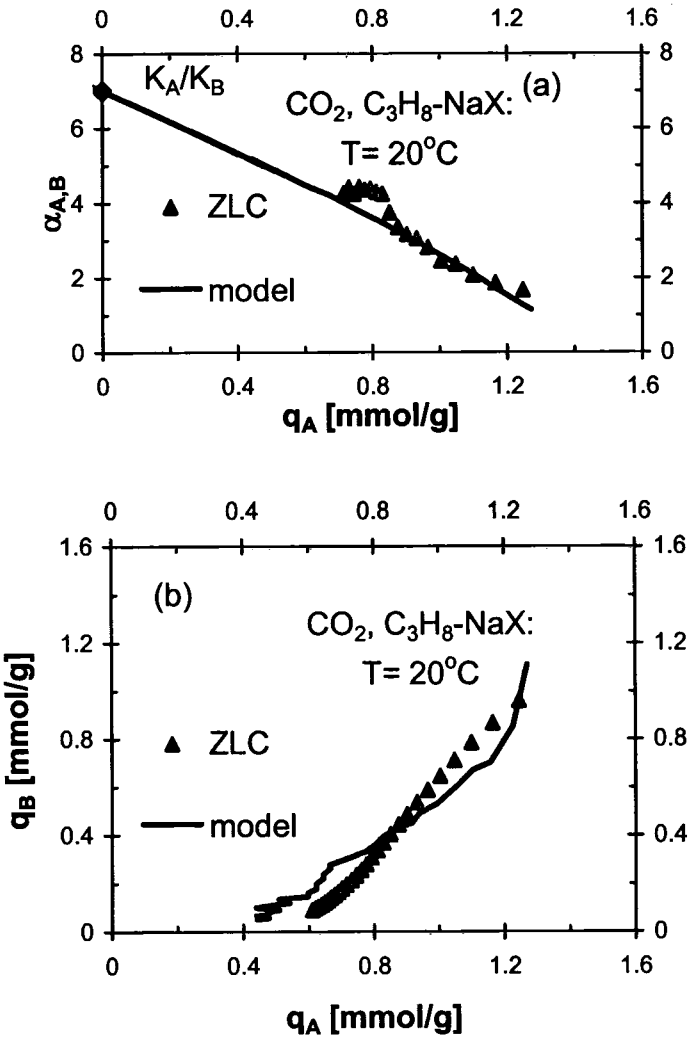

Figure 5.8: (a) Variation of Separation Factor with CO_2 Loading and (b) Path of Desorption for CO_2/C_3H_8 on NaX at 20°C, $p^\circ_A = p^\circ_B = 23.5$ Torr. Theoretical curves are calculated from Eqs 2.23 and 5.1 with parameters given in Table 5.1.

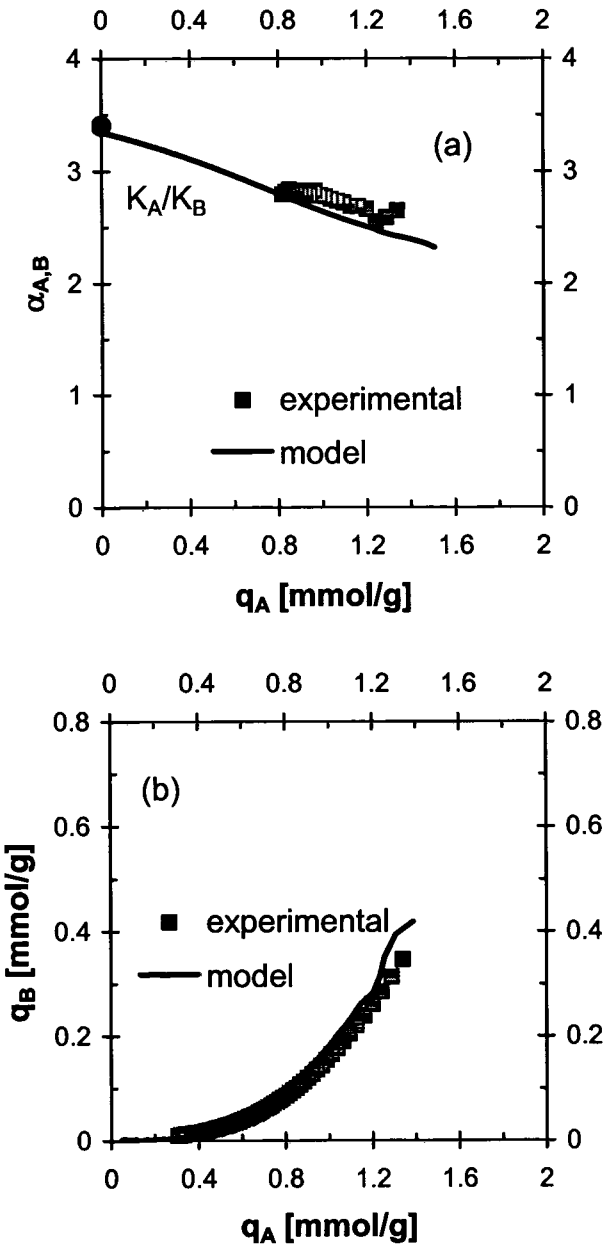

Figure 5.9: (a) Variation of Separation Factor with CO_2 Loading and (b) Path of Desorption for CO_2/C_2H_4 on NaX at 20°C, $p^\circ_A = p^\circ_B = 23.5$ Torr. Theoretical curves are calculated from Eqs 2.23 and 5.1 with parameters given in Table 5.1.

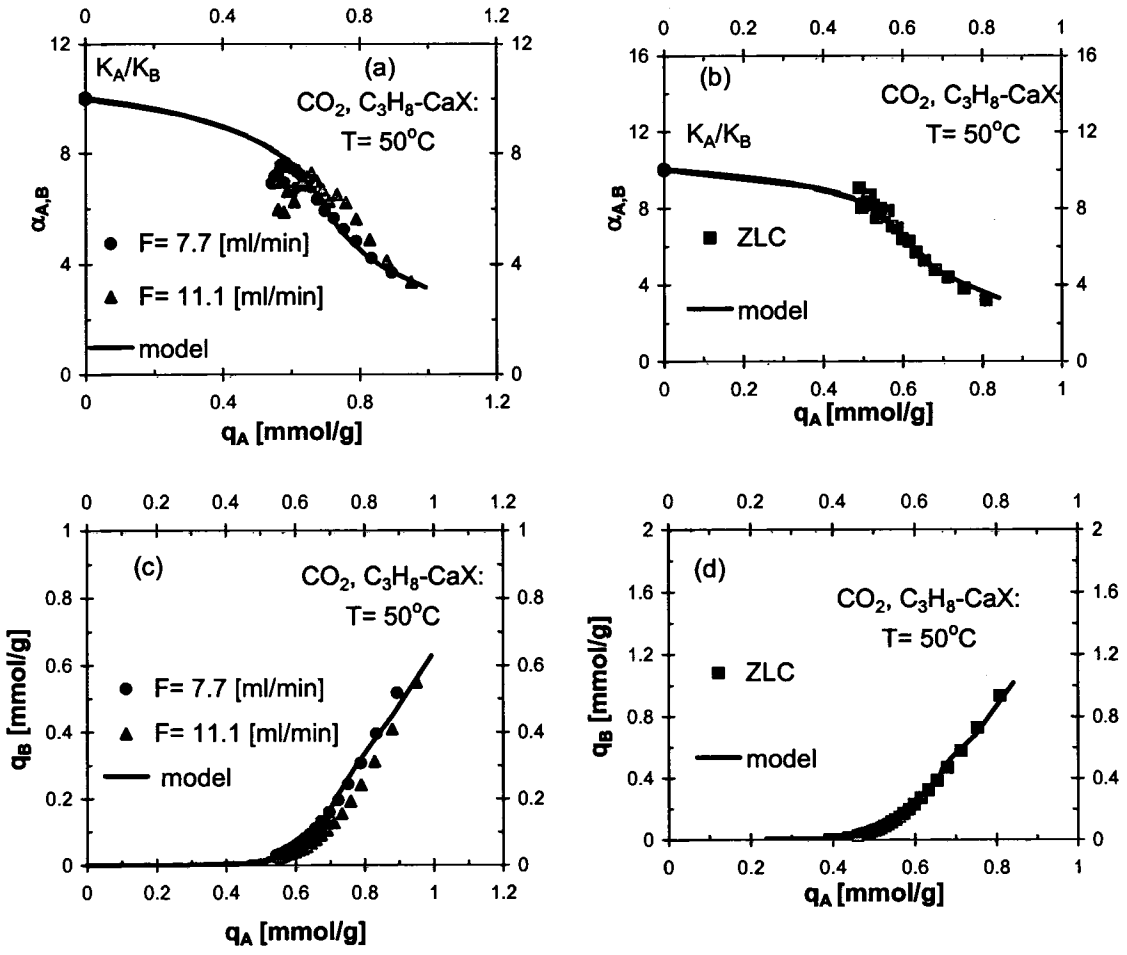

Figure 5.10: (a,b) Variation of Separation Factor with CO_2 Loading and (c,d) Path of Desorption for CO_2/C_3H_8 on CaX at 50°C. (a,c) p^o_A= 23.5 Torr, p^o_B= 47 Torr; (b,d) p^o_A= 23.5 Torr, p^o_B= 94 Torr. Theoretical curves are calculated from Eqs 2.23 and 5.1 with parameters given in Table 5.1.

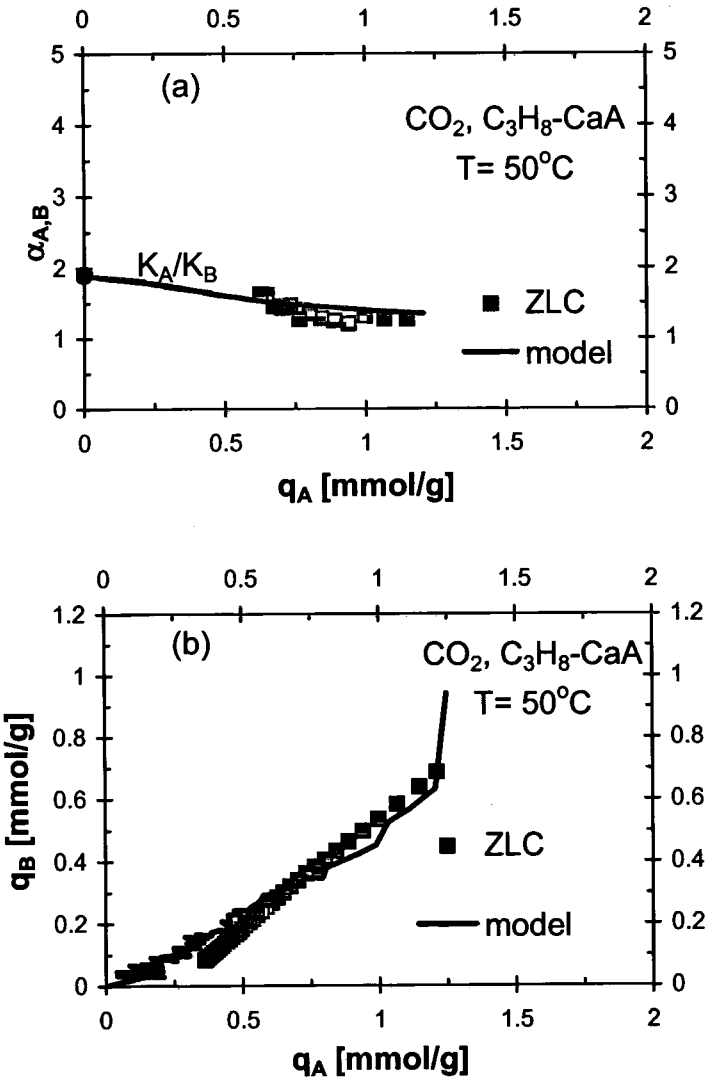

Figure 5.11: (a) Variation of Separation Factor with CO_2 Loading and (b) Path of Desorption for CO_2/C_3H_8 on CaA at 50°C, $p^\circ_A = p^\circ_B = 23.5$ Torr. Theoretical curves are calculated from Eqs 2.23 and 5.1 with parameters given in Table 5.1.

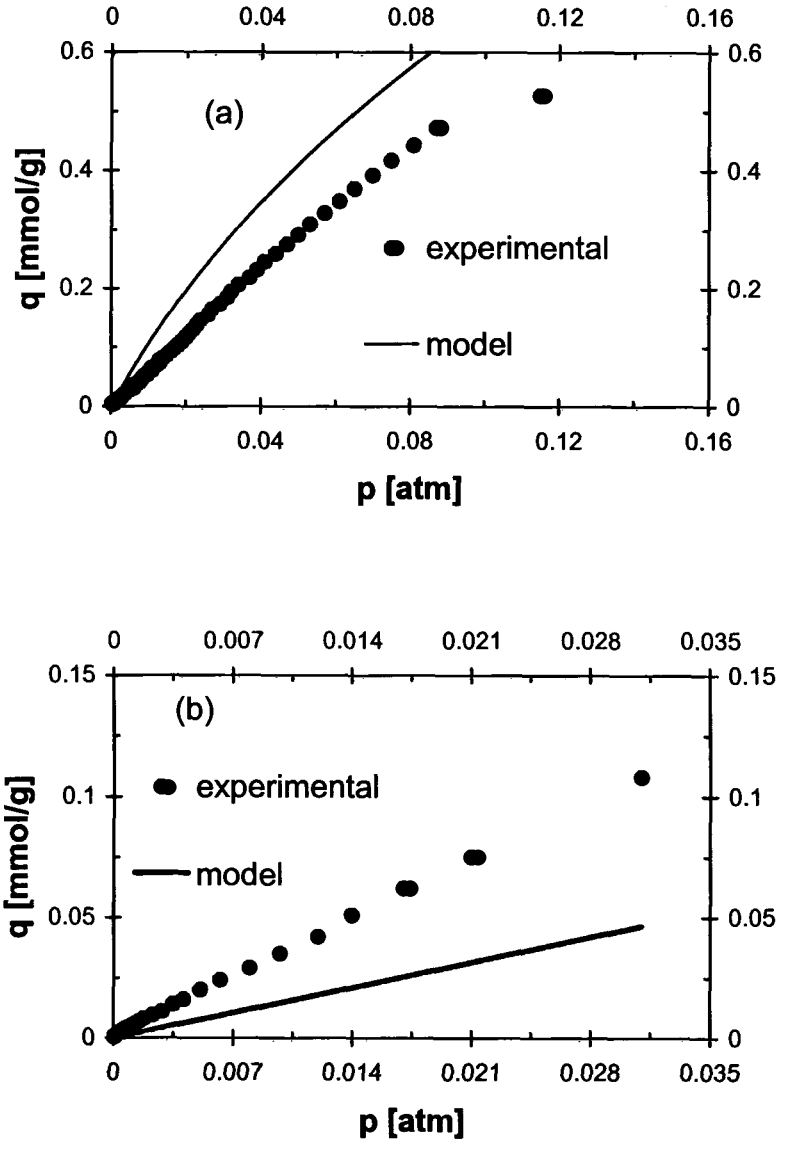

Figure 5.12: Partial Isotherm for (a) CO_2 on CaX in One Atmosphere of C_3H_8 and (b) C_3H_8 on CaX in One Atmosphere of CO_2 at 50°C. Theoretical curves are calculated from Eq.5.1 with the parameters given in Table 5.1.

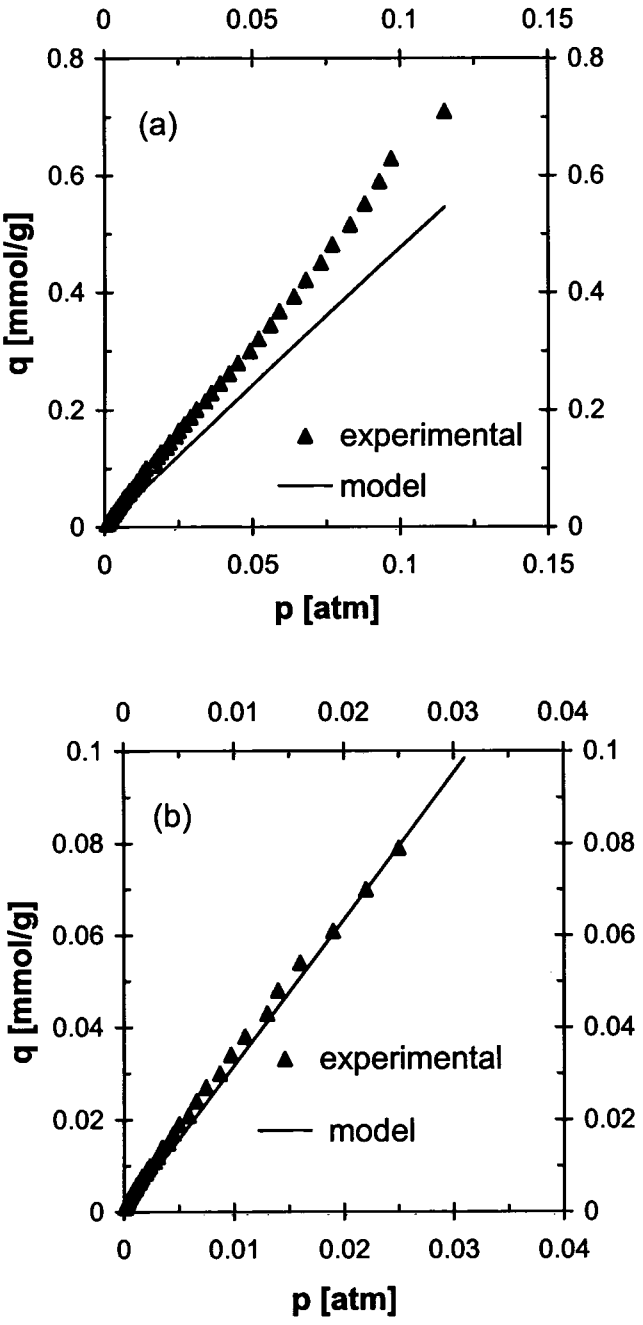

Figure 5.13: Partial Isotherm for (a) CO_2 on CaA in One Atmosphere of C_3H_8 and (b) C_3H_8 on CaA in One Atmosphere of CO_2 at 50°C. Theoretical curves are calculated from Eq.5.1 with the parameters given in Table 5.1.

5.3 The Dual Site Langmuir Model

To account quantitatively for the observed trends requires a model equation for the binary isotherms. Clearly the simple binary Langmuir model cannot account for the behavior since it predicts a constant separation factor. The simplest physically reasonable model which can account for the observed trends is the binary dual site Langmuir model:

$$q_A^* = \frac{b_{1A} q_{1S} p_A}{1 + b_{1A} p_A + b_{1B} p_B} + \frac{b_{2A} q_{2S} p_A}{1 + b_{2A} p_A + b_{2B} p_B} \tag{5.1}$$

with an equivalent expression for q_B^*. The strong sites (type 1) represent the localized cation sites while the weak (type 2) sites represent adsorption on the rest of the framework and within the micropore space.

Eq.5.1 contains six parameters (q_{s1}, q_{s2}, b_{1A}, b_{1B}, b_{2A}, b_{2B}) but all these can be obtained, in principle, from the single component isotherms. However, in practice only the parameters for the strong (type 1) sites can be determined from the single component isotherms with any degree of confidence since the experimental data do not extend to high enough loading levels to yield reliable parameters for the weak sites. The procedure adopted was as follows:

1. The single component isotherms for both components were fitted to Eq.5.1 to provide initial estimates of all parameters.

2. The Henry constants for both components are taken to be accurate. Matching the Henry constants yields:

$$\left.\begin{aligned} K_A &= b_{1A}q_{s1} + b_{2A}q_{s2} \\ K_B &= b_{1B}q_{s1} + b_{2B}q_{s2} \end{aligned}\right\} \qquad (5.2)$$

3. The value of q_{s1} was taken as the average of the q_{s1} values obtained for each component from the single component isotherm.
4. The above procedure yields three equations relating the six constants. The binary data were then fitted using a least squares approach to choose the set of parameter values that, subject to these three restrictions, minimizes the deviation between the experimental and calculated loadings for both components. Thus, in effect, three constants are derived by fitting the binary data.

An example of a Mathcad file is shown in Appendix. The theoretical curves calculated from Eq.5.1, with the parameters determined in this way, are shown in Figures 5.6-5.13 and evidently provide good representations of the binary equilibrium data. Even the partial isotherms for CO_2 in the presence of an atmosphere of propane are well replicated (Figs.5.12 and 5.13) although the experimental conditions are well outside the range over which the equilibrium parameters were determined. However, the partial isotherms for propane, which are dominated by adsorption on the framework surface and within the micropore space, are much less well predicted.

It was shown in Chapter 4 that the dual site Langmuir model can provide a good representation of the single component isotherms for these systems. The match

between the theoretical and experimental single component isotherms shown in Figures 5.3-5.5 is however, only semi-quantitative. This is because the isotherm parameters were chosen to optimize the fits of the binary data, with the same q_s value for both components. The deviations seen at higher loading in the single component isotherms show that the model provides only an approximate representation of the system behavior.

The single component isotherms for CO_2, C_2H_4 and C_3H_8 on NaX at 20°C reported by Siperstein and Myers[11] are very similar to the isotherms for these species on the NaLSX adsorbent used in this study (as shown in Chapter 4). Therefore, it was decided to compare their binary equilibrium data for (CO_2, C_3H_8) and (CO_2, C_2H_4) with the experimental data obtained for these systems on NaLSX. To do this, the fitted constants were used to calculate the loadings (q_A, q_B) according to Eq.5.1 at the partial pressures (p_A, p_B) corresponding to the experimental points reported by Siperstein and Myers. The values of q_A, q_B calculated in this way, are compared with their experimental values in Figure 5.14; representative data points are also given in Table 5.2. It is clear that there is good agreement, showing that the equilibrium data measured by the ZLC method are consistent with the independently measured volumetric data. Even though the adsorbent samples were not identical, in view of the similarity of the single component isotherms, this can be considered as an additional validation of the ZLC technique for measuring binary equilibria.

Table 5.2: Comparison of Experimental Binary Equilibrium Loading Data of Siperstein and Myers[11] for CO_2, C_2H_4-NaX and CO_2, C_3H_8-NaX with Values Calculated from the Correlated ZLC Data of the Present Study

System	p_A	p_B	q_A (Expt)	q_A (Calc)	q_B (Expt)	q_B (Calc)
CO_2(A)-C_2H_4(B)	0.0486	0.0496	2.63	2.78	1.17	0.95
	0.077	0.088	2.85	2.89	1.39	1.14
	0.099	0.11	3.05	3.01	1.36	1.12
	0.368	0.107	4.65	3.99	0.55	0.46
	0.0037	0.042	0.495	0.73	2.21	2.03
	0.0084	0.072	0.738	1.03	2.43	2.29
	0.049	0.311	1.41	1.50	2.85	2.76
CO_2(A)-C_3H_8(B)	0.032	0.003	2.96	3.09	0.25	0.268
	0.038	0.0033	3.11	3.24	0.25	0.27
	0.042	0.0072	3.11	3.22	0.5	0.52
	0.0027	0.0016	1.33	1.23	0.25	0.24
	0.0105	0.0088	2.00	2.02	1.00	0.88
	0.018	0.016	2.2	2.28	1.26	1.23
	0.023	0.027	2.19	2.32	1.5	1.65

p_A and p_B are in atmospheres
q_A and q_B are in m moles/gm.

The single component isotherms reported by Costa et al.[32] and Calleja et al.[33] for CO_2, C_2H_4 and C_3H_8 on a sample of commercial NaX differ significantly from those obtained by the ZLC method for an apparently similar adsorbent. Comparison of the isotherms is shown in Figure 5.15. The reason for this discrepancy is not completely clear although inadequate dehydration by Costa et al. of the adsorbent samples is one obvious possibility. Also in this case the parameters obtained by fitting the ZLC experimental curves were used to calculate the loadings (q_A, q_B) according to Eq.5.1 at the partial pressures (p_A, p_B) corresponding to the experimental points reported by Costa et al. Also in light of the differences of the single component isotherms, the prediction of the binary data show significant deviations. As an

example, a plot of calculated loadings vs. experimental data is given in Figure 5.16 for one of the systems studied.

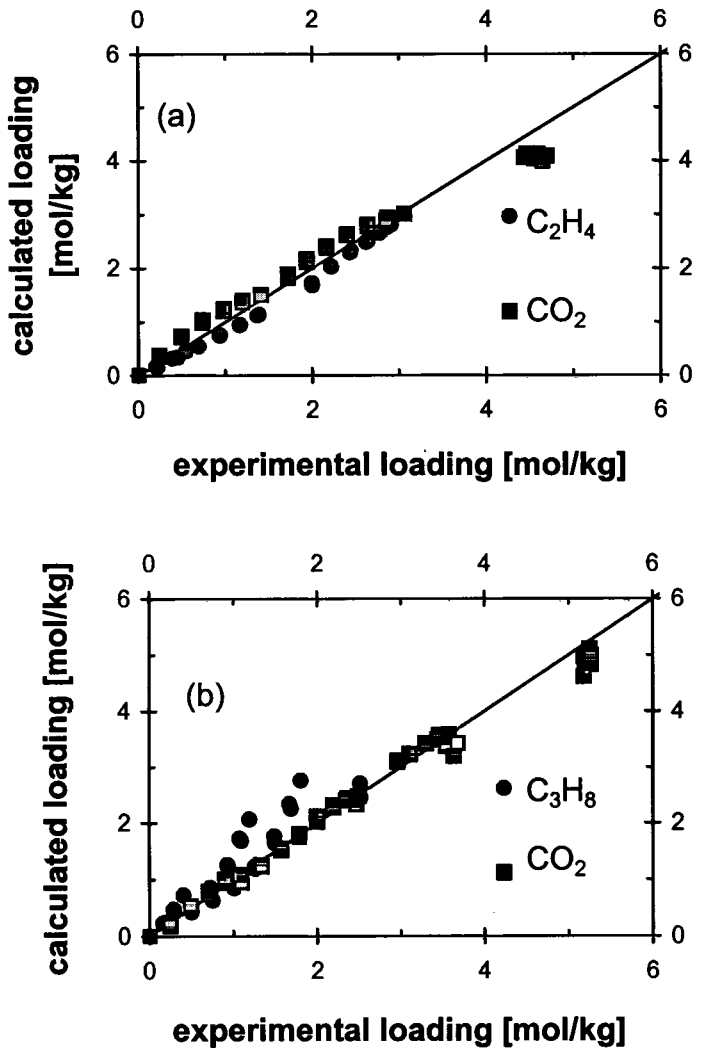

Figure 5.14: Plots of Calculated Loading (from Eq.5.1 with the Parameters Listed in Table 5.1) Against Experimental Loading (Siperstein and Myers[11]) for (a) CO_2/C_2H_4 and (b) CO_2/C_3H_8 on NaLSX at 20°C.

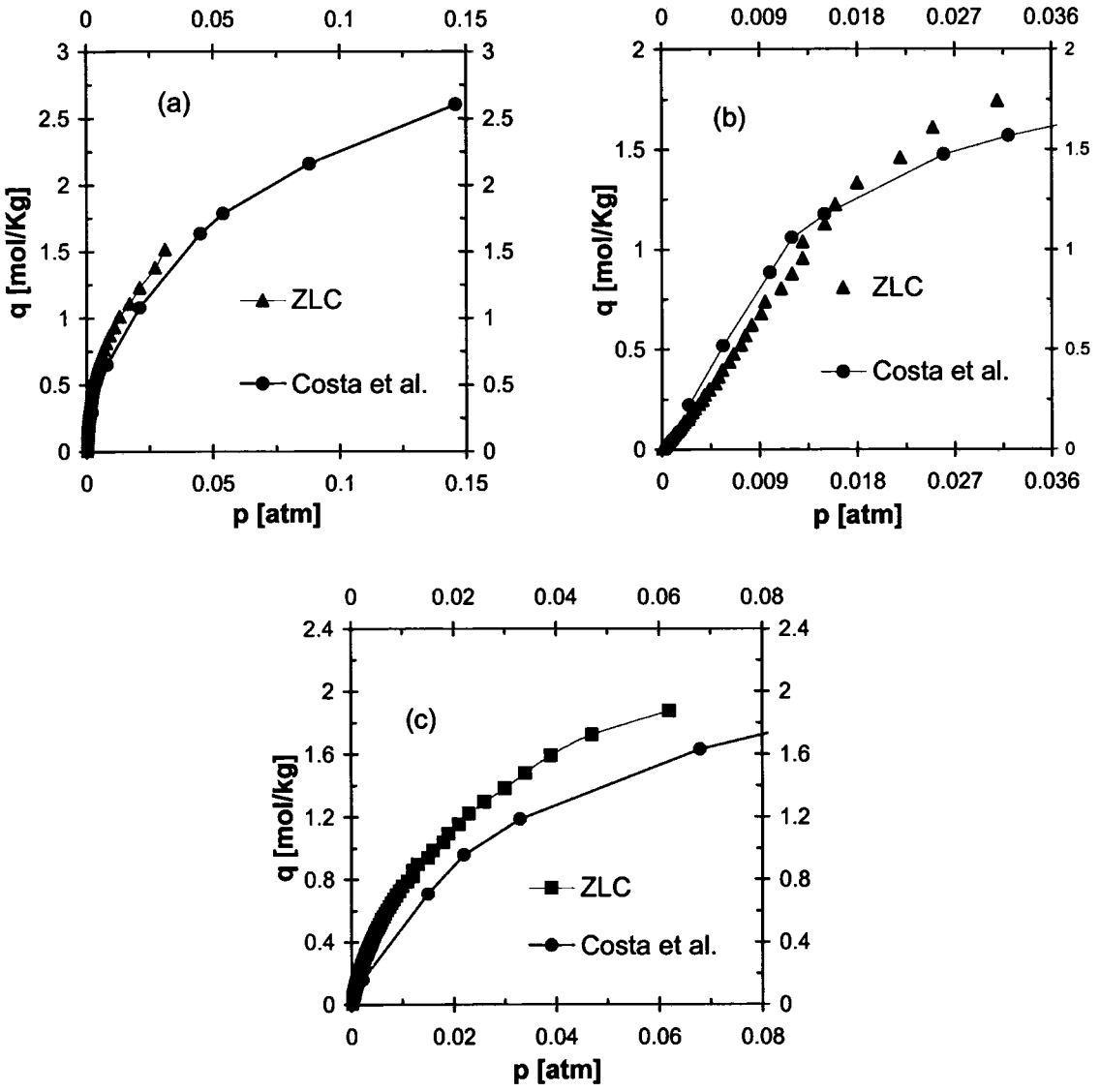

Figure 5.15: Comparison of ZLC Isotherms with those Reported by Costa et al.[32] for (a) CO_2, (b) C_3H_8 and (c) C_2H_4 on NaX at 20°C.

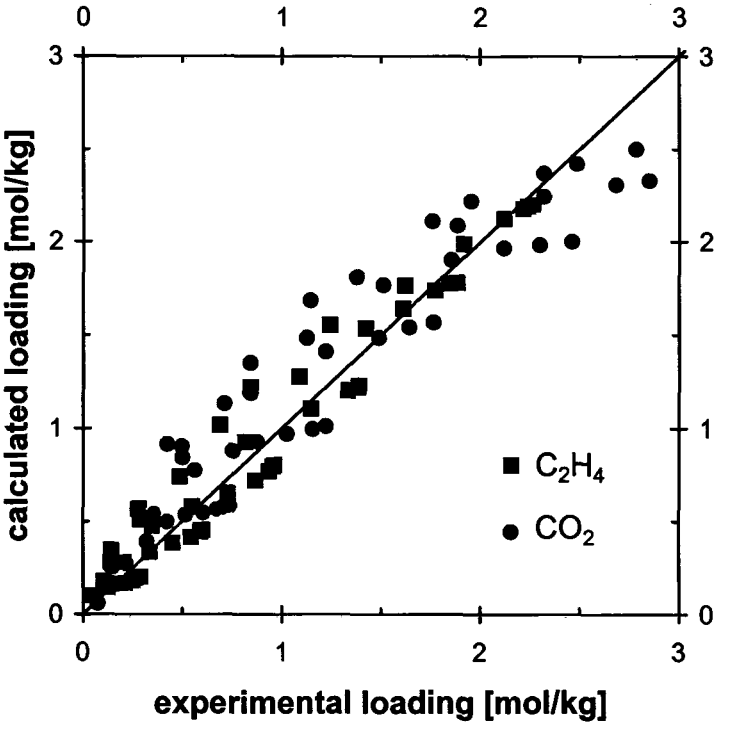

Figure 5.16: Plots of Calculated Loading (from Eq.5.1 with the Parameters Listed in Table 5.1) Against Experimental Loading (Data of Costa et al.[32]) for CO_2/C_2H_4 on NaX at 20°C.

5.4 Conclusions

The ZLC method can be easily extended to the measurement of binary adsorption equilibria. In particular it provides a straightforward way to determine the separation factor as a function of loading and to measure the partial isotherm for one component in an atmosphere of the other. There are, however, some obvious limitations. Clearly the method breaks down for very strongly adsorbed species because of inaccuracy in measuring the very low concentrations in the effluent stream for such species. The method also requires that the affinities of the two sorbates should not be too dissimilar. If the difference in the affinities is too large the two

species desorb sequentially so the separation factor can only be determined at the initial loading point.

The systems studied (CO_2 + hydrocarbon on various cationic zeolites) all show a pronounced decline in separation factor with loading, as is to be expected when one of the components (CO_2) is selectively adsorbed on specific (cation) sites. The single component isotherms and the binary separation factors (and their variation with loading) can all be correlated approximately by the dual site Langmuir model. The binary data correlated in this way are consistent with the reported data of Siperstein and Myers, thus confirming the validity of both the experimental technique and the method of data analysis.

Binary adsorption equilibrium measurements by traditional methods are tedious and time consuming. Adsorbent screening studies are therefore generally based only on single component measurements even though, in some cases, the single component data do not provide a good prediction of the behavior of the binary system. The ZLC method provides a simple and rapid way to measure binary separation factors directly making it potentially useful as a screening tool. Indeed this may well prove to be the most important role for the new technique.

CHAPTER 6

The Effect of Water on the Adsorption of CO_2 and C_3H_8

In previous chapters it was shown that the ZLC method provides a versatile and straightforward approach to the measurement of Henry constants and both single and binary adsorption equilibrium isotherms. The ZLC method also offers the important advantage that it may be easily coupled with temperature programmed desorption (TPD) measurements, thus making it very suitable for measuring the effect of a very strongly adsorbed species such as water, on the isotherm for a weaker species. The practicality of this approach has been demonstrated by measuring the effect of different levels of water on the isotherms for CO_2 (a quadrupolar species) and propane (a non-polar species) on type X zeolites.

The possibility of extending the ZLC technique to the measurement of the water isotherm was also investigated. The results are included in this chapter.

6.1 Experimental Issues for TPD Measurements

The TPD experiment is carried out in the same way as a normal ZLC measurement except that, prior to the isotherm measurement, the adsorbent sample is pre-loaded with water vapor. The sample is then equilibrated, under the experimental conditions, with an inert (He) carrier stream containing a known partial pressure of the sorbate (CO_2). At time zero the flow is switched to a pure He stream and the

desorption curve is measured using an on-line mass spectrometer or other sensitive detector. When the desorption curve is complete the temperature is increased, either continuously or stepwise, to 400°C, with the purge stream still flowing at a constant rate; the TPD response for both residual sorbate and water is recorded. The water loading and any residual (strongly adsorbed) CO_2 are then determined by integration of the TPD response curves. This of course requires calibration of the detector response.

Calibration of the mass spectrometer for CO_2 is straightforward since the relationship between the signal intensity and the CO_2 partial pressure can be obtained directly from the response for a stream containing a known mole fraction of CO_2. This approach is difficult for water since, at the very low partial pressures of interest, water adsorbs strongly on the walls of the tubing etc. As a result the water partial pressure at the detector is not necessarily the same as in the feed stream. An alternative approach was therefore adopted. The zeolite sample was replaced by a ZLC of silicalite, which holds water only rather weakly. Known quantities of water (0.2, 0.4 and 0.7 mg.) were then introduced by syringe (Hamilton 7001KH Syringe) at the upstream side of the ZLC and the TPD curve was measured. The total quantity of water (q') is related to the integral of the TPD response through the mass balance:

$$q' = \int_0^\infty Fcdt = k \int_0^\infty FVdt \qquad (6.1)$$

where F is the He flowrate, k the calibration content and V the signal intensity. Since q', F and the integral are known, the calibration constant is obtained directly. The flow rate is a function of the temperature, which is itself a function of time; therefore, to properly evaluate the integral in Eq.6.1, the temperature increment/time has to be recorded and the flow rate has to be corrected accordingly. Experiments were made with three different water contents. Figure 6.1 represents the TPD response curve for 0.7 mg of water injected into the column. The constant k was evaluated for the three runs according to Eq.6.1. The results were consistent and gave a value for k of 9.215×10^4, for F expressed in ml/sec and q' in mg.

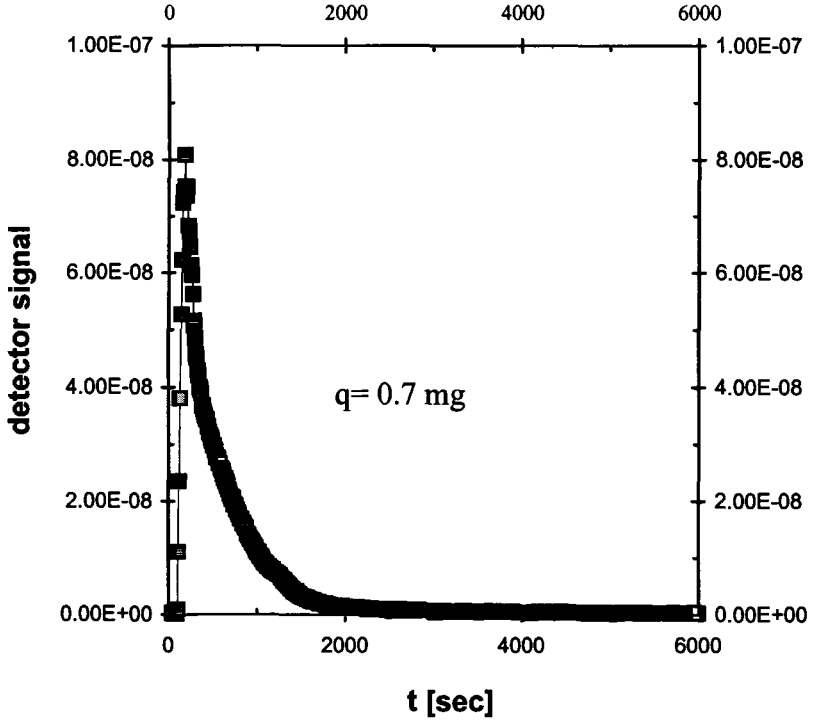

Figure 6.1: Representative TPD Response Curve of Water Calibration Runs. The He flow rate was 10.5 ml/min at 30°C. The temperature was left at 30°C for 2 mins and then raised to 200°C with a 10°C/min increment.

6.2 Dependence of Equilibrium Isotherms on Water Loading

The isothermal ZLC response curve was analyzed in the usual way. At low sorbate concentrations within the Henry's Law region the response is given by:

$$\frac{c}{c_0} = exp\left(\frac{-Ft}{KV_s + V_g}\right) \tag{2.10}$$

Regardless of the concentration level the complete isotherm may be found by integration of the response curve:

$$q^*(p) = \frac{FC}{V_s}\int_0^{\infty}\frac{y}{1-y}dt - \frac{FC}{V_s}\int_0^{t}\frac{y}{1-y}dt - \frac{V_g C}{V_s}y \tag{2.18}$$

The sorbates studied (CO_2 and C_3H_8) are both fairly strongly adsorbed at the relevant temperatures so dead volume corrections were not important. As with all ZLC equilibrium measurements, the response curve, plotted as $\ln(c/c_0)$ vs. Ft should be independent of flow rate. Measurements of at least two flow rates are therefore needed to confirm a close approach to equilibrium.

The adsorbents studied were CaX, LiLSX and NaLSX. Details of these adsorbents are given in Chapter 4. A representative example of the ZLC response curve and the associated TPD response are shown in Figure 6.2. Equilibrium isotherms for CO_2 at various water loading levels are shown in Figures 6.3–6.5;

equivalent data for C_3H_8 on NaLSX at 35°C are shown in Figure 6.6. As expected the equilibrium capacity for CO_2, at a given partial pressure, is strongly reduced by the presence of water and this reduction is much more pronounced for CO_2 than for C_3H_8.

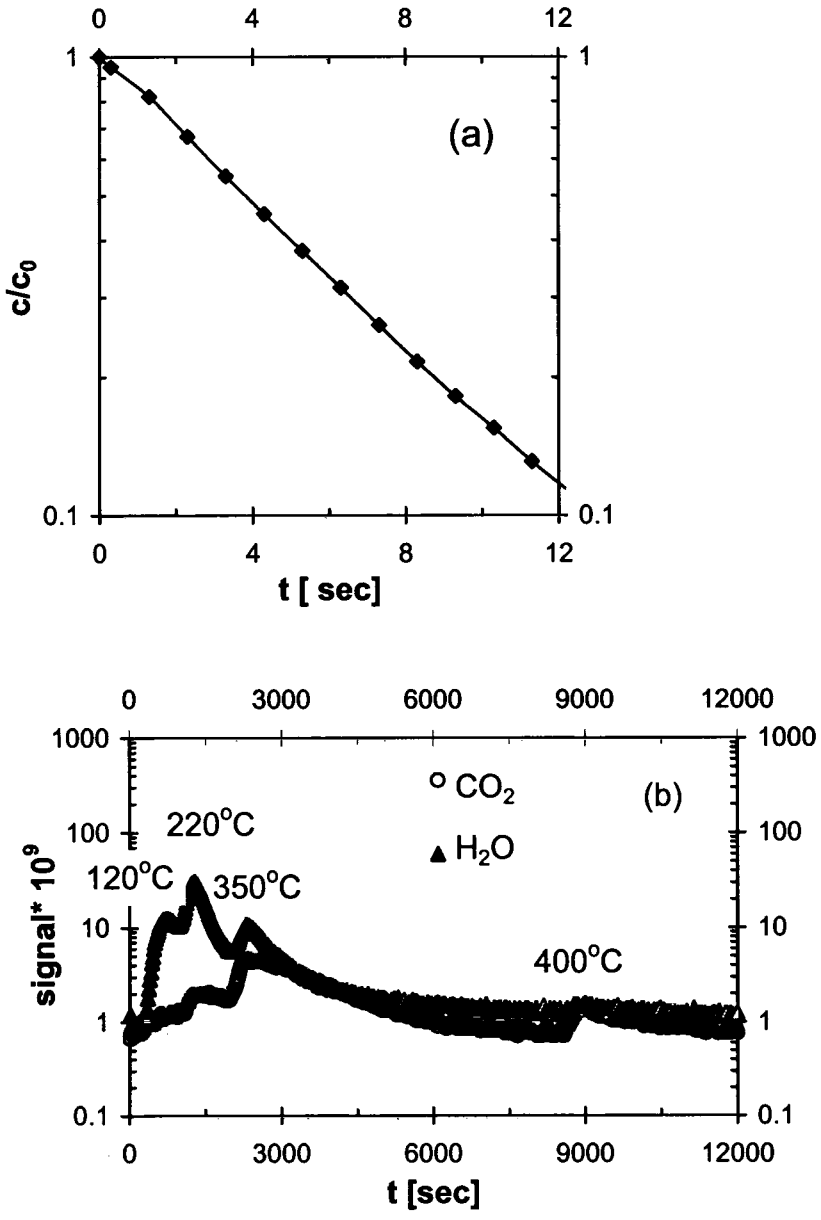

Figure 6.2: (a) Representative ZLC Response Curve and (b) Corresponding TPD Curves for NaLSX at 35°C, Pre-Loaded with 15.4 wt% H_2O. Initial CO_2 pressure= 47 Torr.

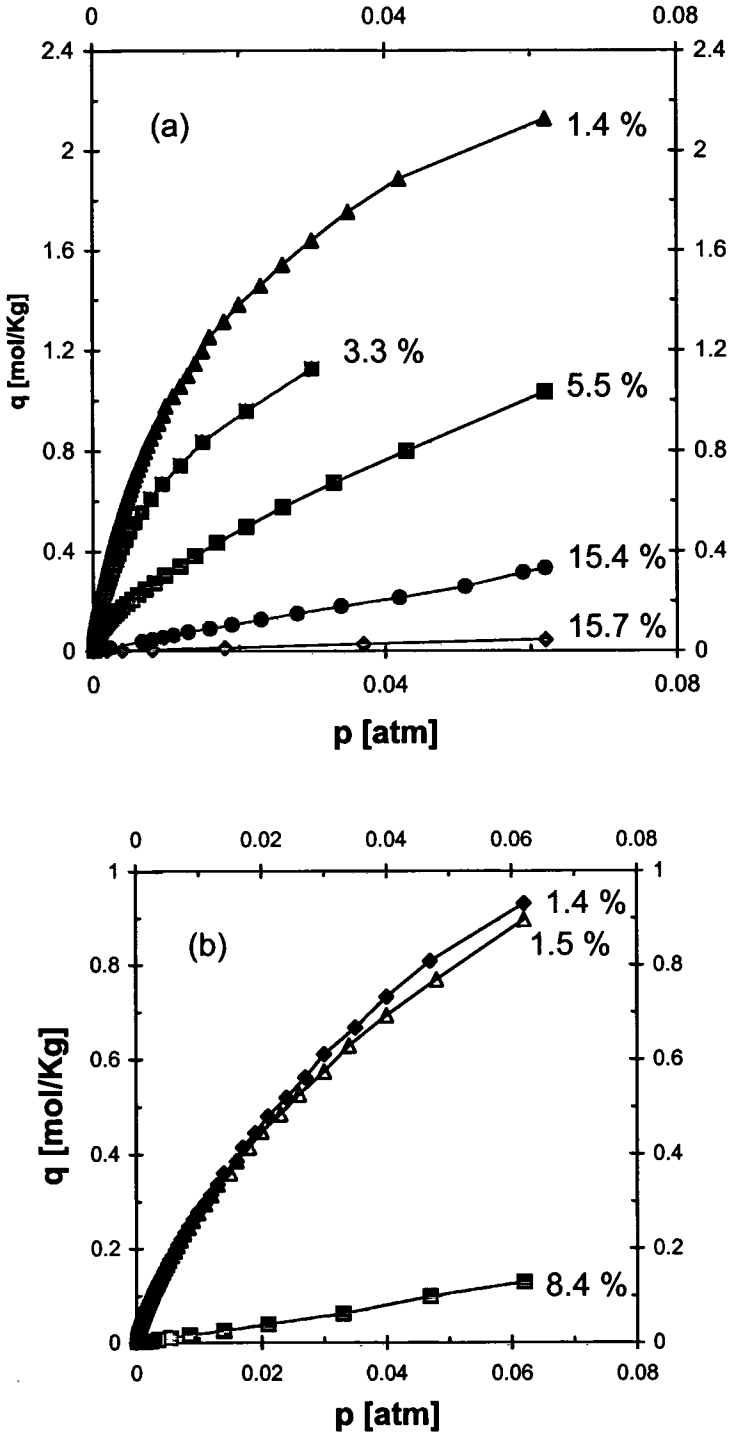

Figure 6.3: Equilibrium Isotherms for CO_2 on NaLSX at (a) 35°C and (b) 70°C Showing Effect of Water (wt%).

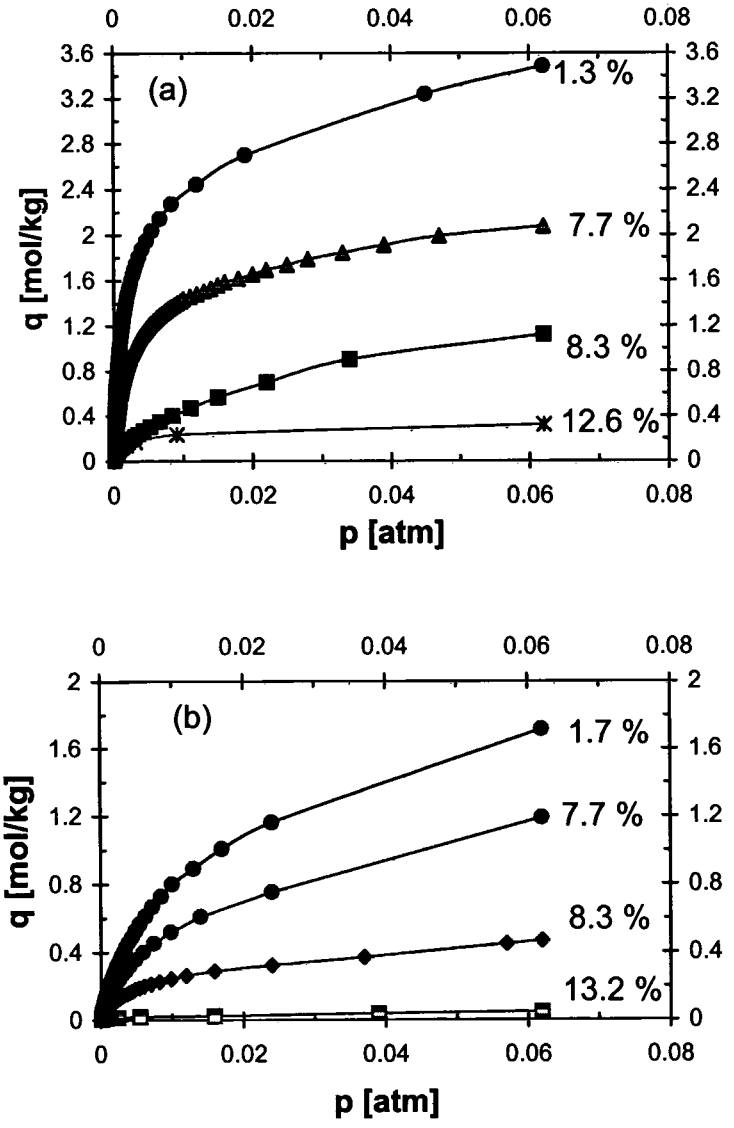

Figure 6.4: Equilibrium Isotherms for CO_2 on LiLSX at (a) 35°C and (b) 75°C Showing Effect of Water (wt%).

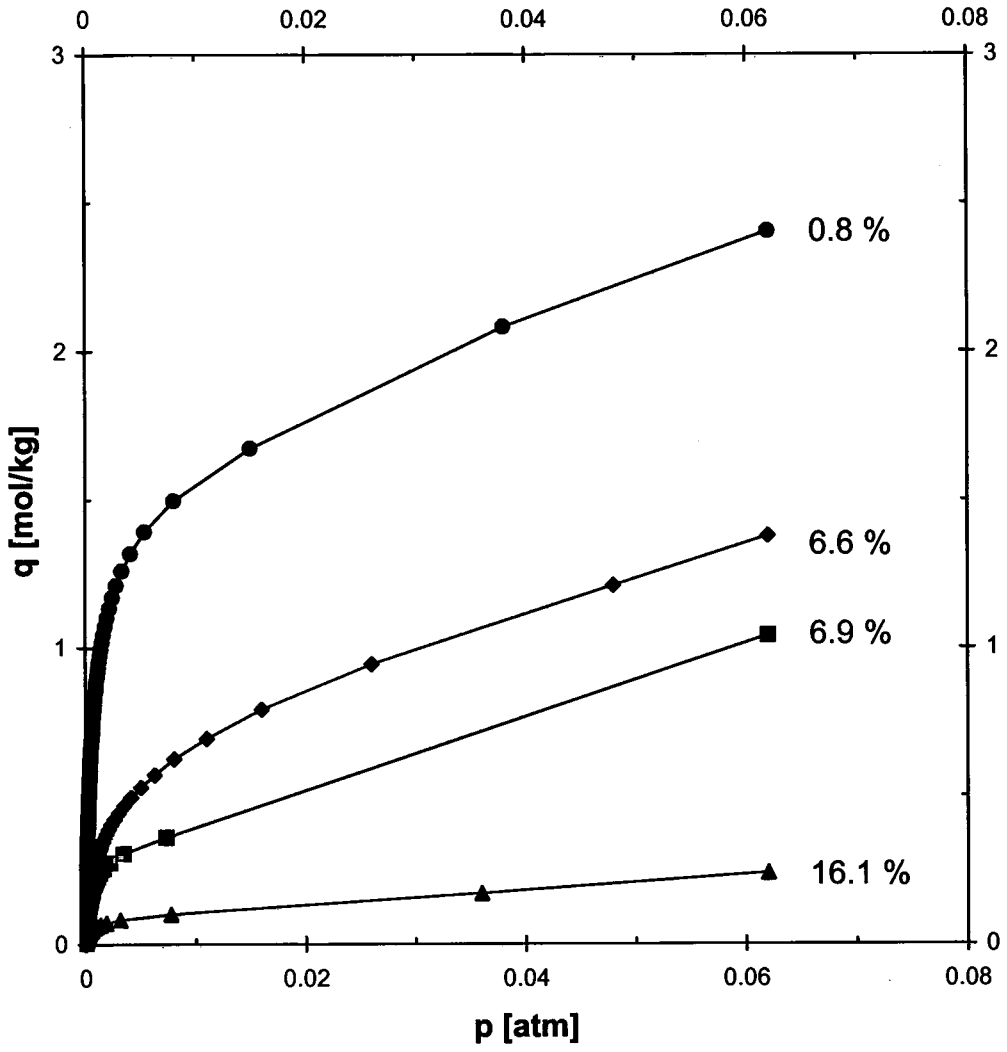

Figure 6.5: Equilibrium Isotherms for CO_2 on CaX at 50°C Showing Effect of Water (wt%).

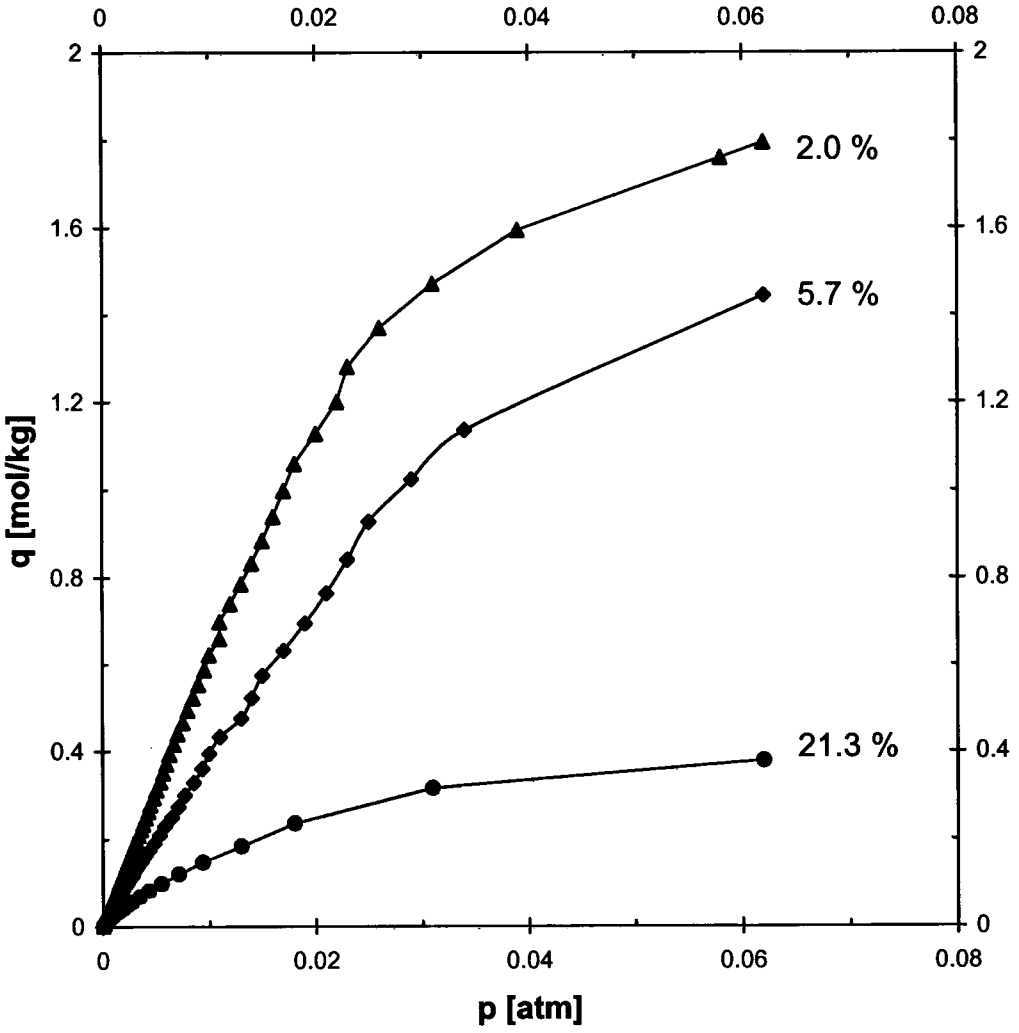

Figure 6.6: Equilibrium Isotherms for C_3H_8 on NaLSX at 35°C Showing Effect of Water (wt%).

In order to quantify this effect Henry constants were calculated and correlated with water loading – see Figures 6.7–6.10. For all adsorbents and temperatures the experimental data reveal an exponential dependence of Henry constant with loading:

$$\frac{K}{K_0} = exp(-\alpha x) \tag{6.2}$$

where x is the water loading. For NaLSX and LiLSX the isotherm measurements were made at two different temperatures (35°C and 70°C). Although the temperature range is modest, both data sets suggest that the parameter α increases approximately in proportion to the absolute temperature. For CO_2 the effect of water is clearly strongest for NaLSX and weakest for CaX, as may be seen from the values of α which are summarized in Table 6.1. The data for C_3H_8 on NaLSX conform to the same general pattern but the effect is much weaker (smaller α).

Table 6.1: Summary of Parameters α and K_o Giving Variation of Henry Constant for CO_2 with Water Loading

Sorbent	Sorbate	T (Deg.C)	α $(wt.\%)^{-1}$	$K_0 \cdot \left(\frac{mmol}{gm \cdot atm}\right)$
NaLSX	C_3H_8	35	0.041	70
	CO_2	35	0.37	619
		70	0.47	95
LiLSX	CO_2	35	0.195	2900
		75	0.215	426
CaX	CO_2	50	0.198	2240

The strong decrease in the isotherms for CO_2 with water loading is to be expected from general theoretical considerations. Water, being strongly polar, is adsorbed strongly on the exchangeable cations, thus reducing the strength and heterogeneity of the electric field. C_3H_8 is a non-polar molecule so the energy of adsorption depends mainly on van der Waals forces with only a relatively minor contribution from electrostatic interaction in the form of the polarization energy. In contrast CO_2 has a high quadrupole moment and the field gradient-quadrupole interaction contributes substantially to the adsorption energy. For such a system any reduction in the strength and heterogeneity of the electric field will obviously have a major impact on the adsorption isotherm.

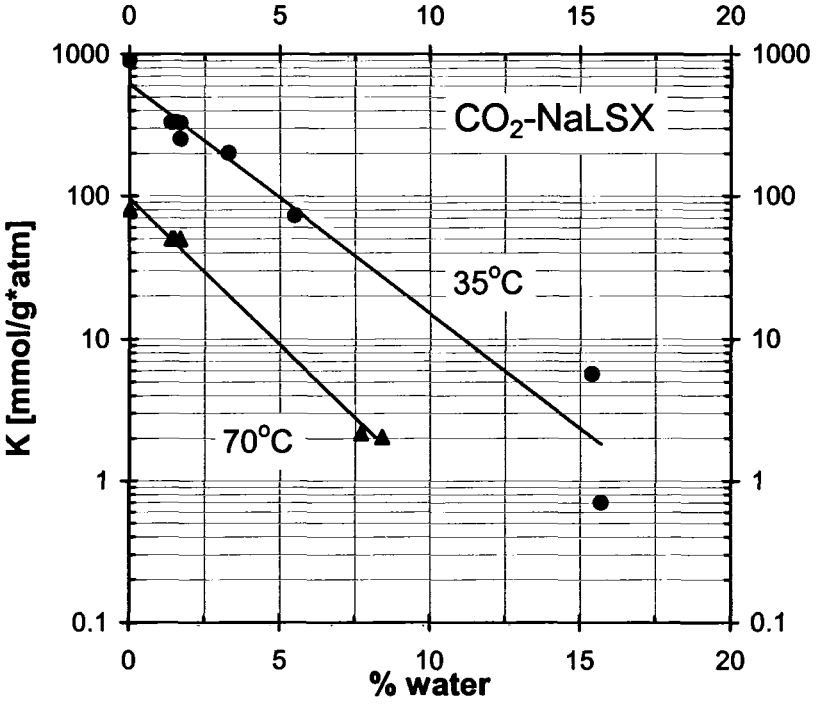

Figure 6.7: Variation of Henry Constant for CO_2 on NaLSX with Water Loading

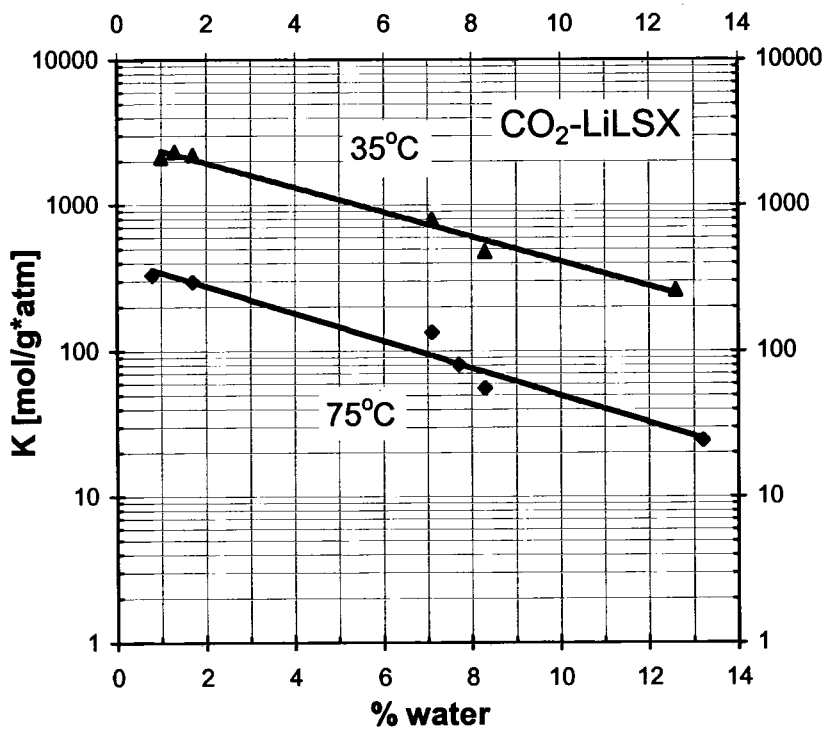

Figure 6.8: Variation of Henry Constant for CO_2 on LiLSX with Water Loading.

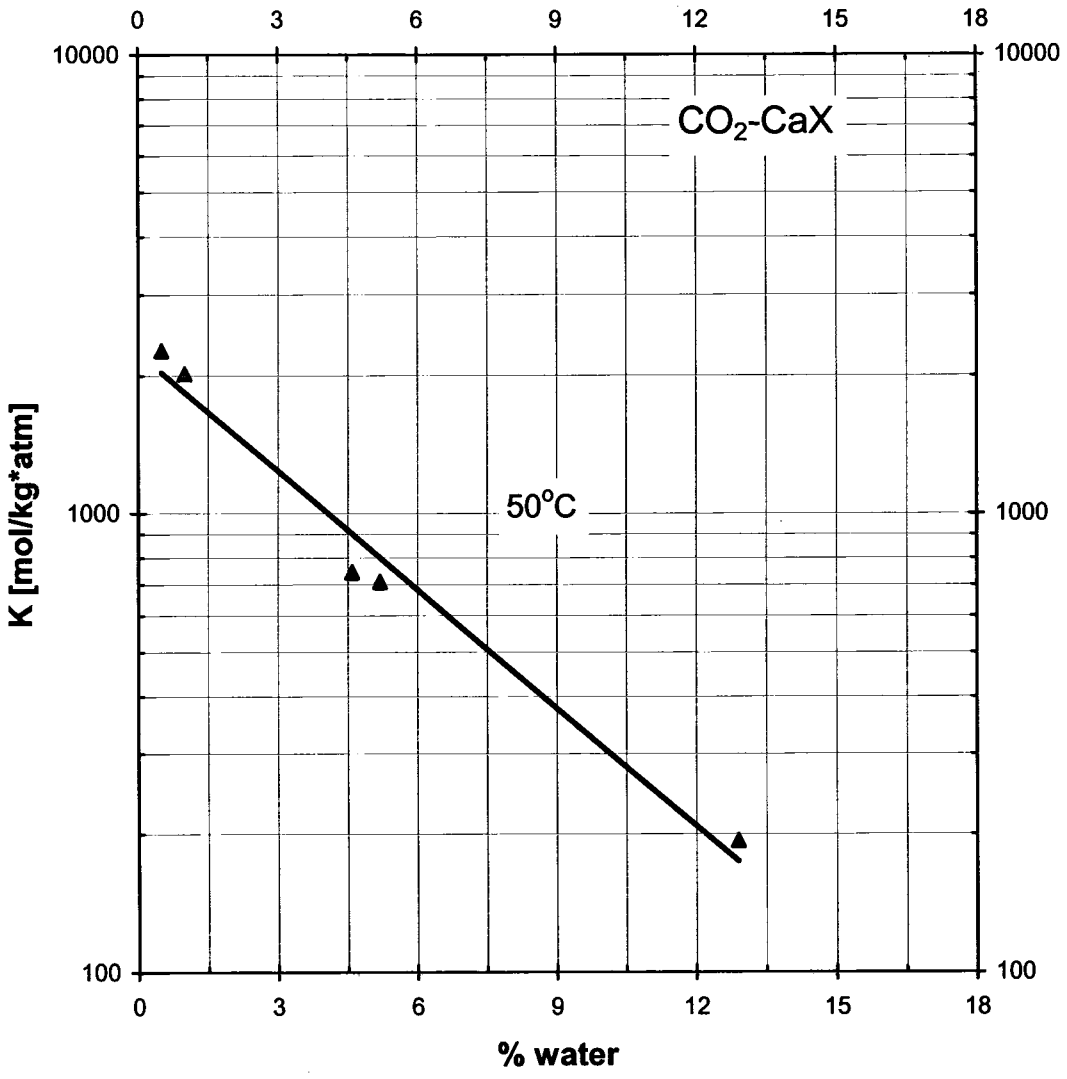

Figure 6.9: Variation of Henry Constant for CO_2 on CaX with Water Loading.

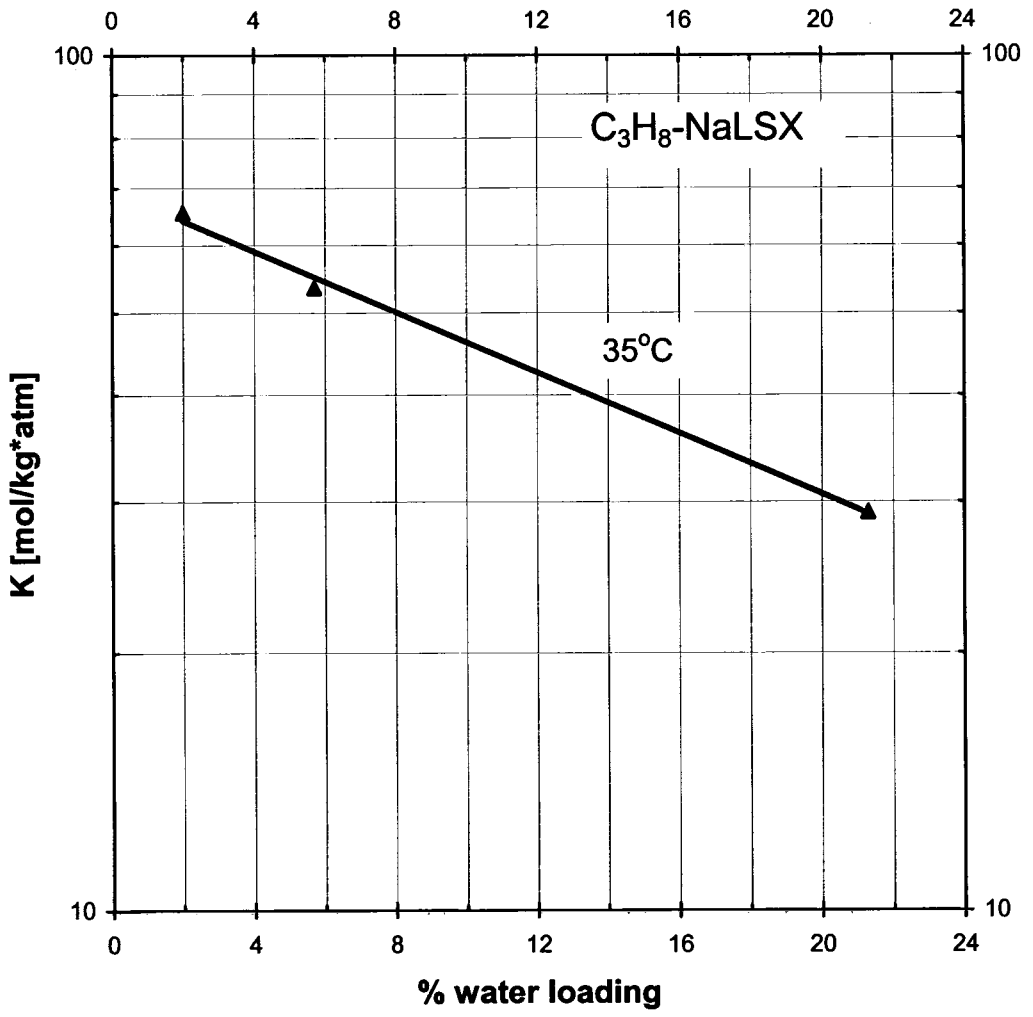

Figure 6.10: Variation of Henry Constant for C_3H_8 on NaLSX with Water Loading.

The initial expectation was that, in NaLSX and LiLSX, water would be expected to be adsorbed preferentially on the exposed type III cations (approximately 3 per supercage). It was therefore expected to see a sharp drop in the Henry constant at a loading corresponding to saturation of these sites by water (approximately 3 wt.%). In fact the experimental data reveal that the exponential decline in the Henry constant continues uninterrupted to substantially higher water loadings. It seems clear

that the presence of water mainly affects the average interaction energy for the sorbate, rather than being site specific. This would be consistent with a delocalized model in which the guest CO_2 molecules are mobile within the supercage, rather than being confined at a particular site (see section 1.1).

If it is assumed that the dimensionless average enthalpy of adsorption (for CO_2) decreases linearly with the water loading the result is:

$$\frac{\Delta H}{RT} = \frac{\Delta H_0}{RT} - \alpha x \tag{6.3}$$

and since the Henry constant is related to the energy through the vant Hoff equation and the Henry constant for a dry adsorbent (K_o) is given by:

$$K_0 = K_\infty \, exp\left(-\frac{\Delta H_0}{RT}\right) \tag{6.4}$$

This yields the form of Eq.6.2. To explain the observed correlation fully requires only the further assumption that the constant of proportionality (α) is proportional to the absolute temperature.

6.3 Residual Loading Data

In addition to providing an accurate measurement of the adsorbed water the TPD data yield information concerning the ease with which the water is desorbed and a quantitative measurement of any residual sorbate (CO_2 or C_3H_8) which is not

removed during the isothermal ZLC desorption experiment. The results are summarized in Table 6.2. No residual propane was detected, indicating complete desorption at 35°C in the ZLC experiments. The values for both residual CO_2 and high temperature water show a good deal of scatter from run to run. Residual CO_2 does not appear to be directly related to water loading except that, when water loading is very high (>7%) we see also high residual CO_2. Both total residual CO_2 and high temperature residual CO_2 (desorbed above 300°C) appear to be independent of water loading. It may be reasonable to assume that

Table 6.2: Total and High Temperature (>300°C) Residual CO_2

Sorbent	HT CO_2	Total CO_2 (m.mole/g)
NaLSX	0.13	0.23
LiLSX	0.05	0.17
CaX	0.09	0.24

the difference between these two quantities reflects reversibly but strongly adsorbed CO_2 that would eventually be desorbed at low temperature after prolonged purging. However, the high temperature residual CO_2 (about one half to one third of the total residual CO_2) clearly represents CO_2 that is held essentially irreversibly. From infrared spectroscopic data Bertsch and Habgood[34] concluded that a small fraction of the adsorbed CO_2 (up to 0.15 m.mole/g) is held essentially irreversibly in the form of either a carbonate or carboxylate. The data obtained are quantitatively consistent with this conclusion although the TPD technique does not provide any evidence as to the form in which the strongly bound CO_2 is held.

The high temperature residual water, for CaX, shows a clear trend with total water loading up to about 4.0 m.mole/g and a more or less constant value (~1.5 m.mole/g) at higher water levels – see Fig. 6.11. The data for NaLSX and LiLSX show more scatter. The general trend is qualitatively similar although the plateau value (about 0.3 m.mole/gm) is substantially smaller. The strongly held water probably represents water held at defect sites.

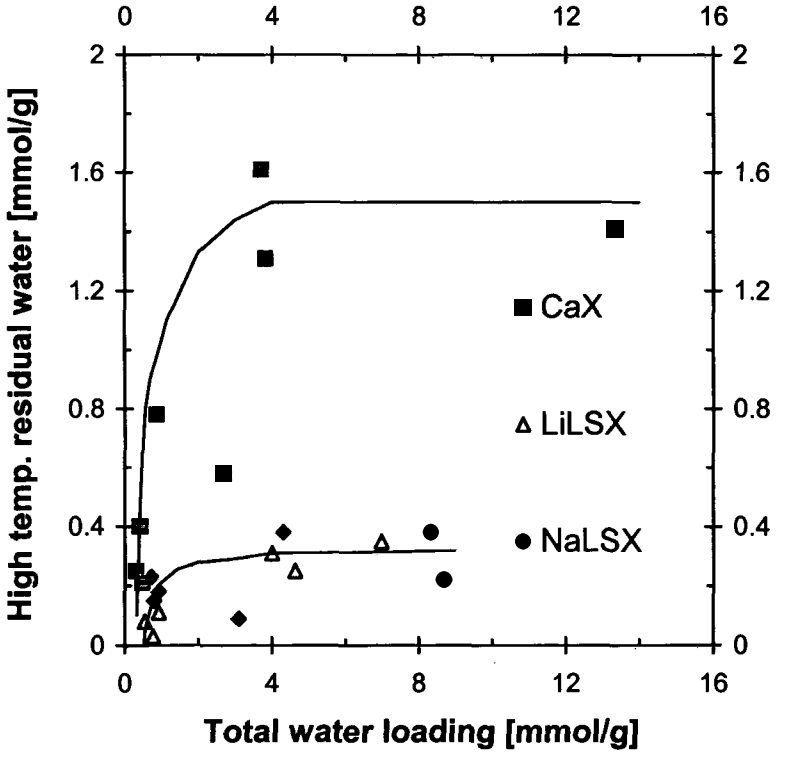

Figure 6.11: Variation of High Temperature Residual Water with Total Water Loading.

Spectroscopic evidence suggests that the water is adsorbed in molecular form rather than as hydroxyls (Bertsch and Habgood[34]).

6.4 Spectroscopic Data

Early infrared spectroscopic studies carried out by Ward and Habgood[35] suggest that, in zeolite X, CO_2 is present mainly in physisorbed but also to a minor extent in chemisorbed forms. Evidence for chemisorption comes from bands at 1700 and at 1340 cm^{-1} (approx.) which were attributed to carbonate like structures. These bands were more intense for NaX than for LiX and essentially absent in CaX.

Essentially similar results were found in a recent study carried out at the Air Products Laboratory in a DRIFT system. The TPD data for CO_2 in LiLSX and NaLSX appear to be quite consistent with these observations since the high temperature residual CO_2 (presumably corresponding to the carbonate like form identified spectroscopically) was present at substantially higher concentrations in NaLSX and NaX than in LiLSX. Very little if any carbonate was observed in either CaA or CaX, suggesting that carbonate formation may require the presence of cations in type III sites. The spectra for CO_2 adsorption on LiLSX, NaLSX and CaX are shown in Figures 6.12-6.14.

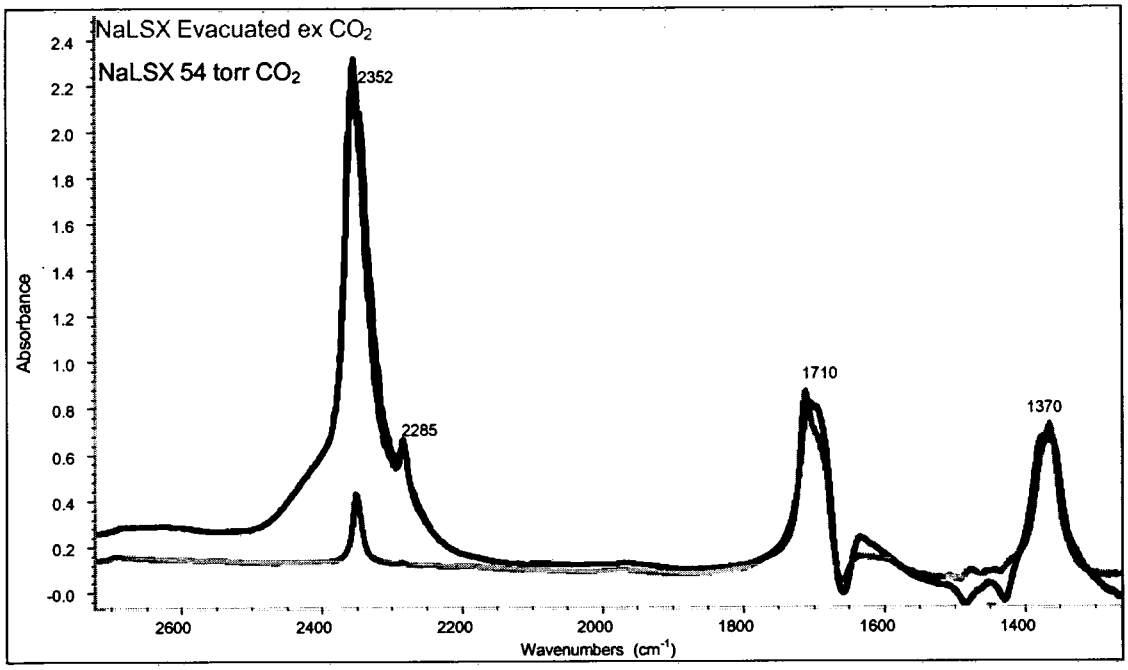

Figure 6.12: IR Spectra for CO_2 on NaLSX. The large complex peak in the region of 2300 cm^{-1} represents physisorbed CO_2. The peaks at about 1710 and 1370 cm^{-1} represent the carbonate species

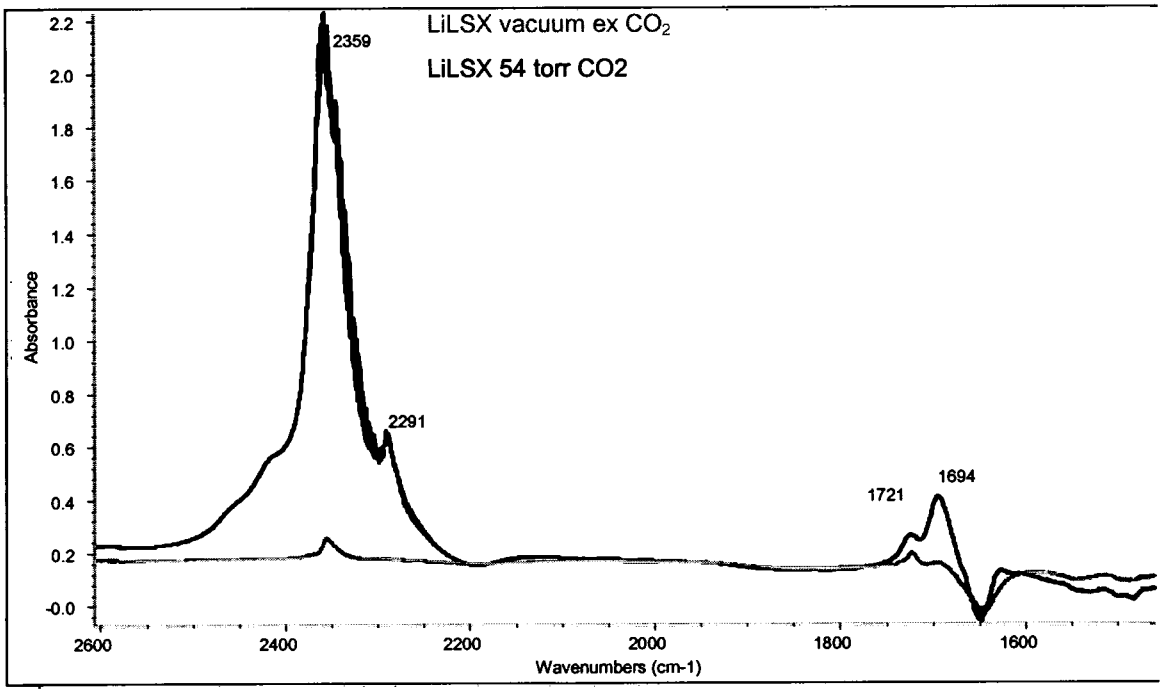

Figure 6.13: IR Spectra for CO_2 on LiLSX. The large complex peak in the region of 2300 cm^{-1} represents physisorbed CO_2. The peaks at about 1710 and 1370 cm^{-1} represent the carbonate species.

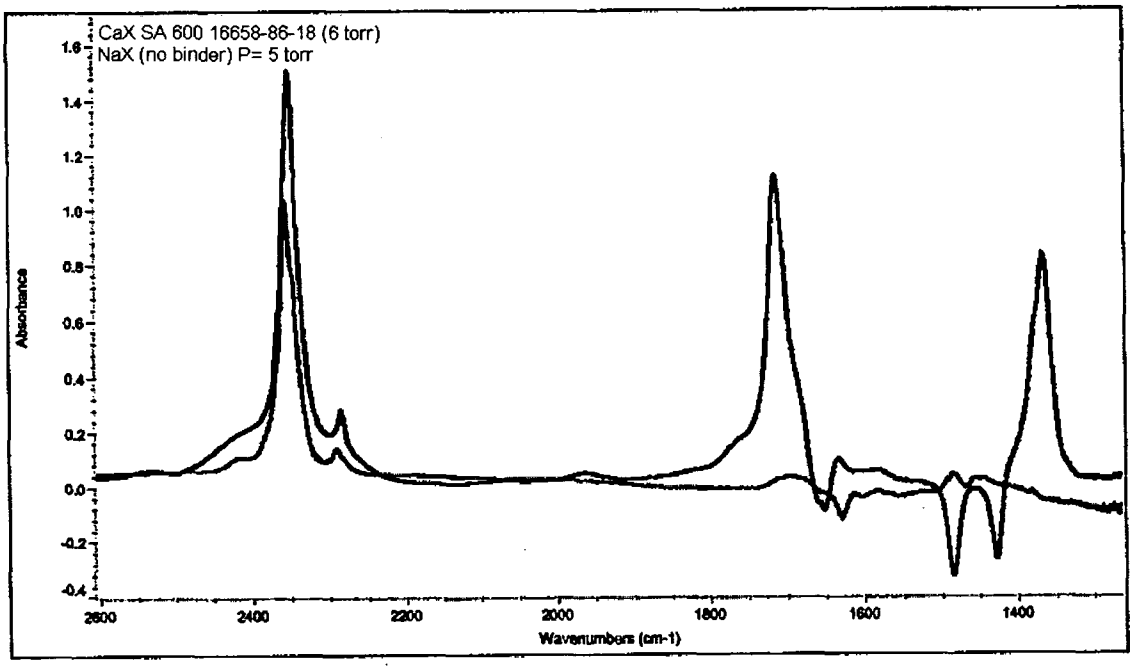

Figure 6.14: IR Spectra for CO_2 NaX and CaX. The large complex peak in the region of 2300 cm^{-1} represents physisorbed CO_2. The peaks at about 1710 and 1370 cm^{-1} represent the carbonate species. Note that these peaks are essentially absent from the CaX spectrum .

6.5 Measurement of Water Isotherms

At ambient temperatures water is very strongly (indeed almost irreversibly) adsorbed on cationic rich zeolites. Such highly favorable isotherms are not amenable to measurement by the ZLC technique since desorption occurs only very slowly and at extremely low water partial pressures. However, the strength of adsorption is greatly reduced at elevated temperatures so it was decided to attempt to measure the water isotherm for 4A zeolite at 149°C (300°F).

To measure the ZLC response curve for water the experimental system was modified to include a bubbler, maintained at 0°C in an ice bath. This provided a

constant water vapor pressure of about 4.6 Torr in the saturated He stream. The ZLC was equilibrated with the stream at the selected temperature and then, at time zero, the valve was switched to purge the sample with a dry He stream.

The ZLC desorption curve is shown in Figure 6.15a and the corresponding isotherm, derived by integration of the ZLC response curve according to Eq.2.18. is shown in figure 6.15b.

Following completion of the desorption curve at 149°C the temperature was raised to 400°C (from 149°C to 250°C at 34°C/min, then the sample was left at 250°C for 30 mins, then from 250°C to 325°C at 25°C/min, then left at 325°C for 170 mins and finally from 325°C to 400°C at 19°C/min) and the TPD desorption curve, shown in Figure 6.16, was obtained. The residual water loading from the TPD measurement is 2.9 mmole/gm, which is actually somewhat greater than the amount of water desorbed during the ZLC experiment. In order to estimate the isotherm, the quantity of water desorbed in the TPD (2.9 mmole/gm) was added to the ZLC isotherm, to yield the composite isotherm curve shown in Figure 6.17. This isotherm is similar to the published UOP isotherm for 4A sieve at this temperature although the slope is different.

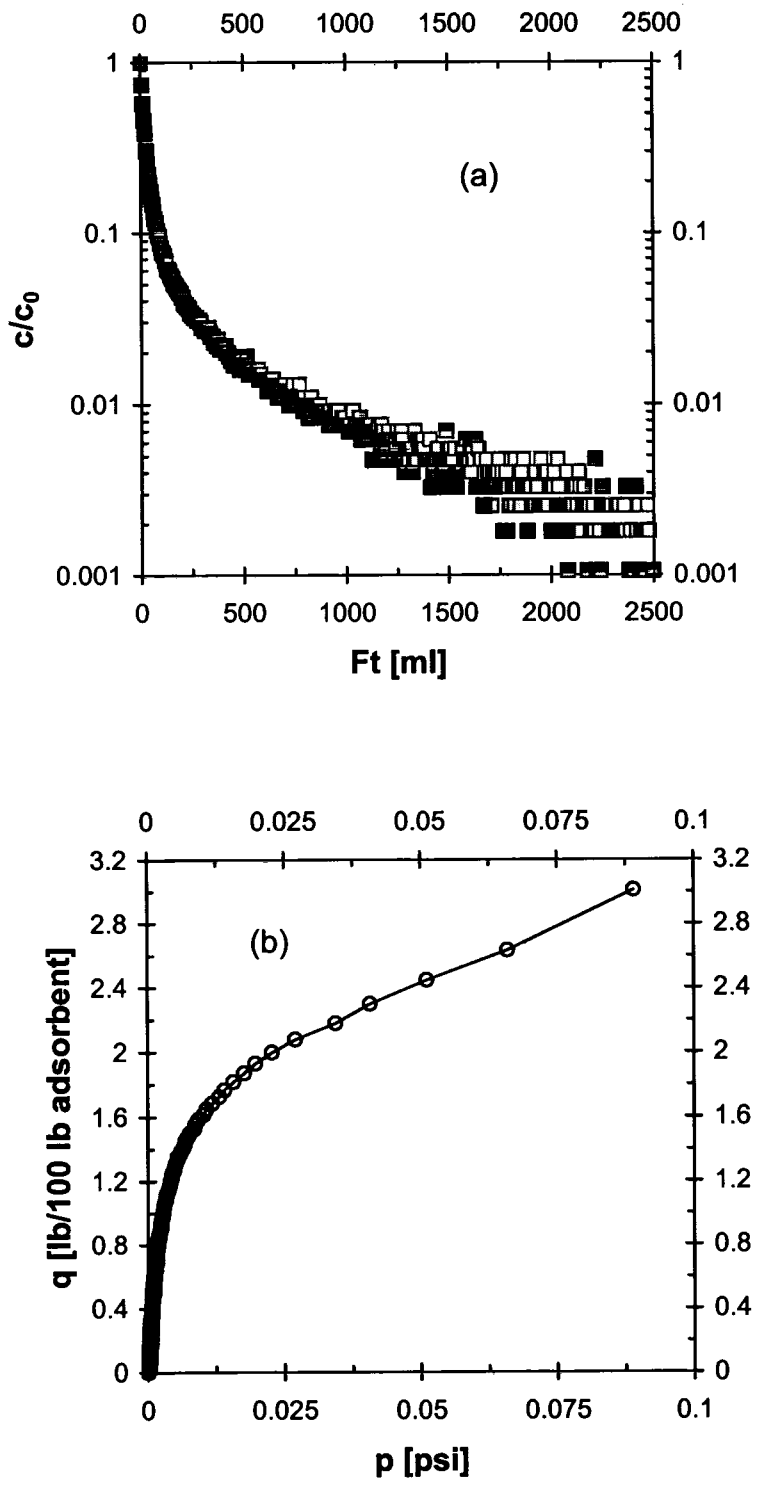

Figure 6.15: (a) ZLC Response Curve for H_2O-4A at 300°F Plotted vs. Ft and (b) Corresponding Isotherm.

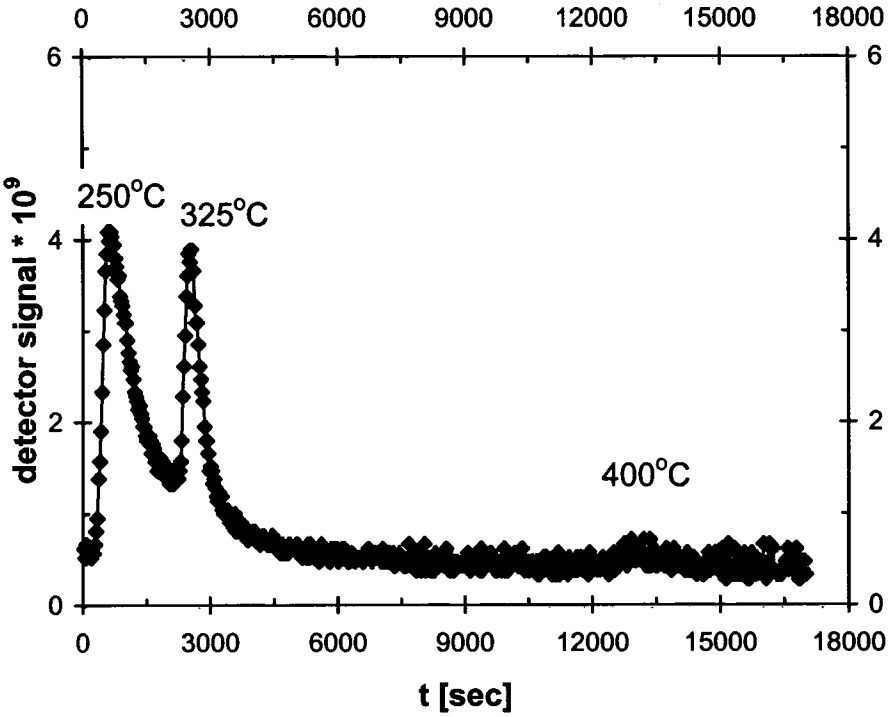

Figure 6.16: TPD Response Curve for H_2O-4A, with a Dry He Flow Rate of 15.0 ml/min (at 149°C).

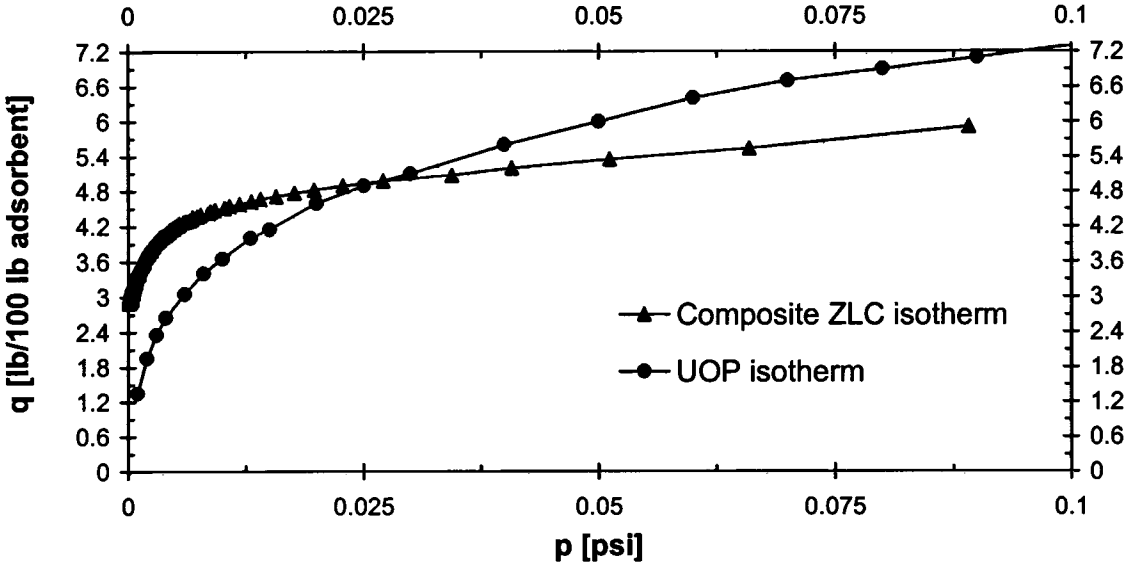

Figure 6.17: Comparison of ZLC Composite Isotherm for H_2O-4A (Obtained from Isotherm in Figure 6.13b by Adding 2.9 mmol/g of Residual Water Determined from TPD) with UOP Isotherm.

The conclusion drawn from these studies was that, even at elevated temperatures, the ZLC method does not provide a quantitatively useful technique for measuring the isotherms for water on cationic zeolites. It seems reasonable to assume that the water isotherm for a weaker desiccant, such as silica gel, could indeed be determined in this way. However, since the focus of this research was on zeolite adsorbents, this was not pursued.

6.6 Conclusions

With TPD measurements the ZLC technique provides a useful method for studying the effect of water on the CO_2 isotherm. The results show an exponential decrease of the Henry constant with water loading. As expected the effect on a non-polar species such as C_3H_8, is weaker than that on a quadupolar molecule such as CO_2. In addition TPD measurements provide a simple way to verify for complete desorption and to measure quantitatively any strongly held residuals. The data obtained with TPD measurements are consistent with spectroscopic results which show that a small fraction of CO_2 is adsorbed as carbonate or carboxylate.

It was also shown that the ZLC technique does not work well for measuring water isotherms on hydrophilic zeolite materials.

CHAPTER 7

Conclusions and Recommendations

This study has been focused on the development of the ZLC technique with respect to its application to the experimental measurement of adsorption equilibria. The main advantages and limitations of this approach have been noted in Chapters 4-6 in the conclusions and discussions of the results obtained from the experimental studies. This information is summarized and reviewed in the present chapter in order to present an overview of the advantages and disadvantages of this technique in comparison with more conventional methods for measurement of adsorption equilibria. In the present study the ZLC approach has been applied to three distinct problems: measurement of single component Henry constants and equilibrium isotherms; measurement of separation factors in binary adsorption systems; determination of strongly held residual adsorption by TPD. This review will follow the same sequence

7.1 General Considerations

The ZLC method depends on following the desorption curve measured at a sufficiently slow flow rate that the gas leaving the ZLC cell is essentially at equilibrium with the adsorbed phase. This clearly places limits on its applicability. For example the method would generally not be applicable to chemisorption systems in which there is a significant activation energy for adsorption/desorption. Even for

physical adsorption the method will break down for very strongly (irreversibly or nearly irreversibly) adsorbed species. For such systems the sorbate will be desorbed only at very low partial pressures, outside the range of accurate measurement, and at an overall rate that is extremely slow, making the desorption time unacceptably long. This behavior is exemplified by the water-4A system discussed in section 6.5.

The ZLC isotherm measurement depends on achieving essentially complete desorption under isothermal conditions. If desorption is incomplete the results will clearly be in error. It is therefore desirable to run a TPD experiment at the end of the ZLC measurement, at least during initial studies of a new system, to confirm that desorption is indeed complete. This is easily accomplished simply by raising the temperature at the end of the run.

In the analysis of the ZLC response isothermal behavior is assumed. The validity of this assumption has to be considered, especially when the method is applied to sorbates with a high heat of adsorption. However, such sorbates will generally have a highly favorable isotherm so the applicability of the method would in any case be restricted by irreversibility, as discussed above.

For the range of systems where the ZLC method is applicable (moderately to weakly adsorbed species) the issue of non-isothermality is in fact less severe than may appear at first sight. The major resistance to heat transfer is the gas film resistance (Ruthven[3]) and this varies with flow rate. The standard test of making replicate measurements at different purge flow rates and confirming the invariance of the response curve plotted in terms of the product Ft (see section 4.1). should

therefore detect any intrusion of thermal effects in addition to confirming mass transfer equilibrium.

The above considerations restrict the applicability of the method for very strongly adsorbed species. The method also fails when adsorption is very weak. To make accurate equilibrium measurements it is essential that the quantity of the sorbate adsorbed is at least comparable with and preferably greater than the amount contained in the gas phase within the dead volume of the ZLC cell (and associated piping) - see section 3.4 -. In quantitative form the criterion is $KV_s \geq V_g$. For weak adsorbents (small K) this criterion can sometimes be satisfied by increasing the quantity of the adsorbent (but there are limits to this approach since when the adsorbent bed becomes too large the basic assumption of ZLC behavior obviously breaks down) or by lowering the experimental temperature. In practice, based on the experience gained in this study, ZLC measurements become challenging when the dimensionless Henry constant (K) is less than about 30 and unreliable when K is less than 15.

With strongly hydrophilic adsorbents it is essential to keep all traces of water out of the system. This requires careful attention to the drying of the gases, elimination of all leaks and high temperature *in situ* degassing the adsorbent. With careful attention to such details it is indeed possible to keep the system dry but this is certainly more difficult in a ZLC system where there is a continuous flow of carrier or purge gas than in a conventional volumetric or gravimetric system. Of course with hydrophobic adsorbents or even moderately hydrophilic materials this is no longer a significant issue.

7.2 Single Component Systems

For single component systems the ZLC method provides a simple and convenient way of estimating the Henry constant directly from the limiting slope of the ZLC response curve and for determining the full isotherms (by integration of the response curve). The purge flow rate must be properly chosen to fulfill the requirements noted above and replicate measurements at different purge rates should be made to confirm the validity of the basic assumptions of the method. The blank response should also be determined to confirm that the requirement $KV_s \geq V_g$ is fulfilled. This is particularly important for weakly adsorbed species. A TPD measurement should also be run at the conclusion of the ZLC experiment to confirm that any residual amounts of strongly held sorbate are negligible or, if not negligible, to allow a proper correction to be applied to the ZLC isotherm.

Even allowing for the time required to complete the replicate runs and blank response measurements the ZLC technique is relatively rapid, allowing a complete isotherm to be measured in minutes rather than hours or days as for conventional piezometric/volumetric or gravimetric measurements. However, because of errors in the measurement of the flow rate and partial pressures and in the weight of the sample (which is only a few mg) as well as the possibility that small amounts of residual sorbate may not be detected, the ZLC Henry constants and isotherms are probably subject to somewhat greater overall errors than conventional gravimetric or volumetric measurements. The experience gained in this study however shows that, for identical adsorbent samples, agreement is achieved within 5-10%, which may be

considerd as best estimate of the overall margin of uncertainty. While the method cannot compete with conventional methods in terms of accuracy its advantages in term of speed and simplicity are overwhelming. The greatest potential use of the technique is therefore for rapid screening studies where high accuracy is secondary to time requirements.

7.3 Binary Systems

While traditional methods of measuring single component isotherms are straightforward, even if somewhat time consuming, the measurement of binary and multicomponent adsorption equilibria by conventional methods is very labor intensive, requiring point by point measurements of both pressures and compositions. The mass balances required to determine the adsorbed phase loading must be carefully executed to avoid cumulative errors. In adsorbent screening studies it is therefore common practice to rely simply on estimating separation factors based on the ratio of the single component Henry constants. However, as shown in Chapter 5, this assumption is often invalid except at very low loadings. There is therefore a real need for a simple and rapid method for measuring separation factors in binary (and higher order multicomponent) systems at loadings beyond the Henry's Law range. The binary ZLC technique appears to have the potential to fill this requirement.

Of course the binary measurements are subject to the restrictions and limitations noted above (for example proper choice of flow rate, dry system etc) and in addition the method only works well when the two components have similar

affinities. It is however precisely for such systems that binary equilibrium measurements are often required. It has been shown in Chapter 5 that binary separation factors measured by the ZLC method agree well with the values determined by conventional methods but the time required for the measurement is substantially smaller. The method thus appears to be viable and potentially useful, subject to the limitations already noted. As with the single component measurements the greatest use of the ZLC technique is likely to be in screening studies where a simple, rapid approximate measurement of the separation factor is required, under particular conditions, at a loading beyond the Henry region.

It is in principle possible to map the complete binary isotherm from a sufficiently large number of binary ZLC measurements with properly selected different feed compositions. However this requires a relatively large number of individual experiments so the major advantages of speed and simplicity are largely dissipated.

7.4 TPD Measurements

The ZLC method fits very well with temperature programmed desorption (TPD). This greatly increases the value and reliability of the method by providing a simple way to check for complete desorption and to measure quantitatively any strongly held residuals. The applicability of this method has been demonstrated in Chapter 6 by using this approach to measure the effect of water on the equilibrium isotherms for CO_2. Such data is practically important in its own right as it reveals the

great sensitivity of CO_2 selective adsorbents to deactivation by relatively small amounts of water. The method is simple and relatively easily executed, requiring only the calibration of the detector (in addition to fulfilling the normal pre-conditions for reliable ZLC measurements). The same approach could obviously be used to study the effect of other strongly adsorbed species on the isotherms for a weaker sorbate.

7.5 Effect of Cations on CO_2 Adsorption

In Chapter 5 the ZLC method was used to measure the isotherm for CO_2 on a range of different cationic zeolites. The results show clearly the dependence of the Henry constant on the number and nature of the cations and the densities of adsorption sites deduced from the isotherm agree reasonably well with structural information on the occupancy levels of the cationic sites. Clearly such studies could be extended to other sorbates and adsorbents. By making it possible to carry out isotherm measurements relatively rapidly the possibilities for using such measurements to explore structural relationships are obviously enhanced.

7.6 Recommendations

The main focus of this study was to explore the potential of the ZLC technique as a method for equilibrium measurements and to establish its advantages and limitations. This has been accomplished and further studies aimed simply at validating this approach are probably not needed. There is however considerable

scope for further application of the technique both to explore the structural relationships and for measuring binary and multicomponent equilibria. One obvious development would be to extend the method to measurement of isotherms at pressures higher than atmospheric. In principle this requires only the addition of a suitable pressure controller but in practice this may prove difficult

to control both the pressure and the flow rate and, of course, leakage problems will become more severe at higher pressures.

The present experimental system was built and modified as experience was gained. If further work is to be continued it would be desirable to reconstruct the system to higher specifications with a well thought out layout.

REFERENCES

1. L.V.C Rees and D. Shen, *Studies in Surface Science and Catalysis* 137, 579-631 2nd Completely Revised and Expanded Edition, Elsevier, Amsterdam (2001).
2. D.M. Ruthven and M.F.M. Post, *Studies in Surface Science and Catalysis* 137, 525-577 2nd Edition, Elsevier, Amsterdam (2001).
3. D.M. Ruthven, *Principles of Adsorption and Adsorption Processes*, J. Wiley, New York (2001).
4. E. van der Vlist and J. van der Meijden, *J. Chromatography* 79, 1 (1973).
5. D.M. Ruthven and R. Kumar, *Ind. Eng. Chem. Fund.* 19, 27 (1980).
6. D.M. Ruthven, M. Eic and E. Richard, "Diffusion of C_8 Aromatics in Silicalite," *Zeolites* 11, 647-653 (1991).
7. D.M. Ruthven and S. Brandani, "Measurement of Diffusion in Porous Solids by ZLC Methods," pp 187-212 in *Recent Advances in Gas Separation by Microporous Ceramic Membranes*, N.K. Kanellopoulos ed., Elsevier, Amsterdam (2000).
8. S. Brandani and D.M. Ruthven, "Analysis of ZLC Desorption Curves for Gaseous Systems," *Adsorption* 2, 133-143 (1996).
9. P. Graham, A.D. Hughes and L.V.C. Rees, "Sorption of Nitrogen and Carbon Dioxide in Silicalite," *Zeolites* 3, 56-64 (1989).
10. N. Haq and D.M. Ruthven, "Chromatographic Study of Sorption and Diffusion in 5A Zeolite," *J. Colloidal Interface Sci.* 112, 164-169 (1986).

11. F.R. Siperstein and A.L. Myers, "Mixed Gas Adsorption," *AIChE Jl.* 47, 1141-1159 (2001).

12. D. Shen, M. Bulow, F. Siperstein, M. Engelhard and A.L. Myers, "Comparison of Experimental Techniques for Measuring Isosteric Heat of Adsorption," *Adsorption* 6, 275-286 (2000).

13. S-Y. Zhang, O. Talu and D.T. Hayhurst, "High Pressure Adsorption of CH_4 in NaX, MgX, CaX, SrX and BaX," *J. Phys. Chem.* 95, 1722-1726 (1991).

14. P.D. Rolniak and R. Kobayashi, "Adsorption of CH_4 and CO_2 at Elevated Pressures on 5A and 13X Molecular Sieves by Tracer Chromatography," *AIChE Jl.* 26, 616-625 (1980).

15. D.W. Breck, *Zeolite Molecular Sieves*, p. 98, Wiley-Interscience, New York (1974).

16. W.J. Mortier, "Compilation of Extra Framework Sites in Zeolites," 19 Butterworth, Guildford (1982).

17. D.H. Olson, "Crystal Structure of Dehydrated NaX," *Zeolites* 15, 439-443 (1995).

18. L. Xhu and K. Seff, "Reinvestigation of Crystal Structure of Dehydrated NaX", *J. Phys. Chem. B* 103, 9512-9518 (1999).

19. G. Vitale, C.C. Mellot, L.M. Bull and A.K. Cheetham, "Neutron Diffraction and Computational Study of Zeolite NaX: Influence of $SIII^1$ Cations on Benzene Complex," *J. Phys. Chem. B* 101, 4559-4564 (1997).

20. J. Plévert, F. DiRenzo, F. Fajula and G. Chiari, "Structure of Dehydrated Zeolite LiLSX by Neutron Diffraction," *J. Phys. Chem. B* 101, 10340-10346 (1997).

21. J. Plévert, F. DiRenzo, F. Fajula and G. Chiari, "Cation Positions in Dehydrated Zeolites LiLSX and Li, NaLSX," 135-139 12th Int. Zeolite Conf. Proceedings, Materials Research Soc. (1999).

22. Y.F. Shepelev, A.A. Anderson and Y.I. Smolin, "Crystal Structure of Partially Li Exchanged X Zeolite in Hydrated and Dehydrated States," *Zeolites* 10, 61-62 (1990).

23. D. Shen and M. Bülow, "Isosteric Study of Sorption Thermodynamics of Single Gases and Multicomponent Mixtures on Microporous Materials," *Mesoporous Materials* 22, 237-249 (1998).

24. J. Dunne, R. Mariwala, M. Roo, S. Sircar, R.J. Gorte and A.L. Myers, "Heats of Adsorption of Polar and Non-Polar Gases in Homogeneous and Heterogeneous Adsorbents," pp. 277-284 in *Fundamentals of Adsorption*, M.D. LeVan (ed.) Klewer, Boston, MA (1996).

25. R.M. Barrer and R.M. Gibbons, "Zeolitic CO_2: Energetics and Equilibria in Relation to Exchangeable Cations in Faujasite," *Trans. Faraday Soc.* 61, 948-961 (1965).

26. S.R. Jale, M. Bülow, F.R. Fitch. N. Perelman and D. Shen, "Monte Carlo Simulation of Sorption Equilibrium for N_2 and O_2 in LiLSX," *J. Phys. Chem. B* 104, 5272-5280 (2000).

27. J. Plévert, L.C. de Menorval, F. DiRenzo and F. Fajula, "Accessibility of Cation Sites by ^{6}Li MAS NMR Spectroscopy using Paramagnetic O_2 as a Chemical Shift Agent," *J. Phys. Chem. B* 102, 3412-3416 (1998).

28. M. Feuerstein and R.F. Lobo, "Influence of O_2 and N_2 on ^7Li MAS NMR Spectra of Zeolite LiX-1.0," *Chem. Commun.* 1647-1648 (1998).

29. V.B. Kazansky, M. Bulow and E. Tichinivova, "Specific Sorption Sites for N_2 in Zeolites NaLSX and LiLSX," *Adsorption* 7 241-299 (2001).

30. C.G. Coe, "Structural Effects on the Adsorptive Properties of Molecular Sieves for Air Separation," pp. 213-229 in *Access in Nanoporous Materials*, T. Pinnavaia and M.F. Thorpe eds., Plenum Press, New York (1995).

31. A. Cornu and R. Massot, *Compilation of Mass Spectral*, Heyden & Son, London (1966).

32. E. Costa, G. Calleja, A. Jimenez and J. Pau, "Adsorption Equilibrium of C_2H_4, C_3H_8, C_3H_6, CO_2 and their Mixtures on 13X Zeolite," *J. Chem. Eng. Data* 36, 218-224 (1991).

33. G. Calleja, A. Jimenez, J. Pau, L. Dominguez and P. Perez, "Multicomponent Sorption Equilibria of C_2H_4, C_3H_8, C_3H_6 and CO_2 on 13X Zeolite," *Gas Separation and Purification* 8, 247-256 (1994).

34. L. Bertsch and H.W Habgood, "An Infrared Spectroscopic Study of the Adsorption of Water and Carbon Dioxide by Linde Molecular Sieve X," *J. Phys. Chem.* 67, 1621-1628 (1963).

35. J.W. Ward and H.W Habgood, "The IR Spectrum of CO_2 on Zeolite X," *J. Phys. Chem.* 70, 1178-1182 (1966).

APPENDIX

Mathcad File for Fitting Binary Data with the Dual Site Model

The example refers to the system CO_2/C_3H_8 on NaLSX with p^0_{CO2}= 23.5 Torr and p^0_{C3H8}= 47 Torr

$A = CO_2$, $B = C_3H_8$

$\begin{pmatrix} PureC3H8 \\ PureCO2 \\ Binary \end{pmatrix} :=$

ZLC: CO_2-C_3H_8	on NaLSX	on NaLSX	ZLC: CO_2-C_3H_8
23-Sep	23-Sep	23-Sep	23-Sep
p_{C3H8}=47 Torr	p_{CO2}= 23.5 Torr	p_{CO2}= 23.5 Torr	p_{C3H8}=47 Torr
p_{CO2} [atm]	q_{CO2} [mmol/g]	p_{C3H8} [atm]	q_{C3H8} [mmol/g]
0.031	1.879	0.062	1.275
0.02	1.749	0.027	1.063
0.016	1.688	0.021	0.983
0.014	1.636	0.018	0.918
0.013	1.589	0.015	0.862
0.012	1.547	0.014	0.812
0.011	1.509	0.013	0.767
0.00998	1.473	0.011	0.726
0.008951	1.441	0.011	0.689
0.008358	1.412	0.011	0.652

$K_A := 958$ experimental Henry constant for CO_2 on NaLSX determined from single component experiment [mmol/(g*atm)]

$K_B := 180$ experimental Henry constant for C_3H_8 on NaLSX determined from single component experiment [mmol/(g*atm)]

$NA := 996$ number of experimental points for the CO_2 on NaLSX isotherm

$NB := 133$ number of experimental points for the C_3H_8 on NaLSX isotherm

$NBin := 200$ number of experimental points for CO_2/C_3H_8 on NaLSX isotherm

Expressions for the Dual Site Model

$$q(P,K1,K2,b1,b2) := \frac{|K1|\cdot P}{1+|b1|\cdot P} + \frac{|K2|\cdot P}{1+|b2|\cdot P}$$

$$qA_{bin}(PA,PB,K1A,K1B,b1A,b2A,b1B,b2B) := \frac{K1A\cdot PA}{1+|b1A|\cdot PA+|b1B|\cdot PB} + \frac{|K_A - K1A|\cdot PA}{1+|b2A|\cdot PA+|b2B|\cdot PB}$$

$$qB_{bin}(PA,PB,K1A,K1B,b1A,b2A,b1B,b2B) := \frac{K1B\cdot PB}{1+|b1A|\cdot PA+|b1B|\cdot PB} + \frac{|K_B - K1B|\cdot PB}{1+|b2A|\cdot PA+|b2B|\cdot PB}$$

Routine for fitting CO_2 on NALSX single component experimental data with dual site model

$$QA(K1,b1,b2) := \left| \begin{array}{l} Q \leftarrow 0.0 \\ K2 \leftarrow K_A - K1 \\ \text{for } j \in 0,1..NA \\ \quad P \leftarrow PureCO2_{j,0} \\ \quad qA \leftarrow q(P,K1,K2,b1,b2) \\ \quad Q \leftarrow Q + (PureCO2_{j,1} - qA)^2 \\ Q \end{array} \right.$$

K1A := 600 b1A := 10 b2A := 10

Given

QA(K1A,b1A,b2A) = 0 K1A < K_A

A := Minerr(K1A,b1A,b2A)

$$A = \begin{pmatrix} 919.225 \\ 418.38 \\ 3.142 \end{pmatrix}$$

K1A := A_0 K2A := K_A − K1A b1A := A_1 b2A := A_2

$j := 0, 1 .. NA$

$$\frac{q(PureCO2_{j,0}, K1A, K2A, b1A, b2A)}{PureCO2_{j,1}}$$

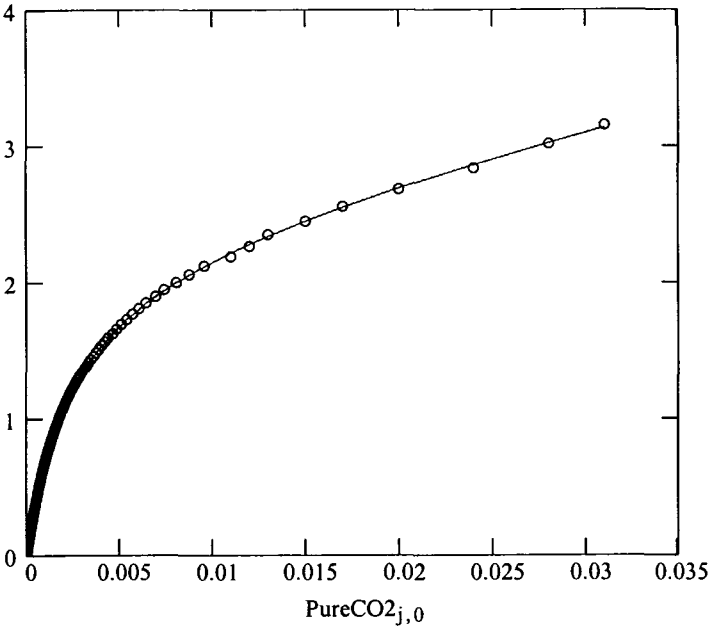

Routine for fitting C_3H_8 on NaLSX single component experimental data with dual site model

$QB(K1, b1, b2) :=$
- $Q \leftarrow 0.0$
- $K2 \leftarrow K_B - K1$
- for $j \in 0, 1 .. NB$
  - $P \leftarrow PureC3H8_{j,0}$
  - $qB \leftarrow q(P, K1, K2, b1, b2)$
  - $Q \leftarrow Q + (PureC3H8_{j,1} - qB)^2$
- Q

$K1B := 70 \qquad b1B := 10 \qquad b2B := 3$

Given

$QB(K1B, b1B, b2B) = 0 \quad K1B < K_B$

$A := \text{Minerr}(K1B, b1B, b2B)$

$$A = \begin{pmatrix} 180 \\ 33.808 \\ 11.516 \end{pmatrix} \qquad K1B := A_0 \qquad K2B := K_B - K1B \qquad b1B := A_1 \qquad b2B := A_2$$

$j := 0, 1 .. NB$

$$\frac{q(PureC3H8_{j,0}, K1B, K2B, b1B, b2B)}{PureC3H8_{j,1}}$$

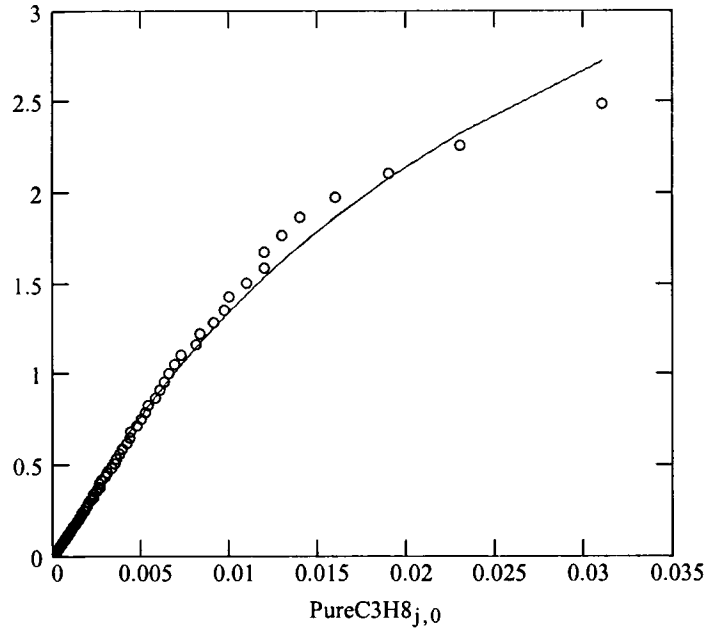

Predicted alpha

$$\alpha(PA, PB, K1A, K2A, K1B, K2B, b1A, b2A, b1B, b2B) := \frac{qA_{bin}(PA, PB, K1A, K1B, b1A, b2A, b1B, b2B)}{qB_{bin}(PA, PB, K1A, K1B, b1A, b2A, b1B, b2B)} \cdot \frac{PB}{PA}$$

$k := 0, 1 .. NBin$

$$\alpha_{Pred_k} := \alpha(Binary_{k,0}, Binary_{k,2}, K1A, K2A, K1B, K2B, b1A, b2A, b1B, b2B)$$

$$\alpha_{Exp_k} := \frac{Binary_{k,1}}{Binary_{k,3}} \cdot \frac{Binary_{k,2}}{Binary_{k,0}}$$

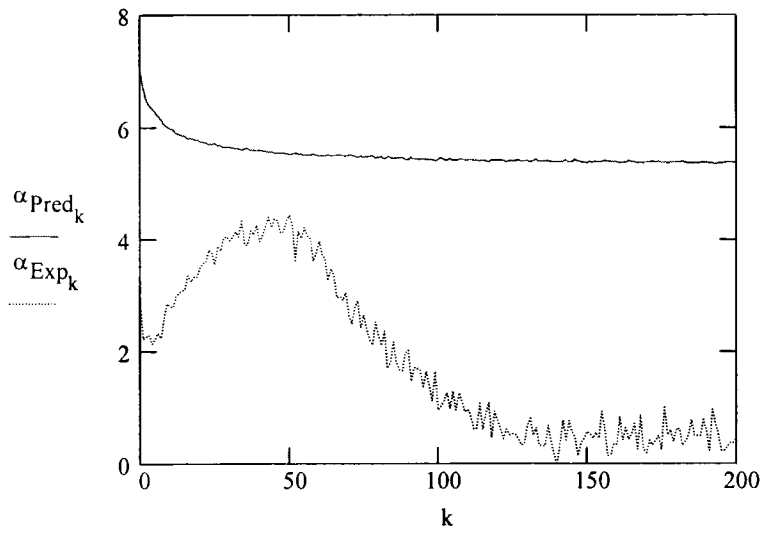

Use only points up to the maximum due to uncertainties in the low loading region

NBin := 45 number of experimental points to be fitted

Routine for fitting CO_2/C_3H_8 on NaLSX experimental data with dual site model

$$
\begin{aligned}
&Q\alpha(K1A, K1B, b1A, b2A, b1B, b2B) := \\
&\quad Q \leftarrow 0.0 \\
&\quad K2B \leftarrow K_B - K1B \\
&\quad K2A \leftarrow K_A - K1A \\
&\quad \text{for } j \in 0, 1 .. NBin \\
&\qquad PA \leftarrow Binary_{j,0} \\
&\qquad PB \leftarrow Binary_{j,2} \\
&\qquad \alpha C \leftarrow \alpha(PA, PB, K1A, K2A, K1B, K2B, b1A, b2A, b1B, b2B) \\
&\qquad Q \leftarrow Q + \left(\alpha_{Exp_j} - \alpha C\right)^2 \text{ if } j > 3 \\
&\quad Q
\end{aligned}
$$

Given

$QB(K1B, b1B, b2B) = 0$

$K1B < K_B - 0.1$ $\quad b1A > 0$ $\quad b2A > 0$

$QA(K1A, b1A, b2A) = 0$

$b1B > 0$ $\quad b2B > 0$

$K1A < K_A - 0.1$

$Q\alpha(K1A, K1B, b1A, b2A, b1B, b2B) = 0$

$A := \text{Minerr}(K1A, K1B, b1A, b2A, b1B, b2B)$

$$A = \begin{pmatrix} 920.259 \\ 117.08 \\ 417.306 \\ 2.303 \\ 36.811 \\ 29.262 \end{pmatrix}$$

$K1A := A_0$ $\quad K1B := A_1$ $\quad b1A := A_2$ $\quad b2A := A_3$

$b1B := A_4$ $\quad b2B := A_5$ $\quad K2A := K_A - K1A$ $\quad K2B := K_B - K1B$

$k := 0, 1 .. NBin$ $\quad \alpha Calc_k := \alpha(Binary_{k,0}, Binary_{k,2}, K1A, K2A, K1B, K2B, b1A, b2A, b1B, b2B)$

$$\alpha Exp_k := \frac{Binary_{k,1}}{Binary_{k,3}} \cdot \frac{Binary_{k,2}}{Binary_{k,0}}$$

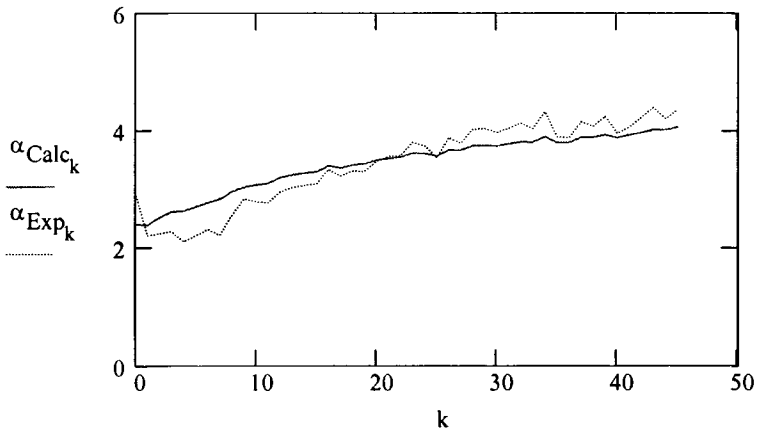

BIOGRAPHY OF THE AUTHOR

Federico Brandani was born in L'Aquila, Italy on February 17, 1967. He graduated from Liceo Scientifico Statale "Andrea Bafile" of L'Aquila in 1985. He attended the Università degli Studi de L'Aquila and graduated in 2000 with a Laurea degree in Chemical Engineering. He entered the Chemical Engineering graduate program at The University of Maine in the winter of 2001.

Federico has been accepted as a Marie Curie Fellow and after receiving his degree will join the University of Leipzig (Germany) for a post-doc position. Federico is a candidate for the Doctor of Philosophy degree in Chemical Engineering from The University of Maine in August, 2002.